Signal Processing and Communication with Solitons

Andrew C. Singer

RLE Technical Report No. 599

June 1996

The Research Laboratory of Electronics
MASSACHUSETTS INSTITUTE OF TECHNOLOGY
CAMBRIDGE, MASSACHUSETTS 02139-4307

This research was generously supported in part by the Defense Advanced Research Projects Agency under Grant N00014-89-J-1489, in part by Lockheed Martin Sanders, in part by the U.S. Navy Office of the Chief of Naval Research under Grant N00014-93-1-0686, and in part by U.S. Air Force Office of Scientific Research under Grant AFOSR-91-0034.

Report Documentation Page

Form Approved
OMB No. 0704-0188

Public reporting burden for the collection of information is estimated to average 1 hour per response, including the time for reviewing instructions, searching existing data sources, gathering and maintaining the data needed, and completing and reviewing the collection of information. Send comments regarding this burden estimate or any other aspect of this collection of information, including suggestions for reducing this burden, to Washington Headquarters Services, Directorate for Information Operations and Reports, 1215 Jefferson Davis Highway, Suite 1204, Arlington VA 22202-4302. Respondents should be aware that notwithstanding any other provision of law, no person shall be subject to a penalty for failing to comply with a collection of information if it does not display a currently valid OMB control number.

1. REPORT DATE	2. REPORT TYPE	3. DATES COVERED
JUN 1996		**00-06-1996 to 00-06-1996**

4. TITLE AND SUBTITLE	5a. CONTRACT NUMBER
Signal Processing and Communication with Solitons	5b. GRANT NUMBER
	5c. PROGRAM ELEMENT NUMBER
6. AUTHOR(S)	5d. PROJECT NUMBER
	5e. TASK NUMBER
	5f. WORK UNIT NUMBER
7. PERFORMING ORGANIZATION NAME(S) AND ADDRESS(ES) **Massachusetts Institute of Technology,Research Laboratory of Electronics,77 Massachusetts Avenue,Cambridge,MA,02139-4307**	8. PERFORMING ORGANIZATION REPORT NUMBER
9. SPONSORING/MONITORING AGENCY NAME(S) AND ADDRESS(ES)	10. SPONSOR/MONITOR'S ACRONYM(S)
	11. SPONSOR/MONITOR'S REPORT NUMBER(S)

12. DISTRIBUTION/AVAILABILITY STATEMENT
Approved for public release; distribution unlimited

13. SUPPLEMENTARY NOTES

14. ABSTRACT

15. SUBJECT TERMS

16. SECURITY CLASSIFICATION OF:			17. LIMITATION OF ABSTRACT	18. NUMBER OF PAGES	19a. NAME OF RESPONSIBLE PERSON
a. REPORT **unclassified**	b. ABSTRACT **unclassified**	c. THIS PAGE **unclassified**		**142**	

Signal Processing and Communication with Solitons

by

Andrew Carl Singer

Submitted to the Department of Electrical Engineering and Computer Science
on May 14, 1996, in partial fulfillment of the
requirements for the degree of
Doctor of Philosophy

Abstract

Traditional signal processing algorithms rely heavily on models that are inherently linear. Such models are attractive both for their mathematical tractability and their applicability to the rich class of signals that can be represented with Fourier methods. Nonlinear systems that support soliton solutions share many of the properties that make linear systems attractive from an engineering standpoint. Although nonlinear, these systems are solvable through inverse scattering, a technique analogous to the Fourier transform for linear systems. Solitons are eigenfunctions of these systems which satisfy a nonlinear form of superposition and display rich signal dynamics as they interact. By using solitons for signal synthesis, the corresponding nonlinear systems become specialized signal processors which are naturally suited to a number of complex signal processing tasks. Specific analog circuits can generate soliton signals and can be used as natural multiplexers and demultiplexers in a number of potential soliton-based wireless communication applications. These circuits play an important role in investigating the effects of noise on soliton behavior. Finally, the soliton signal dynamics also provide a mechanism for decreasing transmitted signal energy while enhancing signal detection and parameter estimation performance.

Thesis Supervisor: Alan V. Oppenheim
Title: Distinguished Professor of Electrical Engineering and Computer Science

Acknowledgments

I would like to express my sincere gratitude to Professor Alan Oppenheim, for both putting me out on a limb, and for making sure that I did not fall. Through his many roles as an advisor, a mentor, and above all, as a friend, he has had a tremendous impact on both my professional and personal development. I look forward to exploring many more trees together.

For his guidance, encouragement, and friendship, I also wish to thank Professor Gregory Wornell. Our many discussions have greatly influenced the way I think about research problems in general and this thesis in particular. I am sincerely grateful to Professor Ruben Rosales for his many insightful comments, his interest and his encouragement. Thanks also to Dr. Jim Kaiser of Bellcore and Dr. Doug Mook of Lockheed Sanders for numerous discussions relating to this work. Lloyd D'Souza deserves thanks for his many hours of circuit hacking and development.

The friendly atmosphere and productive research environment of the Digital Signal Processing Group have made my experiences as a graduate student both challenging and rewarding. Thanks to John Buck, Babis Papadopoulos, and Kathleen Wage for their help with various parts of this thesis and to Paul Beckmann, Steve Isabelle, Stephen Scherock, and Kambiz Zangi for many years of friendship and thought-provoking discussion. Thanks also to Jeff Ludwig, Lon Sunshine and Yakov Royter for their camaraderie and our many athletic pursuits.

I am especially grateful to Giovanni Aliberti both for his computer expertise and friendship. Special thanks go to Maggie Beucler, Janice Zaganjori and Sally Bemus for administrative support and for help in preparing this document.

This research has been generously supported by the Defense Advanced Research Projects Agency, Lockheed Martin Sanders, the Department of the Navy Office of the Chief of Naval Research, and the Air Force Office of Scientific Research.

Finally, I would like to thank my parents for their love and support and for being my very first teachers. Also, thanks to my sister Amy for reminding me what it's like to be a big brother. Most importantly, thanks to my loving wife, Cathy, for her unending love and encouragement.

Contents

List of Figures

Chapter 1

Introduction

Many traditional signal processing applications rely on models that are inherently linear and time-invariant (LTI). Much of the success of such methods can be attributed to their being mathematically tractable, often leading to efficient signal representations and fast algorithms. Linear techniques have also proven effective for modeling a variety of signals of practical interest such as speech or financial time-series and systems of interest such as the telephone or radio broadcast channels. However, we increasingly turn to nonlinear models to capture some of the more salient behavior of physical or natural systems that cannot be expressed by linear means, such as threshold phenomena, amplitude-dependence, or chaotic behavior. Nonlinear systems also hold the potential to produce more efficient algorithms or models for a variety of signal processing and communication problems where linear techniques are suboptimal.

Systems that support solitons may be a natural choice for a class of nonlinear systems to explore since they share many of the properties that make LTI systems attractive from an engineering standpoint. Although nonlinear, these systems are solvable through inverse scattering, a technique analogous to the Fourier transform for linear systems [1]. Solitons are eigenfunctions of these systems which satisfy a nonlinear form of superposition. We can therefore decompose complex solutions in terms of a class of signals with simple dynamical structure. Solitons have been observed in a variety of natural phenomena from water and plasma waves [31, 57] to crystal lattice vibrations [14] and energy transport in proteins [31]. Solitons can also be found in

a number of man-made media including super-conducting transmission lines [56] and nonlinear circuits [29, 60]. Recently, solitons have become of significant interest for optical telecommunications, where optical pulses have been shown to propagate as solitons for tremendous distances without significant loss or dispersion [23].

In this thesis, we view solitons from a decidedly different perspective. Rather than focusing on the propagation of solitons over nonlinear channels, we consider using these nonlinear systems to both generate and process signals for transmission over traditional linear channels. By using solitons for signal synthesis, the corresponding nonlinear systems become specialized signal processors which are naturally suited to a number of complex signal processing tasks. This thesis can be viewed as an exploration of the properties of solitons as signals. In the process, we explore the possibility of using these signals in a potential multi-user wireless communication context.

For example, we consider the problem of multiplexing a number of users onto a single carrier for transmission over a lossy channel. A variety of linear multiplexing schemes have been proposed such as time-, frequency-, or code-division multiple access systems. However, the number of nonlinear multiplexing strategies available is rather limited. One potential benefit to using solitons as carrier signals and the nonlinear systems as multiplexors, is that the soliton signal dynamics provide a mechanism for simultaneously decreasing transmitted signal energy and enhancing communication performance.

1.1 Outline of the Thesis

There is a large body of literature on soliton theory spanning over a century of research. Rather than attempting to provide a self-contained summary, in Chapter 2 we present a brief overview of the components of soliton theory that we will draw upon throughout the thesis. The chapter includes an introduction to solitons and some of the nonlinear systems that support them. We focus our discussion on the Toda lattice, a particularly simple soliton system that forms the basis of many of our

examples throughout the thesis. In order to exploit the rich mathematical structure of these systems, we review some elements from inverse scattering theory. In addition to providing an efficient mechanism for the construction of soliton signals and the solutions to their dynamics, the inverse scattering framework can also be used to synthesize families of soliton systems. Throughout the thesis, the inverse scattering transform plays an analogous role to the Fourier transform in the analysis and processing of soliton signals in the presence of noise.

To facilitate real-time generation and processing of soliton signals, it will be important to explore implementations of these nonlinear systems. In Chapter 3 we develop new circuit models for two soliton systems. The first is a diode ladder implementation of the Toda lattice which appears to be the first circuit implementation to display true soliton behavior. We also develop a lattice-circuit implementation of the discrete-KdV equation, which will be important for processing discrete-time soliton signals.

These circuit models then form the basis for a communication paradigm presented in Chapter 4, where multiple signals can be multiplexed onto soliton carriers using such circuits as tuned modulators and demodulators. As we will see, the nonlinear interaction of multiple solitons can be exploited as a means for reducing the transmitted signal energy in a multi-user communication context. Such low power transmission techniques may be applicable to a variety of portable or power-limited communication applications.

Before soliton systems can be used in a practical communication context, we need accurate models for the effects of disturbances on the dynamics of these systems. The robustness of such systems to additive corruption will have a direct impact on the demodulation performance of the nonlinear receivers. In Chapter 5, we analyze the effects of small amplitude corruption on the dynamics of solitons in the Toda lattice and characterize the statistics of the noise as it is propagates through the system.

In order to develop effective communication strategies by modulating the parameters of soliton carriers, we need to have accurate models for the ability of a receiver to resolve these parameters. In Chapter 6, we compute Cramér-Rao bounds for their

estimation error variance. We show that in addition to reducing signal energy, the nonlinear interaction of multiple solitons can also enhance parameter estimation performance. Based on our characterization of the noise, we develop a set of parameter estimation algorithms in which maximum-likelihood (ML) estimates can be obtained from corrupted measurements. In Chapter 7, we demonstrate how soliton circuits can be used to enhance the detection of multiple solitons in noise.

Finally, Chapter 8 summarizes the main contributions of the thesis and indicates some interesting and potentially important directions for future study.

Chapter 2

Soliton Systems

Solitons play an important role in the study of a large class of nonlinear evolution equations. As we shall see, the ability to describe their long-term behavior analytically makes this class of systems attractive for modeling a variety of nonlinear phenomena in a number of diverse areas in mathematics, physics, biology, and engineering. Examples include topics from surface or internal water waves, to energy transport along long protein chains, and the propagation of optical pulses along nonlinear fibers. Furthermore, the development of optical and electrical analogs for many of these systems makes soliton signals of great practical interest.

The theory of solitons dates back to the work of Korteweg and de-Vries, and was motivated by attempts to explain the unusual water wave observations of Scott Russell in 1834. The method of solution for soliton systems began with the work of Gardner, Greene, Kruskal, and Miura on the Korteweg-de Vries (KdV) equation [18]. These techniques were generalized by Lax [42] and then by Ablowitz et al. [1] and used to solve what is now a large class of solvable nonlinear evolution equations.

This chapter is designed as a brief overview of the components of soliton theory that we will draw upon throughout the thesis. Although no new results will be presented, this chapter serves several purposes. First, we present an introduction to solitons and to some of the nonlinear systems that support them. We will focus our attention on the Toda lattice, a simple mechanical system that will form the basis of many of the examples throughout the thesis. Second, we summarize some of the

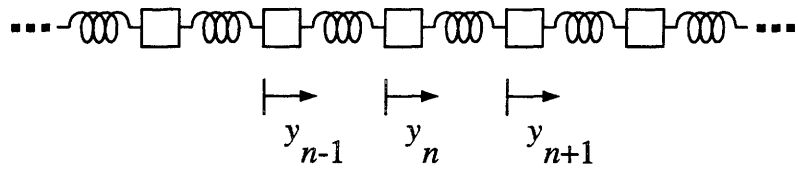

Figure 2-1: The Toda Lattice.

main results of inverse scattering theory, the method by which soliton systems can be solved analytically. Rather than attempting to fully develop this topic, we concentrate on portions of the theory that we will exploit in the applications developed in later chapters of the thesis. Finally, we mention a few of the techniques that can be used to construct families of soliton systems. As we will see in later chapters, these systems are potentially useful for a number of communication applications. Therefore, there may be a practical use for the generation of increasingly complex soliton systems.

2.1 The Toda Lattice

The Toda lattice is a conceptually simple mechanical example of a nonlinear system with soliton solutions. A comprehensive treatment of the lattice and its associated soliton theory can be found in the monograph by Toda [69]. As shown in Fig. 2-1, the Toda lattice equations describe the displacements of an infinite chain of masses connected with nonlinear springs. Each of the springs satisfies the nonlinear force law

$$f_n = a(e^{-b(y_n - y_{n-1})} - 1), \tag{2.1}$$

where f_n is the force on the spring between masses with displacements y_n and y_{n-1} from their rest positions. The equations of motion for the lattice are given by

$$m\ddot{y}_n = a\left(e^{-b(y_n - y_{n-1})} - e^{-b(y_{n+1} - y_n)}\right), \tag{2.2}$$

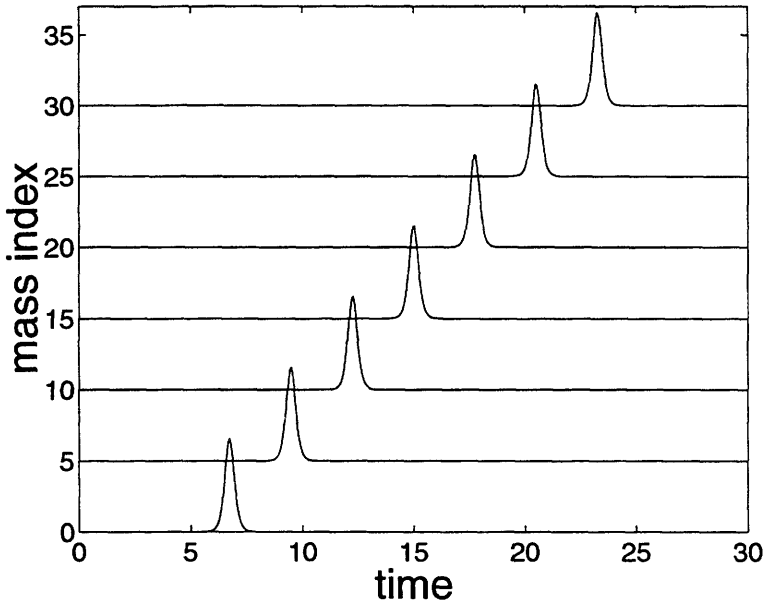

Figure 2-2: A propagating wave solution to the Toda lattice equations. Each trace corresponds to the force $f_n(t)$ stored in the spring between mass n and $n-1$.

where y_n is the displacement of the n-th mass from its rest position, m is the mass, and a and b are constants. This equation admits pulse-like solutions of the form

$$f_n(t) = \left(\frac{m}{ab}\right) \beta^2 \mathrm{sech}^2(\sinh^{-1}(\sqrt{m/ab}\ \beta)n - \beta t), \tag{2.3}$$

which propagate as compressional waves stored as forces in the nonlinear springs. A single right-traveling wave $f_n(t)$ is shown in Fig. 2-2. The bottom trace in the figure corresponds to the force in the spring between masses "zero" and "one" of an infinite-length Toda chain. This compressional wave is localized in time, and propagates along the chain maintaining constant shape and velocity. Since, for example, the wave $f_n(t)$ appears on the thirtieth mass at a later point in time, this wave is therefore propagating to the right along the lattice as viewed in Fig. 2-1. The parameter β appears in both the amplitude and in the temporal- and spatial-scales of this one-parameter family of solutions giving rise to tall, narrow pulses which propagate faster then small, wide pulses. This type of localized pulse-like solution is what is often referred to as a *solitary wave.*

Definition 1: *A* **solitary wave** *solution to a partial differential equation for dependent variable, y, with temporal and spatial variables, t and n, is a traveling-wave solution of the form,*

$$y(n,t) = f(n - ct) = f(z), \tag{2.4}$$

where c is a fixed constant, and the energy of $f(z)$ is localized.

The history of solitary waves dates back to the work of John Scott Russell in 1834 and perhaps the first recorded sighting of a solitary wave. Here is his original account of his sighting:

> I was observing the motion of a boat which was rapidly drawn along a narrow channel by a pair of horses, when the boat suddenly stopped — not so the mass of water in the channel which it had put in motion; it accumulated round the prow of the vessel in a state of violent agitation, then suddenly leaving it behind, rolled forward with great velocity, assuming the form of a large solitary elevation, a rounded, smooth and well defined heap of water, which continued its course along the channel apparently without change of form or diminution of speed. I followed it on horseback and overtook it still rolling on at a rate of speed some eight or nine miles an hour, preserving its original figure some thirty feet long and a foot to a foot and a half in height. Its height gradually diminished and after a chase of one or two miles I lost it in the windings of the channel. Such in the month of August 1834 was my first encounter with that singular and beautiful phenomenon... [58].

What Scott Russell actually observed was a solitary wave solution to what is now known as the KdV equation [57]. The Toda lattice is in many ways analogous to KdV; in fact, KdV can be derived as a continuum limit. A detailed discussion of linear and nonlinear wave theory including KdV can be found in [75]. In a 1965 paper, Zabusky and Kruskal performed numerical experiments with KdV and noticed that these solitary wave solutions retained their identity upon collision with other solitary waves. Since the velocities of KdV solitary waves are proportional to their amplitudes, a collision of solitary waves will occur for any solution with a taller pulse to the left of a shorter pulse. As the individual solitary waves approach one-another, they begin to interact nonlinearly. However, after passing through one-another, they regain their shape and speed with only a slight positional shift as evidence of their interaction [78].

This process indicates that the nonlinear dynamic system has a generalized coordinate transformation, or underlying dynamic structure which produces a set of "normal modes" that are almost completely uncoupled.

Zabusky and Kruskal's discovery that these solitary wave solutions behaved much like particles in that they essentially retained their identity after collisions prompted them to coin the term *soliton* implying that these solitary waves possess a particle-like nature. This is the type of behavior we would expect for linear wave equations, that is, the ability to form solutions from a superposition of simpler waves. However, that a nonlinear equation such as KdV or the Toda lattice permits such a form of superposition is an indication that it belongs to a rather remarkable class of nonlinear systems. This property distinguishes solitons from other solitary waves. We will adopt the following working definition of solitons:

Definition 2: *A* **soliton** *solution to a partial differential equation is a solitary wave which asymptotically retains its shape and velocity upon collision with another soliton, i.e.*

$$y(n,t) = \begin{cases} f(n-ct), & t \to -\infty, \\ f(n-ct+\delta), & t \to +\infty, \end{cases} \tag{2.5}$$

for $(n-ct)$ *fixed and* δ *an arbitrary constant.*

As we shall see, the term soliton often implies additional mathematical structure involving the inverse scattering transform.

Returning to the Toda lattice, Fig. 2-3 illustrates soliton behavior for two solutions of the form of Eq. (2.3). The bottom trace in the figure corresponds to the force in the spring between masses with indices zero and one in the lattice. Note that as a function of time, a smaller, wider soliton appears before a taller, narrower one. However, as viewed by, e.g., the thirtieth mass in the lattice, the larger soliton appears first as a function of time, i.e. has traveled faster. Note that when the larger soliton catches up to the smaller soliton as viewed on the fifteenth node, the combined amplitude of the two solitons is actually less than would be expected for a linear system, which would display a linear superposition of the two amplitudes. Also, the signal shape changes

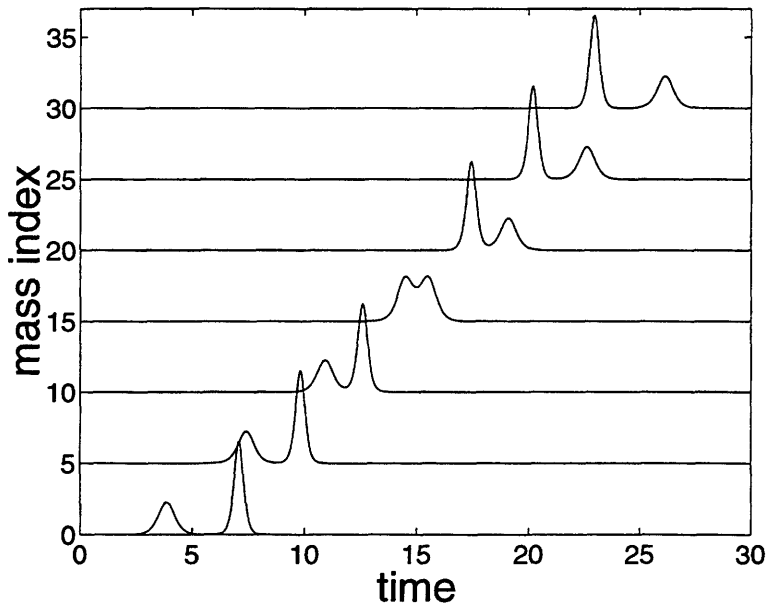

Figure 2-3: Two solitary wave solutions to the Toda lattice.

significantly during this nonlinear interaction. Both of these characteristics of soliton interaction will have useful implications in the context developed in Chap. 4.

An analytic expression for the two-soliton solution for $\beta_1 > \beta_2 > 0$ is given by [29]

$$f_n(t) = \frac{m}{ab} \frac{\beta_1^2 \mathrm{sech}^2(\eta_1) + \beta_2^2 \mathrm{sech}^2(\eta_2) + A \mathrm{sech}^2(\eta_1)\mathrm{sech}^2(\eta_2)}{\left(\cosh(\phi/2) + \sinh(\phi/2)\tanh(\eta_1)\tanh(\eta_2)\right)^2}, \tag{2.6}$$

where

$$A = \sinh(\phi/2)\left(\left(\beta_1^2 + \beta_2^2\right)\sinh(\phi/2) + 2\beta_1\beta_2\cosh(\phi/2)\right), \tag{2.7}$$

and

$$\phi = \ln\left(\frac{\sinh((p_1 - p_2)/2)}{\sinh((p_1 + p_2)/2)}\right), \tag{2.8}$$

and $\beta_i = \sqrt{ab/m}\sinh(p_i)$, and $\eta_i = p_i n - \beta_i(t - \delta_i)$.

Although Eq. (2.6) appears rather complex, Figure 2-3 illustrates that for large separations, $|\delta_1 - \delta_2|$, $f_n(t)$ essentially reduces to the linear superposition of two solitons with parameters β_1 and β_2. As the relative separation decreases, the multiplicative cross term becomes significant, and the solitons interact nonlinearly. This

asymptotic behavior can also be evidenced analytically,

$$\begin{aligned} f_n(t) &= \frac{m}{ab}\beta_1^2 \mathrm{sech}^2(p_1 n - \beta_1(t-\delta_1) \pm \phi/2) \\ &+ \frac{m}{ab}\beta_2^2 \mathrm{sech}^2(p_2 n - \beta_2(t-\delta_2) \mp \phi/2), \quad t \to \pm\infty, \end{aligned} \tag{2.9}$$

where each component soliton experiences a net displacement ϕ from the nonlinear interaction.

The Toda lattice also admits periodic solutions which can be written in terms of Jacobian elliptic functions $\mathrm{dn}(\cdot)$ and $\mathrm{sn}(\cdot)$. These solutions can be expressed

$$f_n(t) = \frac{(2K\nu)^2}{ab/m}\left\{\mathrm{dn}^2\left[2\left(\frac{n}{\lambda} \pm \nu t\right)K\right] - \frac{E}{K}\right\}, \tag{2.10}$$

for wavelength λ and frequency ν, with

$$2K\nu = \sqrt{\frac{ab}{m}}\left(\mathrm{sn}^{-2}(2K/\lambda) - 1 + \frac{E}{K}\right)^{-1/2}. \tag{2.11}$$

For further description of Jacobian elliptic functions, the reader is referred to [2] and [69].

An interesting observation can be made when the Toda lattice equations are written in terms of the forces,

$$\frac{d^2}{dt^2}\ln\left(1 + \frac{f_n}{a}\right) = \frac{b}{m}(f_{n+1} - 2f_n + f_{n-1}). \tag{2.12}$$

If the substitution

$$f_n(t) = \frac{d^2}{dt^2}\ln\phi_n(t) \tag{2.13}$$

is made into Eq. (2.12), then the lattice equations become,

$$\frac{m}{ab}\left(\dot{\phi}_n^2 - \phi_n\ddot{\phi}_n\right) = \phi_n^2 - \phi_{n-1}\phi_{n+1}. \tag{2.14}$$

In view of the Teager energy operator introduced by Kaiser in [35], the left hand side of Eq. (2.14) is the Teager instantaneous-time energy at the node n, and the right

hand side is the Teager instantaneous-space energy at time t. In this form, we may view solutions to Eq. (2.14) as propagating waveforms that have equal Teager energy as calculated in time and in space, a relationship also observed by Kaiser [36].

2.2 The Inverse Scattering Transform

Perhaps the most significant discovery in soliton theory was that under a rather general set of conditions, certain nonlinear evolution equations such as KdV or the Toda lattice could be solved analytically. That is, given an initial condition of the system, the solution can be explicitly determined for all time. This discovery eventually led to a theory of solvable nonlinear dynamic systems to which KdV and Toda belong along with many other nonlinear systems which exhibit soliton behavior. Since much of inverse scattering theory is beyond the scope of this thesis, we will only present some of the basic elements of the theory which we will exploit in later chapters and refer the interested reader to the comprehensive treatment given in the text by Ablowitz and Clarkson [1].

The nonlinear systems which have been solved by inverse scattering belong to a class of systems called conservative Hamiltonian systems. These are state-variable systems where the dynamics can be written explicitly in terms of the gradient of an energy function, or the Hamiltonian of the system, $\mathcal{H}(\mathbf{x})$. For example, if the state of the system were given by $\mathbf{x}$, and the Hamiltonian were $\mathcal{H}(\mathbf{x})$, then the dynamics could be written in the form

$$\dot{\mathbf{x}} = \begin{bmatrix} 0 & I \\ -I & 0 \end{bmatrix} \nabla \mathcal{H}(\mathbf{x}). \tag{2.15}$$

For conservative Hamiltonian systems, $\mathcal{H}(\mathbf{x})$ will not be a function of time. A rigorous treatment of Hamiltonian systems can be found in the text [41]. Conditions under which conservative Hamiltonian systems become solvable can be found in [3]. For the nonlinear systems we discuss in this thesis, an integral component of their solution lies in the ability to write the dynamics of the system implicitly in terms of an operator

differential equation of the form,

$$\frac{dL(t)}{dt} = B(t)L(t) - L(t)B(t), \tag{2.16}$$

where $L(t)$ is a symmetric linear operator, $B(t)$ is an anti-symmetric linear operator, and both $L(t)$ and $B(t)$ depend explicitly on the state of the system $\mathbf{x}(t)$. Lax has shown [42] that when the dynamics can be written in the form of Eq. (2.16), then the eigenvalues of the operator $L(t)$ are time-invariant, i.e. $\dot{\lambda} = 0$. The ability to write the dynamics implicitly in the form of Eq. (2.16), coupled with the structure of conservative Hamiltonian systems is sufficient to guarantee the solvability of each of the soliton systems that will be discussed in this thesis.

Using the Toda lattice as an example, the operator L would be the symmetric matrix

$$L = \begin{bmatrix} \ddots & a_{n-1} & \\ a_{n-1} & b_n & a_n \\ & a_n & \ddots \end{bmatrix}, \tag{2.17}$$

where

$$a_n = \frac{1}{2}e^{(y_n - y_{n+1})/2}, \qquad b_n = \frac{\dot{y}_n}{2}, \tag{2.18}$$

for mass positions y_n in a solution to Eq. (2.2). When B is given by the anti-symmetric matrix

$$B = \begin{bmatrix} \ddots & -a_{n-1} & \\ a_{n-1} & 0 & -a_n \\ & a_n & \ddots \end{bmatrix}, \tag{2.19}$$

then Eq. (2.16) implicitly contains the Toda lattice equations. Although each of the entries of $L(t)$ evolve with the state of a solution to the Toda lattice, the eigenvalues of $L(t)$ remain constant.

If we assume that the motion on the lattice is confined to lie within a finite region of the lattice, i.e. the lattice is at rest for $|n| \to \infty$, then the spectrum of eigenvalues for the matrix $L(t)$ can be separated into two sets. As depicted in Fig. 2-4, there is a continuum of eigenvalues $\lambda \in [-1, 1]$ and a discrete set of eigenvalues for which

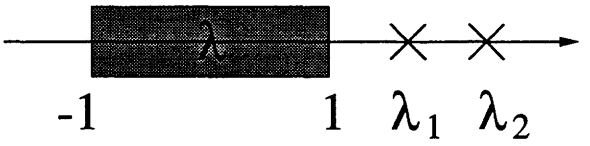

Figure 2-4: Spectrum of eigenvalues of the matrix $L(t)$ for the Toda lattice.

$|\lambda_k| > 1$. For any solution to the infinite-length Toda lattice, the continuous set of eigenvalues will all be present. However the discrete eigenvalues will only exist if there are solitons present in the lattice — one discrete eigenvalue for each soliton excited. This separation of eigenvalues of $L(t)$ into discrete and continuous components is common to all of the nonlinear systems solved with inverse scattering.

The inverse scattering method of solution for soliton systems is schematically similar to methods used to solve linear evolution equations. For example, consider a linear evolution equation of the form

$$\frac{d}{dt}y(x,t) = \mathcal{L}(t,x,y), \tag{2.20}$$

where $\mathcal{L}$ is a linear function of time t, space x, the state y and its derivatives. Given an initial condition of the system, $y(x,0)$, a standard technique for solving for $y(x,t)$ employs Fourier methods. By decomposing the initial condition into a superposition of simple harmonic waves of the form,

$$y(x,0) = \frac{1}{2\pi}\int_{-\infty}^{\infty} Y(k,0)e^{jkx}dk, \tag{2.21}$$

each of the component harmonic waves can be independently propagated using the dispersion relation defined by $\mathcal{L}$. Given the Fourier decomposition of the state at time t, the harmonic waves can then be recombined to produce the state of the system $y(x,t)$. This process is depicted schematically in Fig. 2-5.

An outline of the inverse scattering method for soliton systems is similar. Given an initial condition for the nonlinear system, $y(x,0)$, the eigenvalues λ and eigenfunctions $\psi(x,0)$ of the linear operator $L(0)$ can be obtained. This step is often called *forward scattering* by analogy to quantum mechanical scattering. To obtain

$$
\begin{array}{lll}
y(x,0) & \longrightarrow F.T. \longrightarrow & k, Y(k,0) \\
 & & \Downarrow \text{ Evolve simply in time} \\
 & & \Downarrow \quad e^{-j\omega(k)t} \\
y(x,t) & \longleftarrow I.F.T. \longleftarrow & k, Y(k,t)
\end{array}
$$

Figure 2-5: Schematic solution to linear evolution equations.

$$
\begin{array}{lll}
y(x,0) & \longrightarrow F.S. \longrightarrow & \lambda, \psi(x,0) \\
 & & \Downarrow \text{ Evolve simply in time} \\
 & & \Downarrow \quad e^{j\beta(k)t} \\
y(x,t) & \longleftarrow I.S. \longleftarrow & \lambda, \psi(x,t)
\end{array}
$$

Figure 2-6: Schematic solution to soliton equations.

the eigenvalues and eigenfunctions at a point in time t, all that is needed is the time evolution of the eigenfunctions, since the eigenvalues do not change with time. For these soliton systems, the eigenfunctions evolve simply in time, according to linear differential equations. Given the eigenvalue-eigenfunction decomposition of $L(t)$, through a process called *inverse scattering*, the state of the system $y(x,t)$ can be completely reconstructed. This process is depicted in Fig. 2-6 in a similar fashion to the linear solution process.

Once again, we turn to the Toda lattice as an example to illustrate the inverse scattering method in slightly more detail. Although the discussion that follows is specific to the Toda lattice, the general approach and much of the theory applies directly to all soliton systems.

Once a pair of linear operators for the nonlinear evolution equation is known, the dynamics of the nonlinear system can be inferred through the behavior of the eigenvalues and eigenfunctions of $L(t)$. Here we consider the eigenvalue-eigenfunction decomposition

$$L(t)\psi(t) = \lambda\psi(t), \tag{2.22}$$

the n-th row of which corresponds to

$$(L(t)\psi(t))_n = a_{n-1}(t)\psi(n-1,t) + b_n(t)\psi(n,t) + a_n(t)\psi(n+1,t) = \lambda\psi(n,t). \quad (2.23)$$

The eigenfunctions satisfy,

$$\frac{d\psi(n,t)}{dt} = B(t)\psi(n,t), \quad (2.24)$$

the n-th row of which yields,

$$\frac{d\psi(n,t)}{dt} = a_{n-1}(t)\psi(n-1,t) - a_n(t)\psi(n+1,t). \quad (2.25)$$

Assuming that the lattice is at rest ($a_n = 1/2$ and $b_n = 0$) for $|n| \gg 1$, the eigenvalues of $L(t)$ consist of a continuum $\lambda \in [-1,1]$, and a finite set of discrete eigenvalues $|\lambda_k| > 1$. The corresponding eigenfunctions can be specified in terms of their asymptotic behavior in the regions where the motion on the lattice vanishes. Specifically, the eigenfunctions $\zeta_k(n,t)$ corresponding to the discrete eigenvalues λ_k are specified as

$$\zeta_k(n,t) \approx c_k(t) z_k^n, \quad n \to \infty, \quad (2.26)$$

where $|z_k| < 1$ and $\lambda_k = (z_k + z_k^{-1})/2$, with

$$\sum_{n=-\infty}^{\infty} (\zeta_k(n,t))^2 = 1. \quad (2.27)$$

The eigenfunctions $\psi(n,t)$ corresponding to the eigenvalues λ in the continuum are specified as

$$\psi(n,t) \approx z^{-n} + R(z,t)z^n, \quad n \to \infty, \quad (2.28)$$

$$\psi(n,t) \approx \frac{z^{-n}}{\alpha(z,t)} \quad n \to -\infty, \quad (2.29)$$

for $\lambda = (z + z^{-1})/2$.

We can now solve the initial value problem for the Toda lattice. Given $y_n(0)$, the initial eigenvalue-eigenfunction decomposition can be found for $L(0)$. The collec-

tion of discrete eigenvalues and the asymptotic description of both the discrete and continuous eigenfunctions are often referred to as the nonlinear spectrum for soliton systems. Here our nonlinear spectrum consists of

$$S(\lambda,0) = \left[\{(z_k, c_k(0)) : 1 \le k \le N\}, R(z,0), \alpha(z,0)\right]. \tag{2.30}$$

From (2.25), the time evolution of the nonlinear spectrum can be expressed as

$$\begin{aligned} c_k(t) &= c_k(0)e^{\beta_k t}, \quad \beta_k = (z_k^{-1} - z_k)/2 && (2.31)\\ \alpha(z,t) &= \alpha(z,0), && (2.32)\\ R(z,t) &= R(z,0)e^{2\beta t}, \quad \beta = (z^{-1} - z)/2 && (2.33) \end{aligned}$$

which yields the nonlinear spectrum at time t, $S(\lambda,t)$. The inverse scattering problem is then to reconstruct the state of the system, $a_n(t)$, and $b_n(t)$ at time t, given $S(\lambda,t)$. From the nonlinear spectrum, we can define the following function,

$$F(n,t) = \sum_{k=1}^{N} c_k^2(t) z_k^n + \frac{1}{2\pi i}\oint R(z,t) z^{n-1} dz. \tag{2.34}$$

We then seek a solution $K(n,m,t)$ to the Gel'fand-Levitan-Marchenko (GLM) equation,

$$\kappa(n,m,t) + F(n+m,t) + \sum_{n'=n+1}^{\infty} \kappa(n,n',t) F(n'+m,t) = 0, \quad m > n, \tag{2.35}$$

where,

$$K(n,n,t)^{-2} = 1 + F(2n,t) + \sum_{n'=n+1}^{\infty} \kappa(n,n',t) F(n'+m,t), \tag{2.36}$$

and

$$\kappa(n,m,t) = \frac{K(n,m,t)}{K(n,n,t)}. \tag{2.37}$$

The GLM equation form a linear discrete-integral equation in the terms $\kappa(n,m,t)$.

The solution $y_n(t)$ can then be found from

$$\begin{aligned} a_n(t) &= \frac{K(n+1,n+1,t)}{2K(n,n,t)}, \\ b_n(t) &= \frac{K(n,n+1,t)}{2K(n,n,t)} - \frac{K(n-1,n,t)}{2K(n-1,n-1,t)}. \end{aligned} \tag{2.38}$$

The forces on the springs, $f_n(t)$, can be obtained directly

$$f_n(t) = \left[\frac{K(n,n,t)}{K(n-1,n-1,t)}\right]^2 - 1. \tag{2.39}$$

For a large class of soliton systems, the inverse scattering method generally involves solving either a linear integral equation or a linear discrete-integral equation. The general form of the GLM equation follows that for the Toda lattice. Although the equation is linear, finding the solution of the GLM is often very difficult in practice. However, when the reflection coefficient, $R(z)$, is zero, then Eq. (2.35) reduces a set of simultaneous linear equations. This corresponds to a solution made up of pure solitons, one soliton for each discrete eigenvalue. Examples of this method for the Toda lattice are carried out for a single soliton and a multi-soliton solution as well as a solution with a single pole reflection coefficient in Appendices 2.A–2.C.

2.3 Other Systems Exhibiting Solitons

Since the discovery of the inverse scattering method for the solution to KdV, there has been a large class of nonlinear wave equations, both continuous and discrete, for which similar solution methods have been obtained. In most cases, solutions to these equations can be constructed from a nonlinear superposition of soliton solutions. For a comprehensive study of inverse scattering and equations solvable by this method, the reader is referred to the text by Ablowitz and Clarkson [1]. We briefly mention a few to indicate the rich class of such equations.

1. The sine-Gordon equation

$$\psi_{xx} - \psi_{tt} = \sin(\psi). \tag{2.40}$$

The sine-Gordon (SG) equation has been used as a model for a variety of physical phenomena including the propagation of crystal dislocation [57] and the propagation of magnetic flux along a Josephson strip line [56]. A simple physical model can be constructed by hanging pendula from an elastic line – the angular displacement of the pendula are approximately governed by the SG equation. A soliton solution is given by

$$\psi(x,t) = 4\tan^{-1} e^{\pm\left(\frac{x-ut}{\sqrt{1-u^2}}\right)}, \tag{2.41}$$

which is often called a "kink" soliton since it corresponds to a change in phase. An inverse scattering solution for the SG equation has been developed by Ablowitz, Kaup, Newell, and Segur [1].

2. The Nonlinear Schrödinger Equation

$$iu_t + u_{xx} \pm k|u|^2 u = 0. \tag{2.42}$$

The most widely-known application of the nonlinear Schrödinger (NLS) equation has been to describe the propagation of lightwave pulses along nonlinear fiber-optic cables [23]. Other applications include the propagation of heat in solids, and Langmuir waves in plasma [57]. The NLS equation admits envelope solitons of the form

$$u = u_0 \mathrm{sech}\left(\sqrt{k}2u_0(x - v_e t)\right) e^{i(v_e/2)(x - v_c t)}, \tag{2.43}$$

where v_e and v_c are the envelope and carrier velocities respectively [57]. The inverse scattering solution to the NLS equation was given by Zakharov and Shabat [79].

3. The Discrete-KdV Equation

$$\dot{u}_n = e^{u_{n-1}} - e^{u_{n+1}}. \tag{2.44}$$

The discrete-KdV (dKdV) equation was discussed by Kac and Van Moerbeke in relation to the Toda lattice. Manakov also studied the dKdV lattice for its relation to a model for Langmuir oscillations in plasma. An inverse scattering theory for dKdV was developed by each independently in [33] and [45]. Manakov presents the single soliton solution for $N_n = e^{u_n}$,

$$N_n(t) = \frac{\cosh(\eta(n - x_0 - 2))\cosh(\eta(n - x_0 + 1))}{\cosh(\eta(n - x_0 - 1))\cosh(\eta(n - x_0))}, \tag{2.45}$$

where

$$x_0(t) = x_0(0) + \frac{\sinh(2\eta)}{\eta}t. \tag{2.46}$$

4. Cellular Automata

A number of fully-discrete dynamic systems, or cellular automata (CA), have been shown to possess solutions with many of the properties of solitons. Ablowitz et al. have shown several automata that possess soliton-like solutions which are remarkably similar to the solitons of KdV or the Toda lattice [1, 52] as shown in Fig. 2-7. Park, Steiglitz and Thurston have also observed soliton-like behavior in automata, and even suggested possible computational applications of such systems [53, 63, 62]. Takahashi has presented a CA similar to the automata of Ablowitz et al., which also not only possesses soliton-like solutions, but also has an infinite number of conserved quantities, a property shared by solvable nonlinear systems [66].

2.4 Soliton Hierarchies

In this section we mention a few of the techniques that can be used to construct families of solvable nonlinear evolution equations. Since we shall see that the soliton

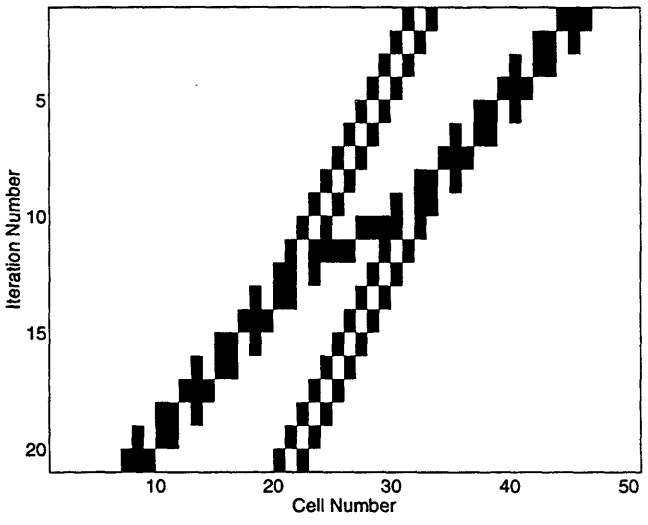

Figure 2-7: Soliton-like solutions to the automata of Ablowitz et al.

solutions of such systems are potentially useful for communication, there may be a practical use for the generation of increasingly complex soliton systems.

Many solvable nonlinear evolution equations, including the Korteweg-de Vries and nonlinear Schrödinger equations, can be written in the form

$$\frac{du(x,t)}{dt} = K(u), \tag{2.47}$$

where $K(u)$ may be a function of u and its x-derivatives. In [42], Lax demonstrated conditions under which the eigenvalues of a self-adjoint linear operator L, parameterized by u, would remain invariant under time evolution of $u(x,t)$ and hence, of $L(t)$. This is the so-called Lax equation, $\dot{L} = BL - LB$, where B is an anti-symmetric operator.

In many cases this leads directly to an inverse scattering framework, from which the nonlinear evolution equations can be solved. Unfortunately, given a nonlinear evolution equation, there is no constructive means known to generate a Lax pair for the system or even to tell if one exists. Lax does indicate in [42] how given an operator, L, an associated operator B may be constructed such that the resulting nonlinear evolution equation is nontrivial. Although such evolution equations have

often been discounted for having no physical analog, such equations clearly can be used in the signal processing contexts discussed in this thesis either through numerical integration or with the aid of high-speed nonlinear circuitry.

A similar technique was applied to the matrix $L(t)$ for the Toda lattice, viz.,

$$L[n,m] = a_{n-1}\delta_{n,m+1} + b_n\delta_{n,m} + a_n\delta_{n+1,m}, \tag{2.48}$$

by Moser in [48]. Here, the evolution equation will be defined in terms of $\dot{L}$; hence we require $BL - LB$ to be a tridiagonal symmetric matrix yielding the evolution of the parameters, $a_n(t)$ and $b_n(t)$. A Toda lattice hierarchy can be found by specifying an algorithm for selecting the antisymmetric matrix, B, though the calculations are cumbersome. The first of such matrices would be the simple matrix,

$$B_1[n,m] = c_{n-1}\delta_{n,m+1} - c_n\delta_{n+1,m}, \tag{2.49}$$

which leads to the following set of evolution equations,

$$\begin{aligned} \dot{a}_n &= a_n(b_n - b_{n+1}) \\ \dot{b}_n &= 2c(a_{n-1}^2 - a_n^2). \end{aligned} \tag{2.50}$$

With $c = 1$, Eqs. (2.50) are the Toda lattice equations.

The next in the Toda hierarchy can be found by allowing the matrix B to be a penta-diagonal matrix,

$$B_2[n,m] = d_{n-2}\delta_{n-2,m} + c_{n-1}\delta_{n-1,m} - c_n\delta_{n+1,m} - d_n\delta_{n+2,m}. \tag{2.51}$$

This leads to the following set of evolution equations,

$$\begin{aligned} \dot{a}_n &= a_n(a_{n-1}^2 - a_{n+1}^2 + b_n^2 - b_{n+1}^2) \\ \dot{b}_n &= 2(a_{n-1}^2(b_{n-1} + b_n) - a_n^2(b_n + b_{n+1})). \end{aligned} \tag{2.52}$$

This higher order lattice equation contains the discrete-KdV equation as a special case, when $b_n = 0$, reduce to

$$\dot{a}_n = a_n(a_{n-1}^2 - a_{n+1}^2). \tag{2.53}$$

Defining a_n as

$$a_n = \frac{1}{2}e^{u_n/2}, \tag{2.54}$$

leads to the discrete-KdV equation,

$$\dot{u}_n = \left(e^{u_{n-1}} - e^{u_{n+1}}\right). \tag{2.55}$$

This system has been studied by Moser in [48]. The inverse scattering solution for this system was given by Manakov for the infinite line case in [45], and Kac and van Moerbeke in [33] and [34] for both the semi-infinite and periodic cases. Though little emphasis has been placed on this system, since it has no physical analog (though Manakov suggests a relation to the spectra of Langmuir oscillations in plasma [45]), realizations of the discrete-KdV system may implemented either numerically or with analog circuits making the system of potential use in the signal processing contexts discussed in this thesis. In Chapter 3, we show both a single circuit implementation of this system, along with an implementation using two Toda lattice circuits based on a relationship suggested by Kac and van Moerbeke [33] and [68].

As the number of nonlinear evolution equations solved using the inverse scattering method grew, more methods for generating hierarchies of nonlinear equations solvable by inverse scattering were developed. Ablowitz, Kaup, Newell, and Segur, developed a framework for generating large classes of nonlinear evolution equations solvable by inverse scattering [1]. This method is a generalization of the ideas of Lax, and centers around a more general form of eigenvalue problem. For further information, the reader is referred to [1], and [49] and the list of references therein.

2.A A Soliton Solution

The discrete integral equation, or GLM, is often difficult to solve, except under certain interesting conditions. Specifically, for the case when the reflection coefficient vanishes identically, $R(z,t) = 0$, the GLM reduces to a set of linear equations which can be solved by simple methods. The only eigenfunctions that result in this case are those corresponding to discrete eigenvalues.

We consider first the case when the solution has no contribution from the continuous eigenvalues, $R(z) = 0$, and has only a single term from the discrete spectrum, which we write,

$$z_0 = \pm e^{-\gamma}. \tag{2.56}$$

That z_0 can be taken as real comes from the symmetric assumption on $L(t)$. We complete the specification of the solution by selecting the initial value of the normalization coefficient, $c_0(0)$. By forming the function,

$$F(m,t) = c_0^2 z_0^m, \tag{2.57}$$

where $c_0 = c_0(0)e^{\beta_0 t}$, and $\beta_0 = \pm\sinh(\gamma)$.

The GLM equation can now be written as

$$\kappa(n,m) + c_0^2 z_0^{n+m} + c_0^2 z_0^m \sum_{n'=n+1}^{\infty} \kappa(n,n') z_0^{n'} = 0. \tag{2.58}$$

Following [15], (2.58) can be solved by assuming a solution of the form,

$$\kappa(n,m) = A_n c_0 z_0^m, \tag{2.59}$$

leading to

$$A_n = \frac{-c_0 z_0^n}{1 + e^{2\delta} z_0^{2(n+1)}}, \tag{2.60}$$

where

$$e^{\delta} = \frac{c_0(t)}{\sqrt{1 - z_0^2}} = e^{\delta_0 + \beta_0 t}. \tag{2.61}$$

Substituting (2.59) into (2.38), after some manipulations, we have

$$e^{-(q_n - q_{n-1})} - 1 = \beta_0^2 \text{sech}^2(\gamma n - \beta_0 t - \delta_0). \tag{2.62}$$

This corresponds to a single soliton solution whose direction of propagation is determined by the sign of β_0, and hence the sign of z_0.

2.B Multi-soliton Solutions

Once again, we consider the case where $R(z) = 0$, and for the discrete spectrum, we allow N eigenvalues corresponding to $z_1, \ldots, z_N$. In this case the function $F(m)$ in the GLM is given by,

$$F(m) = \sum_{j=1}^{N} c_j^2 z_j^m. \tag{2.63}$$

This results in the GLM

$$\kappa(n,m) = \sum_{j=1}^{N} c_j^2 z_j^{n+m} + \sum_{n'=n+1}^{\infty} \kappa(n,n') \sum_{j=1}^{N} c_j^2 z_j^{n'+m} = 0. \tag{2.64}$$

By assuming a solution of the form

$$\kappa(n,m) = \sum_{j=1}^{N} A_{j,n} c_j z_j^m, \tag{2.65}$$

and substituting into (2.64), for each n, after some algebra, we have a set of N linear equations for the N unknowns $A_{j,n}$,

$$\sum_{i=1}^{N} \left(\delta_{i,j} + c_i c_j \frac{(z_i z_j)^{n+1}}{1 - z_i z_j} \right) A_{i,n} = -c_j z_j^n, \quad (j = 1, \ldots, N). \tag{2.66}$$

This can be written in matrix form,

$$B(n) \begin{bmatrix} A_{1,n} \\ \vdots \\ A_{N,n} \end{bmatrix} = \begin{bmatrix} -c_1 z_1^n \\ \vdots \\ -c_N z_N^n \end{bmatrix}, \tag{2.67}$$

which lead to a direct formula for the soliton solution,

$$e^{(q_n - q_{n-1})} - 1 = \frac{|B(n)||B(n-2)|}{|B(n-1)|^2} - 1. \tag{2.68}$$

2.C Single Pole Reflection Coefficient

We now consider an example when the reflection coefficient contains a single pole in the z-plane, at $z = \gamma$, *e.g*,

$$R(z) = \frac{-c}{1 - \gamma z^{-1}}, \tag{2.69}$$

where $\gamma > 0$, and c are constants. Since the discrete spectrum contains zeros of $\alpha(z)$, there must be at least one discrete eigenvalue corresponding to the eigenfunction

$$\phi(z) \sim c\gamma^n, \quad n \to \infty. \tag{2.70}$$

From the definition of the function $F(m)$, we have

$$F(m) = c\gamma^m + \frac{1}{2\pi i} \oint \frac{-c}{1 - \gamma z^{-1}} z^{m-1} dz. \tag{2.71}$$

By the Cauchy residue theorem, the integral on the right hand side evaluates to

$$\frac{1}{2\pi i} \oint \frac{-c}{1 - \gamma z^{-1}} z^{m-1} dz = -c\gamma^m u[m], \tag{2.72}$$

where $u[m]$ is the discrete unit-step function. This results in

$$F(m) = c\gamma^m u[-m-1]. \tag{2.73}$$

The resulting GLM for this nonlinear spectrum is given by

$$\kappa(n,m) + c\gamma^{n+m} u[-(n+m)-1] + \sum_{n'=n+1}^{\infty} \kappa(n,n') c\gamma^{n'+m} u[-(n'+m)-1] = 0, \quad m > n. \tag{2.74}$$

For the diagonal terms, $n = m$, we have

$$K(n,n)^{-2} = 1 + c\gamma^{2n}u[-(2n)-1] + \sum_{n'=n+1}^{\infty} \kappa(n,n')c\gamma^{n'+n}u[-(n'+n)-1]. \quad (2.75)$$

From (2.74) we see immediately that

$$\kappa(n,m) = 0, \qquad n+m \geq 0. \quad (2.76)$$

For $n + m < 0$, we have

$$\kappa(n,m) + c\gamma^{n+m} + \sum_{n'=n+1}^{-m-1} \kappa(n,n')c\gamma^{n'+m} = 0, \qquad m > n. \quad (2.77)$$

One method of solving (2.77), is to take the first difference with respect to m, resulting in

$$\begin{aligned} \kappa(n,m+1) \;-\; & \kappa(n,m) + c\gamma^{n+m}(\gamma-1) + \\ & \left(\sum_{n'=n+1}^{-(m+1)-1} \kappa(n,n')c\gamma^{n'+m+1} - \sum_{n'=n+1}^{-m-1} \kappa(n,n')c\gamma^{n'+m} \right) = 0, \end{aligned}$$

which leads to

$$\begin{aligned} \kappa(n,m+1) \;-\; & \kappa(n,m) + c\gamma^{n+m}(\gamma-1) + \\ & \left(\sum_{n'=n+1}^{-m-1} \kappa(n,n')c\gamma^{n'+m} \right)(\gamma-1) - \kappa(n,-m-1)c = 0. \end{aligned}$$

By substitution, we arrive at

$$\kappa(n,m+1) - \kappa(n,m) + c\gamma^{n+m}(\gamma-1) + (-\kappa(n,m) - c\gamma^{n+m})(\gamma-1) - \kappa(n,-m-1)c = 0, \quad (2.78)$$

which is solved if $c = 1 - \gamma$ and $\kappa(n,m) = (\gamma-1)/\gamma$. Using these values in (2.75),

yields

$$K(n,n) = \begin{cases} 0, & n \geq 0 \\ \sqrt{\frac{\gamma}{2\gamma-1}}, & n < 0 \end{cases} \tag{2.79}$$

$$K(n,m) = \begin{cases} 0, & n+m \geq 0 \\ \frac{(\gamma-1)\sqrt{\gamma(2\gamma-1)}}{\gamma^2}, & n+m < 0. \end{cases} \tag{2.80}$$

The initial condition that led to this one pole nonlinear spectrum is given by

$$a_n = \frac{1}{2} + \frac{\sqrt{\gamma(2\gamma-1)}-\gamma}{2\gamma}\delta[n+1] \tag{2.81}$$

$$b_n = 0 + \frac{(1-\gamma)(2\gamma-1)}{2\gamma^2}\delta[n], \tag{2.82}$$

which is a localized perturbation to the lattice at rest. Even for small disturbances, $|\gamma| \ll 1$, we see that the localized perturbation gives rise to both continuous and discrete components of the spectrum. In [16], Flaschka demonstrates that any localized disturbance must give rise to both continuous and discrete components.

Chapter 3

New Electrical Analogs for Soliton Systems

Since soliton theory has its roots in mathematical physics, most of the systems studied in the literature have at least some foundation in physical systems in nature. For example, the KdV equation was developed to describe the dynamics of small amplitude surface water waves, and a large class of weakly nonlinear systems have been demonstrated to reduce to KdV in a variety of physical applications. Such systems range from ion-acoustic waves in plasma [78], to pressure waves in liquid gas bubble mixtures [57]. As a result, the predominant purpose of soliton research has been to explain physical properties of natural systems. In addition, there are several examples of man-made media that have been designed to support soliton solutions and thus exploit their robust propagation. The use of optical fiber solitons for telecommunications and of Josephson junctions for volatile memory cells are two practical examples [56, 57].

Whether its goal has been to explain natural phenomena or to support propagating solitons, this research has largely focussed on the properties of propagating solitons through these nonlinear systems. In this thesis, we take a decidedly different perspective. We view solitons as signals and consider exploiting some of their rich signal properties in a signal processing or communication context. This perspective is illustrated graphically in Fig. 3-1, where a signal containing two solitons is shown

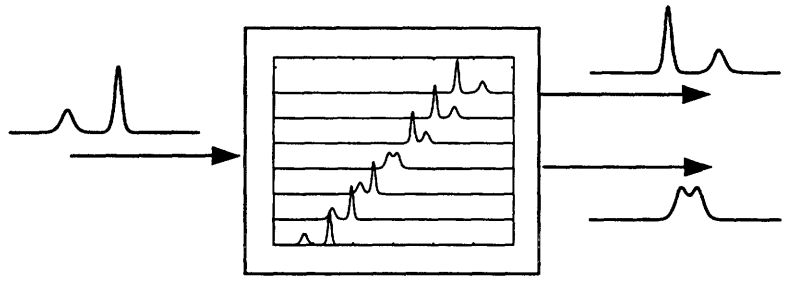

Figure 3-1: Two-soliton signal processing by a soliton system.

as an input to a soliton system which can either combine or separate the component solitons according to the evolution equations. From the "solitons-as-signals" perspective, the corresponding nonlinear evolution equations can be viewed as special purpose signal processors that are naturally suited to performing complex signal processing tasks such as signal separation or sorting. As we shall see, these systems also form an effective means of generating soliton signals.

Although many soliton systems are described by partial differential equations, the concept of performing signal processing operations with partial differential equations, or wave equations, is not new. For example, signal generation and detection in pulse compression radar systems can be accomplished using a dispersive delay line [61]. Such systems can be constructed either using bulk material, like a surface acoustic wave (SAW) device, or with a lumped element line. In either case, a signal is induced into the device and allowed to propagate according to the wave equations that describe the device. Once the signal has propagated along the device and the appropriate delay or other processing has been accomplished, the signal can be extracted from the medium. SAW devices can also be used for a variety of signal processing applications including chirp Z-transforms or digital filtering [11].

In this chapter, we study circuit implementations of two of the nonlinear evolution equations discussed in the previous chapter. The first of these is a nonlinear LC ladder network developed by Hirota and Suzuki [29]. Although this circuit serves as a useful electrical model for the Toda lattice, it is difficult to implement using standard components. We present a new circuit model for the Toda lattice based on a precise electrical analog of the exponential spring mass system. This circuit has

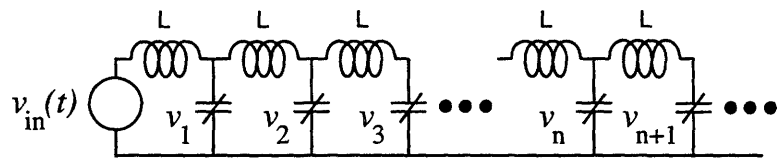

Figure 3-2: Nonlinear LC ladder circuit of Hirota and Suzuki.

been implemented in hardware using standard components and appears to be the first such circuit to display true soliton behavior. We also present a new circuit model for the discrete-KdV equation, for which there is no prior electrical or mechanical analog.

3.1 Toda Circuit Model of Hirota and Suzuki

Motivated by the work of Toda on the exponential lattice, the nonlinear LC ladder network implementation shown in Fig. 3-2 was given by Hirota and Suzuki in [29]. Rather than a direct analogy to the Toda lattice, the authors derived the functional form of the capacitance required for the LC line to be equivalent. The resulting network equations are given by

$$\frac{d^2}{dt^2}\ln\left(1+\frac{V_n(t)}{V_0}\right) = \frac{1}{LC_0V_0}(V_{n-1}(t) - 2V_n(t) + V_{n+1}(t)), \tag{3.1}$$

which is equivalent to the Toda lattice equation for the forces on the nonlinear springs given in Eq. (2.12). This amounts to an implicit mapping from force to voltage, $f_n(t) \rightarrow V_n(t)$. The capacitance required in the nonlinear LC ladder is of the form

$$C(V) = \frac{C_0V_0}{V_0+V}, \tag{3.2}$$

where V_0 and C_0 are constants representing the bias voltage and the nominal capacitance, respectively. In their implementation, varactor diodes with nonlinear capacitance

$$C(V) \approx 27(V - V_b)^{-.48}\text{pF}, \tag{3.3}$$

where V_b is a bias voltage, were used to approximate the required capacitance of Eq. (3.2).

Although the varactor diode capacitance can be biased to yield a fairly good match for small voltages, for larger voltages, the deviations from the ideal capacitance becomes apparent. Moreover, as the length of the lattice increases, the effects on any propagating solitons accumulate. The net result is that interaction between solitary waves of appreciable amplitude will not result in soliton collisions; rather such a collision will also produce a nontrivial amount of ripple [29]. Also, since the circuit is only accurate for small voltages, where the velocity difference between solitons is small, large numbers of nodes are required to bring about collisions.

After publication of their circuit [29] and subsequent publication of modulation experiments using the circuit [64, 65], several papers have appeared in the literature on a variety of related topics. In [39], Kolosick et al. analyze a similar nonlinear network. In [32] Islam, Singh and Steiglitz studied the effects of dissipation on the propagation of individual solitons as well as the interaction of pairs of solitons. They found that dissipative effects led to a decrease in amplitude and an increase in the width of solitons as they propagate through the lattice. These findings are in agreement with the numerical work of Okada, Watanabe and Tanaca in [50], whose studies showed similar effects due to parameter fluctuation in the periodic Toda lattice. In [4] Ballantyne et al. observed the Jacobian elliptic function solutions in a periodic version of the nonlinear LC line. Toda also demonstrated properties of the nonlinear line and illustrated the existence of modulated solitons, by relating the lattice to the nonlinear Schrödinger equation in [68]. Finally, Cho, Wakita and Miyigawa developed a similar nonlinear network as an equivalent circuit model for the propagation of nonlinear surface acoustic waves in thin-bar and broad-plate vibrations. They also have shown that the nonlinear LC network is an accurate model for a metallic grating waveguide and use this circuit model to explain certain nonlinearities observed in SAW devices including the generation of acoustic phase conjugate waves [10].

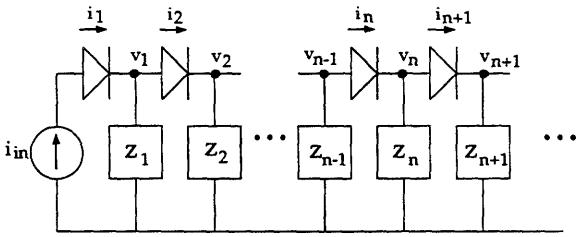

Figure 3-3: Diode ladder network.

3.2 Diode Ladder Circuit Model for Toda Lattice

Although the nonlinear ladder network realizations of the Toda lattice retain many of the properties of the ideal lattice, as suggested in Section. 3.1, the dynamics of these circuits are limited to a small range of voltages and therefore their applicability is inherently limited. In this section, we present a new circuit model that accurately matches the Toda lattice and is a direct electrical analog of the nonlinear spring mass system. If voltages v_{n-1} and v_n are applied to the terminals of a junction diode, then the current through the device is accurately modeled by

$$i_n = I_s \left(e^{(v_{n-1}-v_n)/v_t} - 1 \right), \tag{3.4}$$

where I_s is the saturation current and v_t is the thermal voltage. If we place the diodes in a ladder configuration as shown in Fig. 3-3, then the current through the n-th shunt impedance is given by

$$i_n - i_{n+1} = I_s \left(e^{(v_{n-1}-v_n)/v_t} - e^{(v_n-v_{n+1})/v_t} \right). \tag{3.5}$$

In analogy to (2.2), we see that if the shunt impedance has the following voltage-current relation

$$\frac{d^2 v_n(t)}{dt^2} = \alpha(i_n(t) - i_{n+1}(t)), \tag{3.6}$$

then the governing equations become

$$\frac{d^2 v_n(t)}{dt^2} = \alpha I_s \left(e^{(v_{n-1}(t)-v_n(t))/v_t} - e^{(v_n(t)-v_{n+1}(t))/v_t} \right), \tag{3.7}$$

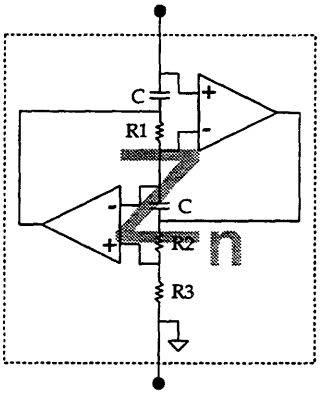

Figure 3-4: Double capacitor circuit diagram.

or,

$$\frac{d^2}{dt^2}\ln\left(1+\frac{i_n(t)}{I_s}\right)=\frac{\alpha}{v_t}(i_{n-1}(t)-2i_n(t)+i_{n+1}(t)), \tag{3.8}$$

where $i_1(t)=i_{\text{in}}(t)$. These are equivalent to the Toda lattice equations with $a/m=\alpha I_s$ and $b=1/v_t$. The required shunt impedance is often referred to as a double capacitor, which can be realized using ideal operational amplifiers in the gyrator circuit shown in Fig. 3-4, yielding the required impedance of $Z_n=\alpha/s^2=R_3/R_1R_2C^2s^2$ [30, 59].

When $i_{\text{in}}(t)$ in Fig. 3-3 is of the form

$$\begin{aligned} i_{\text{in}}(t) &= I_s\Omega^2\text{sech}^2(\gamma t), \\ \gamma &= \Omega\sqrt{I_s\alpha/v_t}, \end{aligned} \tag{3.9}$$

a single soliton is induced in the line resulting in

$$i_n(t)=I_s\Omega^2\text{sech}^2(pn-\gamma t), \tag{3.10}$$

where $\Omega=\sinh(p)$. Note that the saturation current I_s may be absorbed into the parameter Ω, yielding

$$i_n(t)=\beta^2\text{sech}^2(pn-\beta\tau), \tag{3.11}$$

where $\beta=\sqrt{I_s}\sinh(p)$, and $\tau=t\sqrt{\alpha/v_t}$. Since I_s is generally on the order of picoamps, the operating range of the circuit can be on the order of milliamps over a wide

range of values of the soliton wavenumber p. As a result, the diode ladder circuit model is very accurate over a large range of soliton wavenumbers, and is significantly more accurate than the LC circuit of Hirota and Suzuki.

Solitons of the form of Eq. (3.11) are solutions of the infinite-length Toda lattice equations. In practice, a finite-length lattice can be constructed to yield soliton solutions if the diode ladder circuit can be appropriately terminated to limit reflections. As a starting point, we consider the termination that would yield no reflections for the small signal model. This can be obtained from the impedance of the line when the diodes are replaced with their equivalent linearized resistance $R_{\text{eq}} = v_t/i_d$, where i_d is the current in the linearized diode. This results in an impedance

$$Z_{\text{in}} = \frac{R_{\text{eq}}}{2} \pm \sqrt{\frac{R_{\text{eq}}^2}{4} + \frac{R_{\text{eq}}\alpha}{s^2}}. \tag{3.12}$$

For typical component values, $\alpha \approx 10^{11}$. If R_{eq} is taken to be $v_t/25\text{mA} = 1$, then for frequencies below 1 MHz, a load impedance consisting of a 1Ω resistor and a 0.3μF capacitor approximate Eq. (3.12) well and yield negligible reflections in practice.

3.3 Circuit Simulation

The diode lattice has been simulated using realistic component models in the circuit simulation package HSPICE [47]. The diodes used are model `1n4148` with a saturation current of $I_s \approx .01\text{pA}$. Setting the operation range of the circuit to produce solitons on the order of 10mA yields a value of $p \approx 14$. To fix the time scale of the circuit, we set the pulse width of a soliton to approximately 5μs, which leads to

$$\sinh(p)\sqrt{\frac{I_s\alpha}{v_t}} \approx \frac{1}{5\mu s}, \tag{3.13}$$

or $\alpha \approx 10^{11}$. The resistor values in the double capacitor circuits can now be chosen to prevent saturation of the operational amplifiers. By calculating the transfer function from the driving point of the double capacitor to each of the operational amplifier

output voltages, we obtain

$$G_1 = \frac{R_2 + R_3}{R_3}, \tag{3.14}$$

$$G_2 = 1 + \frac{R_2 + 2R_3}{R_3} R_1 C s, \tag{3.15}$$

where G_1 and G_2 are the transfer characteristics from the voltage v_n to the outputs of the top and bottom amplifiers, respectively. In order to select a valid set of resistor values, the range of voltages seen at the top of the double capacitor is needed. For a single soliton solution, the closed form solution for the voltage is

$$v_n(t) = v_t \ln\left\{\cosh\left(p(n) - \beta t\sqrt{\alpha/v_t}\right)\right\} - v_t \ln\left\{\cosh\left(p(n+1) - \beta t\sqrt{\alpha/v_t}\right)\right\} + \text{const.} \tag{3.16}$$

The limiting voltage in Eq. (3.16) is given by

$$\lim_{t\to\infty} v_n(t) = v_t p + \text{constant}, \tag{3.17}$$

and

$$\lim_{t\to-\infty} v_n(t) = -v_t p + \text{constant}. \tag{3.18}$$

Selecting the constants such that $v_n(-\infty) = 0$, gives

$$\lim_{t\to\infty} v_n(t) = 2v_t p. \tag{3.19}$$

For $p \approx 14$, this leads to a final voltage amplitude on the order of $v_n \approx 0.75$ volts. For each soliton that passes through a given node, the voltage on the double capacitor will increase by $2v_t p$. In order to keep the amplifiers from saturating due to a single soliton, G_1 and G_2 must remain less than about a factor of 10. Since each soliton that passes through a given node will result in a similar voltage increase, we would like these gains to be as small as possible to avoid saturation. However, it is also important to maintain voltages levels in the double capacitors that are above the noise level for the circuit, which implies that these gains cannot be too small. A reasonable balance can be obtained by setting $R_2 \approx R_3$, and $R_1 \ll 1/C$ which can be met by selecting

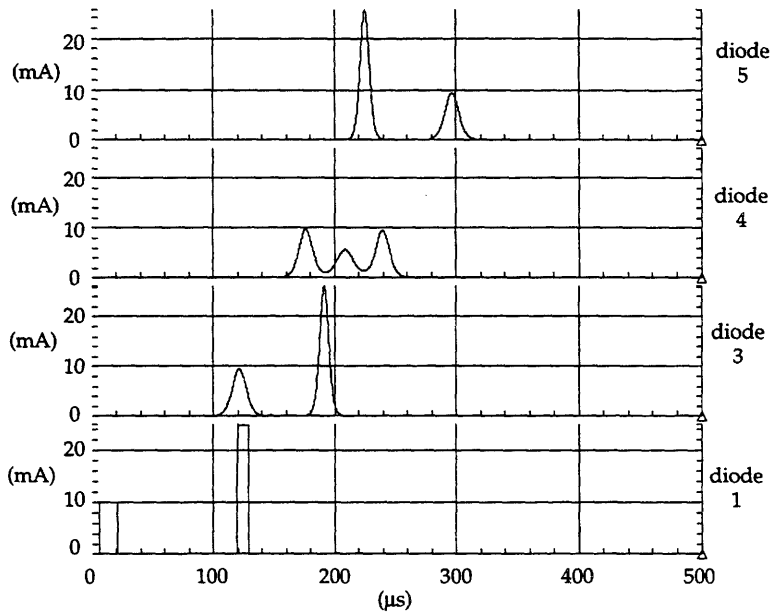

Figure 3-5: HSPICE simulation of the evolution of a two-soliton signal through the diode lattice. Each horizontal trace shows the current through one of the diodes 1, 3, 4 and 5.

$R_1 = R_2 = R_3 = 1\text{k}\Omega$ and $C = .01\mu\text{F}$. These values permit soliton pulse widths of about 5μs with amplitudes of about 10mA and with voltages at the amplifier outputs within the double capacitors on the order of 1 Volt. The double capacitors use precision LT1028A operational amplifiers with a gain bandwidth product of about 65 MHz. Shown in Fig. 3-5 is an HSPICE simulation with two solitons propagating down a length 10 Toda chain.

A significant difference between soliton solutions to this circuit and those of the nonlinear LC line lies in the scale of operation. Due to biasing constraints for the LC line, solitons were generally restricted to a small range of wavenumbers in the neighborhood of $p \approx 1$. Over this range, the propagation velocity of the solitons, which is proportional to $\sinh(p)/p$ does not vary greatly between solitons of different wavenumbers. This led to the use of chains with hundreds of nodes in order to demonstrate soliton collisions. The diode ladder circuit, however, can operate in the range $p \approx 14$ for solitons with amplitudes in the mA range. Due to the exponential nature of the sinh function, the velocities of solitons with slightly different amplitudes for currents in the mA range yield exponentially different velocities. This enables soliton

collisions to take place with far fewer nodes than with the nonlinear LC network.

As illustrated in the bottom trace of Fig. 3-5, a soliton can be generated by driving the circuit with a square pulse of approximately the same area as the desired soliton. As seen on the third node in the lattice, once the soliton is excited, the non-soliton components are quickly stripped away. For the example in the figure, a small pulse followed by a larger pulse are used to drive the circuit giving rise to a small soliton followed by a larger amplitude soliton. This property has been demonstrated experimentally for a number of soliton systems, c.f. [23] for the nonlinear Schrödinger equation and [29] for the Toda lattice. It has been shown theoretically for KdV, c.f. [1] and [12], that practically any smooth, localized disturbance of the proper area will result in a soliton with that area, if such a solution exists. Multi-soliton signals could also be generated by using inverse scattering techniques to determine a drive signal $i_{\text{in}}(t)$ that would give rise to the desired solitons. However, this method requires more complex drive circuitry than simple pulse generators.

Note that as the faster soliton overtakes the slower as viewed on the fourth node in Fig. 3-5, the joint signal amplitude is significantly less than the sum of the individual amplitudes. Also, the signal shape changes significantly during the nonlinear interaction. These two effects will impact both the energy of multi-soliton signals and the ability to recover their signal parameters.

3.4 Circuit Implementation

To perform real-time experimentation and to verify the operation of the model using standard components, the diode ladder circuit has been implemented in hardware. Real-time implementation also enables rapid testing of soliton processing techniques and enables measurements of actual circuit noise levels. Such noise measurements permit experimental verification of some of the theoretical results we obtain in Chap. 5 concerning system noise.

In the construction of the circuit, there were several practical matters to be dealt with. First, the diode ladder is driven by a current source. In our implementation

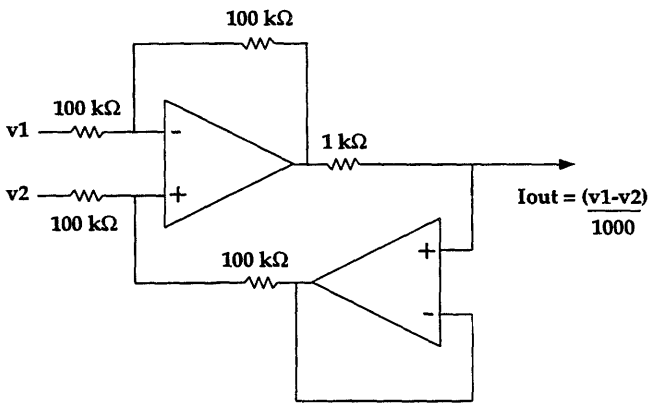

Figure 3-6: Precision bipolar current source.

the precision bipolarity current source shown in Fig. 3-6 taken from [30] was used. When implemented with the low noise LT1028A operational amplifiers, this circuit provides a reliable, accurate current source, with low leakage. In practice, leakage current turns out to be a problem, since the double capacitor circuits are marginally stable. The node voltages are double integrators of their current and therefore any excess current will lead to large deviations in the node voltages and corrupt soliton propagation.

In addition to the voltage deviations from leakage current, each soliton that passes through a node on the ladder contributes a net voltage increase of $2v_tp$ or approximately 1 Volt. Therefore a signal containing three solitons will leave the node with a net voltage increase of nearly 3 volts. If several such signals are processed by this circuit, the operational amplifiers in the double capacitors will eventually saturate. This problem can be overcome by resetting the node voltages after each signal has been processed by the circuit using analog switches as shown in Fig. 3-7.

Finally, since the solitons are present in the diode ladder circuit as current waveforms, there must be an adequate means of measuring the current through the diodes without significantly affecting the dynamics of the circuit. This can be accomplished by placing a small resistance in series with each diode in the lattice a shown in Fig. 3-7. The current through the diodes can then be observed by measuring the voltage drop across each of the resistors with a differential amplifier.

A hardware implementation of the diode ladder circuit with twelve nodes is shown

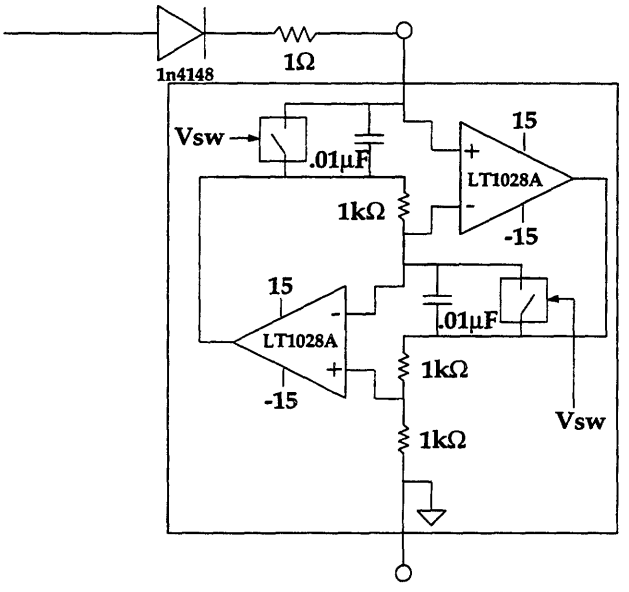

Figure 3-7: Diagram for the double capacitors used in the diode ladder circuit. Analog switches, placed in parallel with the capacitors, are used to reset the circuit after each processed signal.

in Fig. 3-8. Each of the three rightmost bread boards in the figure contains four stages of diodes, series resistors, and double capacitors. The left most bread board contains pulse-generation circuitry, and the remaining bread board contains the voltage-controlled current source. A two-soliton signal generated by this circuit is shown on the oscilloscope traces in Fig. 3-9. The bottom trace in the figure corresponds to the input current to the circuit, and the remaining traces, from bottom to top, show the current through the second, third and fourth diodes in the lattice.

For a more complex example, a simple waveform consisting of three component soliton signals, periodically repeated, was used to drive the diode ladder circuit with several additional stages. Using a digital oscilloscope to sample real-time circuit waveforms, measurements of the diode currents were transferred to a computer, and then plotted online. The measured currents through each of the diodes are shown in Fig. 3-10. The time axis of the figure is such that $t = 0$ corresponds to the beginning of a period. The largest amplitude soliton measures 17mA, with a pulse width of 82μs at the first node. As measured on the fifteenth node, the amplitude is 14mA with pulse width of 86μs. This decay in the soliton amplitude is on the order of 1% per node

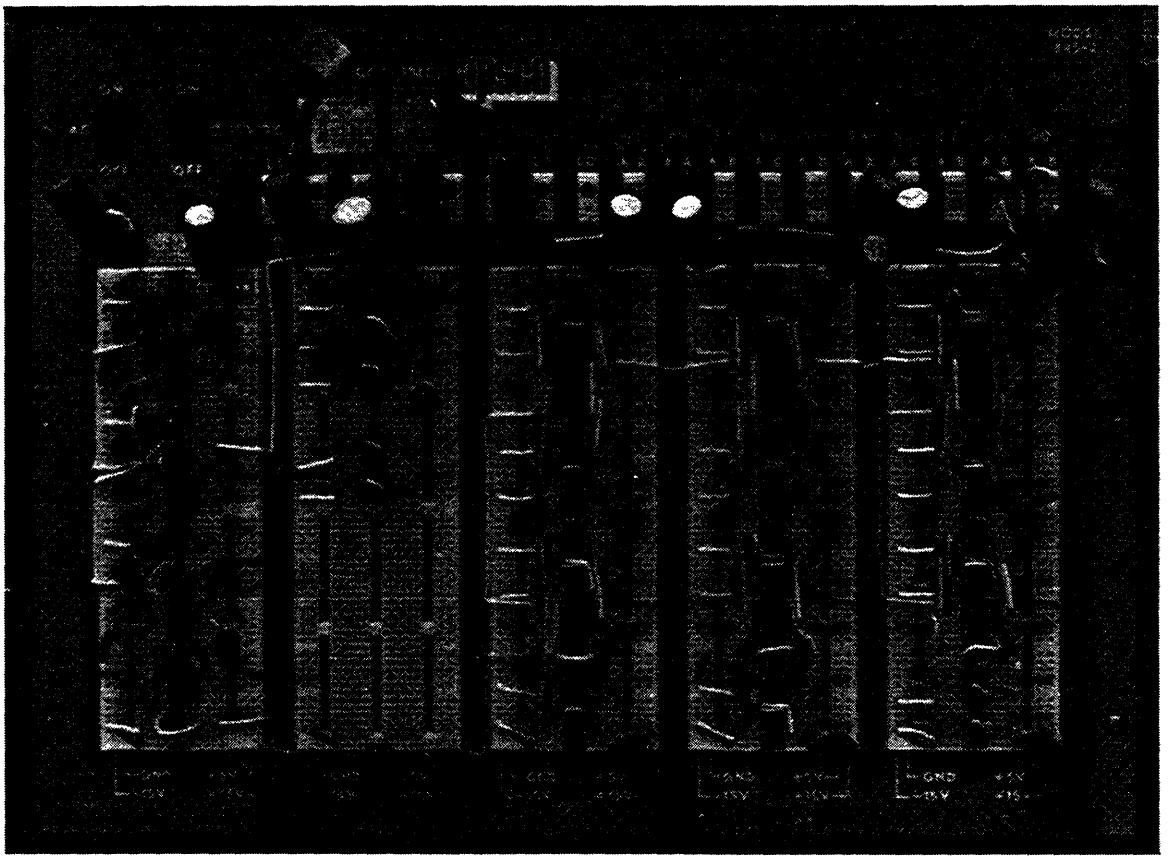

Figure 3-8: Hardware implementation of the diode ladder circuit. The first column from the left contains the pulse-generation circuitry; the second contains the voltage-controlled current source; each of the last three contains four stages of diodes, series resistors and double capacitors.

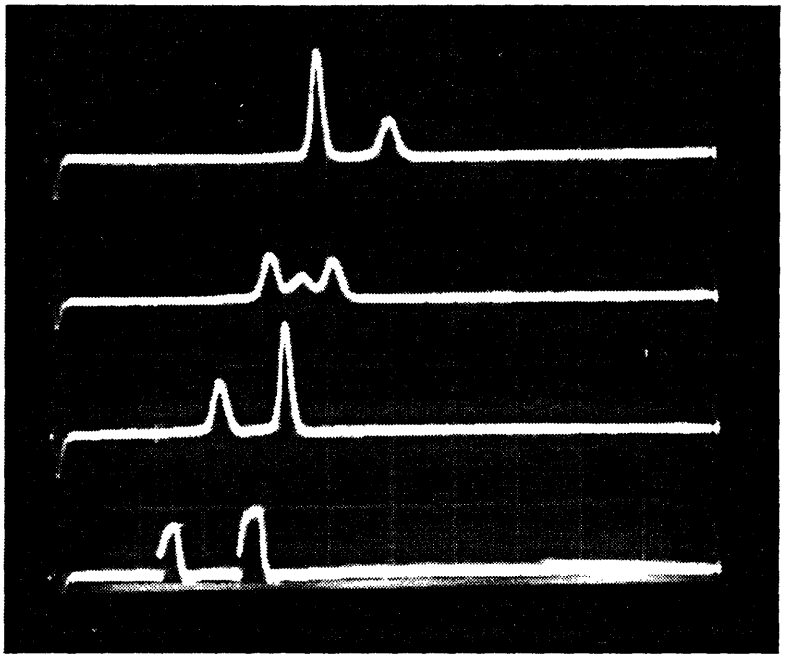

Figure 3-9: Oscilloscope traces for two solitons in the diode ladder circuit. The traces correspond to the currents in the first four diodes.

and may have several causes in addition to deviations of the circuit components from their idealized models. Specifically, as stated in [32], dissipative effects in the lattice are contrary to the conservative nature of the Toda lattice, and will necessarily lead to energy loss. Also, as shown in [50], inter-node parameter fluctuations can lead to dispersion, causing decay as well as additional non-soliton components. This leads to a change in the soliton parameter β, resulting in a decrease in soliton velocity as they propagate through the lattice. In the figure, there is also a small spike that appears in each of the diode currents near the time $t = -1$ms. This results from the reset signal, V_{sw}, propagating down the lattice and resetting adjacent double capacitors at slightly different times.

3.5 Circuit Model for Discrete-KdV

The discrete-KdV equation (dKdV), sometimes referred to as the nonlinear ladder equations [1], or the KM system (Kac and vanMoerbeke) [67] is governed by the

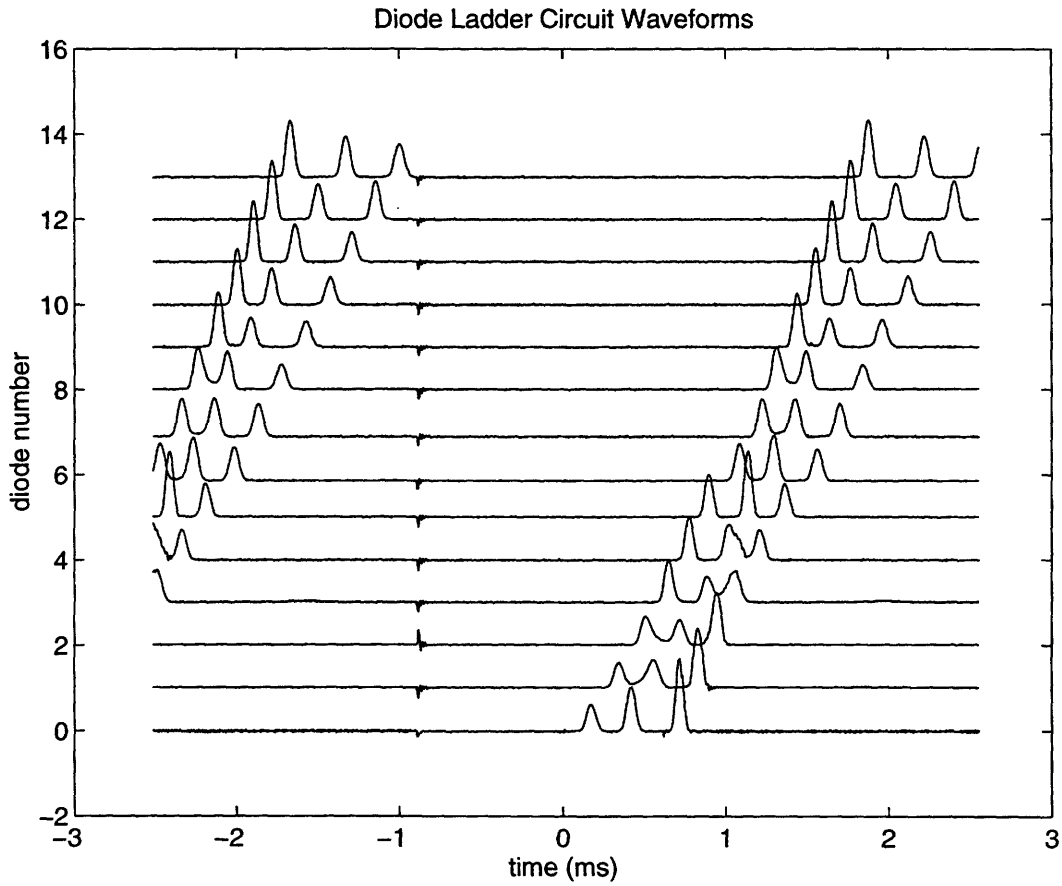

Figure 3-10: Diode currents measured from the diode ladder circuit in operation. The input signal consists of three square pulses of different areas. The spike that appears in the figure near $t = -1$ ms is a result of the signal that resets the lattice.

equations,

$$\dot{u}_n(t) = e^{u_{n-1}(t)} - e^{u_{n+1}(t)}. \tag{3.20}$$

This equation is first order in time, which makes the dynamics less complex than the Toda lattice, yet as evidenced in Sec. 2.2, the inverse scattering framework is very similar. Although much of the theory for this nonlinear system has been developed with the theory for the Toda lattice, the discrete-KdV equations are generally ignored since there is no clear physical analog of these equations. However, there is special relationship known as a Bäcklund transformation which provides a connection between this system and the Toda lattice [67, 33, 34].

Given our success with the Toda lattice using a ladder comprising diodes and double capacitors and the similarity between (3.20) and (3.7), we first consider a ladder of diodes with shunt capacitors. A similar analysis leads to the following set of equations

$$\frac{dv_n(t)}{dt} = \frac{I_s}{C}\left(e^{(v_{n-1}(t)-v_n(t))/v_t} - e^{(v_n(t)-v_{n+1}(t))/v_t}\right), \tag{3.21}$$

which look deceptively similar to (3.20). However, there is no apparent means of decoupling the node voltage, $v_n(t)$ from $v_{n+1}(t)$ and $v_{n-1}(t)$ as would be required. This similarity is not a mere coincidence and actually leads to a realization of the discrete-KdV equation using two Toda circuits. Following [33] and [67], let

$$u_n \to -R_n, \qquad t \to -t, \tag{3.22}$$

which transforms (3.20) to

$$\dot{R}_n = e^{-R_{n-1}} - e^{-R_{n+1}}. \tag{3.23}$$

Letting $q_n = R_n + R_{n+1}$, then q_n satisfies

$$\ddot{q}_n = 2e^{-q_n} - e^{-q_{n-2}} - e^{q_{n+2}}. \tag{3.24}$$

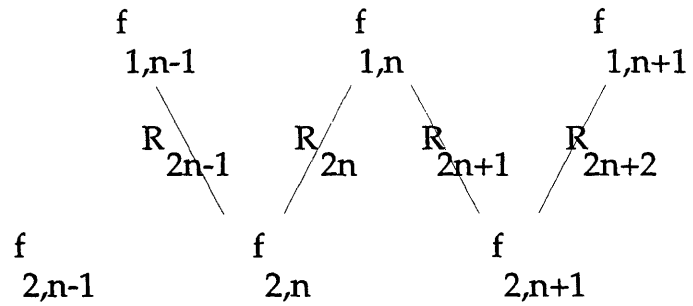

Figure 3-11: Illustration of the relationship between two adjacent Toda lattices, $f_{i,n}, i = 1, 2$ and the discrete-KdV equation. This process suggests a possible implementation of the dKdV equation using two adjacent Toda lattice circuits.

Taking every other term, i.e. $q_{1,n} = q_{2n}, q_{2,n} = q_{2n+1}$, we have

$$\ddot{q}_{i,n} = 2e^{-q_{i,n}} - e^{-q_{i,n-1}} - e^{q_{i,n+1}}, \quad i = 1, 2. \tag{3.25}$$

Setting $q_{i,n} = -\ln(1 + f_{i,n})$, yields

$$\frac{d^2 \ln(1 + f_{i,n})}{dt^2} = f_{i,n-1} - 2f_{i,n} + f_{i,n+1} \quad i = 1, 2, \tag{3.26}$$

which are each a Toda lattice equation. The physical interpretation of this transformation is the following: if $f_{1,n}$ and $f_{2,n}$ are each defined within a different Toda lattice, then R_n defined by $R_{2n} = f_{1,n} - f_{2,n}$, $R_{2n+1} = f_{2,n+1} - f_{1,n}$ satisfies the discrete-KdV equation in the form (3.23). This process is illustrated in Fig. 3-11. Although a dKdV circuit could be so constructed, the resulting circuitry would be twice as complex as the Toda circuit. A much simpler implementation can be found by maintaining the aspects of the diode ladder that are useful, namely the exponential current relationship of the diodes, while removing the aspects which are troublesome, viz. the ladder interconnections.

Since the desired equations are first order, we use capacitor voltages for state variables, i.e. $v_n(t)$ will be the voltage on the n-th capacitor. Rather than assembling the capacitors in a ladder network, we consider a collection of nodes with nearest neighbor coupling as shown in Fig. 3-12. Each node is maintains a node voltage, $v_n(t)$, and also maintains a voltage that is proportional to $e^{v_n(t)}$, which can be accomplished

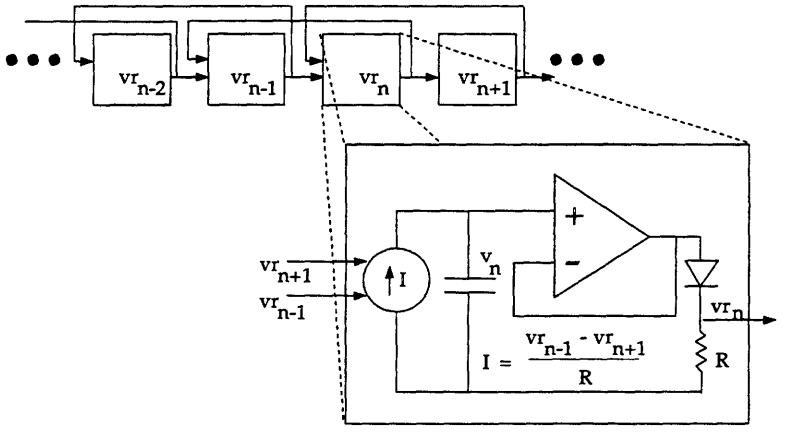

Figure 3-12: Collection of nodes for the discrete-KdV circuit.

with a voltage follower and a diode as shown in Fig. 3-12. Since the voltage follower mirrors the voltage on the capacitor, neglecting the voltage drop from the resistor, the voltage across the diode is approximately $v_n(t)$. Hence the current through the diode is $i_n(t) \approx I_s(\exp(v_n(t)/v_t) - 1)$, where v_t is the thermal voltage. Since each node maintains a node voltage along with a voltage proportional to $\exp(v_n(t))$, all that remains is to construct a current source that is proportional to the difference in the exponential reference voltages of the neighboring nodes. If a current source is used to drive the capacitor as shown in Fig. 3-12, then the node voltage, $v_n(t)$, is governed by

$$\dot{v}_n(t) = \frac{I_s}{C}\left(e^{v_{n-1}(t)/v_t} - e^{v_{n+1}(t)/v_t}\right). \tag{3.27}$$

The required differential voltage controlled current source can be the same as the one that drives the Toda ladder circuit, shown in Fig. 3-6. Therefore, for a collection of nodes such as those in Fig. 3-12, the node capacitor voltages are governed by the discrete-KdV equation.

The time scale of the circuit can be set by proper choice of the ratio I_s/C. Specifically, if $I_s = \alpha v_t C$, the node voltage satisfies,

$$\frac{dv_n(\tau)/v_t}{d\tau} = \left(e^{v_{n-1}(\tau)/v_t} - e^{v_{n+1}(\tau)/v_t}\right), \tag{3.28}$$

where $\tau = t/\alpha$. Thus $v_n(t)/v_t$ satisfies the discrete-KdV equation on a time-scale t/α.

An HSPICE simulation of this circuit indeed verifies the propagation of dKdV solitons. Since this circuit is first order, the state of the system is completely specified by the capacitor voltages. Rather than processing continuous-time signals as with the Toda lattice system, we can use this system to process discrete-time solitons as specified by v_n. For the purposes of simulation, we consider the periodic dKdV equation by setting $v_{n+1}(t) = v_0(t)$ and initializing the system with the discrete-time signal corresponding to a listing of node capacitor voltages. We can place a multi-soliton solution in the circuit using inverse scattering techniques to construct the initial voltage profile. The single soliton solution to the dKdV system is given by

$$v_n(t) = \ln\left(\frac{\cosh(\gamma\,(n-2) - \beta\,t)\cosh(\gamma\,(n+1) - \beta\,t)}{\cosh(\gamma\,(n-1) - \beta\,t)\cosh(\gamma\,n - \beta\,t)}\right) \tag{3.29}$$

where $\beta = \sinh(2\gamma)$. Shown in Fig. 3-13, is the result of an HSPICE simulation of the circuit with 30 nodes in a loop configuration, each with $2nF$ capacitors and diodes with a saturation current chosen to be $I_s = v_t \times 2\text{nA}$. Thus, the time scale of the circuit is unity, $\alpha = 1$. The initial condition was set such that a soliton with $\gamma_1 = 2.5$ was placed on node 0 and a second soliton with $\gamma_2 = 2$ was placed on node 10. As with the diode ladder implementation of the Toda circuit, this circuit model is very accurate, and can support a wide range of soliton wavenumbers. Discrete-time soliton signals could be used as an initial condition to the dKdV lattice and then be processed by their evolution in the circuit.

3.6 Further Considerations

In this chapter we have illustrated three circuits which can be used to both generate and to process soliton signals. The first of the three, developed by Hirota and Suzuki, demonstrated the feasibility of using such nonlinear circuits as analogs of soliton systems. Their results [29, 64, 65], along with the experimental work of Toda in [68], Scott in [56, 57], and a host of others illustrate the potential for development of a variety of analog hardware for soliton processing techniques.

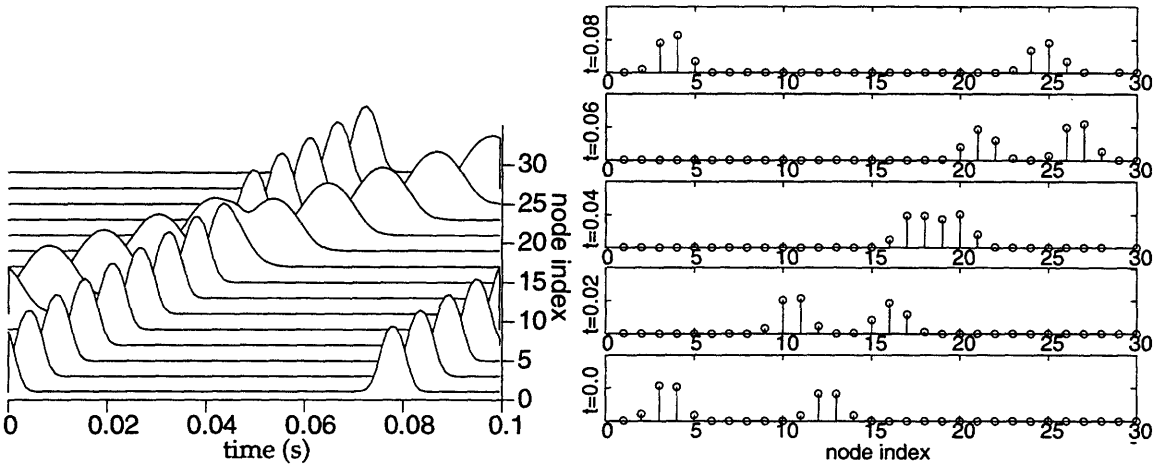

Figure 3-13: To the left, the normalized node capacitor voltages, $v_n(t)/v_t$ for each node is shown as a function of time. To the right, the state of the circuit is shown as a function of node index for five different sample times. The bottom trace in the figure corresponds to the initial condition.

We then presented a new diode ladder circuit which models the Toda lattice more accurately than the nonlinear LC circuit and can be operated over a larger range of soliton amplitudes. Increasing the range of operation has a direct impact on the complexity of the processing hardware that would be used, for example, to separate multi-soliton signals. Specifically, the number of nodes required (length of the lattice) is significantly reduced. A real-time implementation of this circuit was constructed in hardware using standard components which appears to be the first such circuit to experimentally demonstrate true soliton collisions. It remains to be seen whether or not the diode ladder circuit can operate without the need for periodic resetting of the double capacitor sub-circuits. The resolution of this issue might avail the diode ladder circuit to a greater range of potential processing techniques and is therefore an interesting avenue for future work.

Finally, we presented a new circuit which implements the discrete-KdV equation, for which no other circuit models have previously been presented. Experiments using HSPICE demonstrate the viability of the circuit model for a variety of discrete-time soliton processing techniques. As shown, the dKdV circuit is placed in a loop configuration and the circuit iterates forward from an initial condition. This circuit can also process continuous signals in an analogous manner to the Toda lattice. However,

the problem of properly terminating the dKdV circuit differs from its Toda lattice counterpart due to the more complex circuit topology.

The circuits developed in this chapter can be used to generate multi-soliton signals as well as perform a variety of processing operations. For example multiple solitons can be multiplexed by using a signal with solitons arranged in increasing amplitude as input, allowing them to collide, and then extracting the signal from the circuit. Similarly the separation of multiple overlapping solitons could be achieved by allowing them to propagate at different velocities and again extracting the signal after separation. Each of these otherwise complex nonlinear tasks can be completed naturally by the dynamics of the nonlinear systems. Such systems also indicate the viability of analog hardware implementations of a large class of nonlinear systems exhibiting soliton behavior. Additionally, many of the soliton processing techniques could be mapped onto the soliton or soliton-like behavior that has been exhibited by a large class of cellular automata [1, 7, 53, 62, 63, 66], for which many fast algorithms [52] and hardware [46, 70, 71] have been developed.

Chapter 4

Communication with Soliton Signals

Many traditional communication systems use a form of sinusoidal carrier modulation, such as amplitude modulation (AM) or frequency modulation (FM) to transmit a message-bearing signal over a physical channel. The reliance upon sinusoidal signals is due in part to the simplicity with which such signals can be generated and processed using linear systems. More importantly, information contained in sinusoidal signals with different frequencies can easily be separated using linear systems or Fourier techniques. This has led to the development of standards and regulation of the sinusoidal composition of signals transmitted electromagnetically based on the allocation of separate bands of frequencies to different users.

The complex dynamic structure of soliton signals and the ease with which these signals can be both generated and processed with analog circuitry renders them potentially applicable in the broad context of communication in an analogous manner to sinusoidal signals. We have also seen that either by using analog circuitry or the inverse scattering transform, the individual solitons in a multi-soliton signal can also be easily separated. In this chapter we will present a paradigm for modulation of information on soliton carriers and illustrate the potential applicability of such a framework to multi-user communication. Specifically, we consider a scenario in which solitons are used as carrier waveforms in an amplitude- or position-modulation

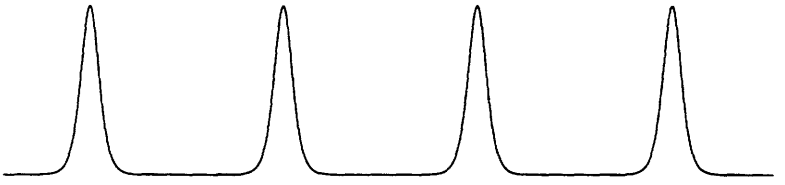

Figure 4-1: A soliton carrier signal for the Toda lattice.

communication system using the soliton systems to perform signal multiplexing and demultiplexing. In this context, we will show that the signal amplitude reduction that occurs during soliton interaction may provide increased energy efficiency, making such techniques particularly attractive for a broad range communication contexts over power-limited channels including portable wireless communication, satellite or deep-space applications.

4.1 Soliton Modulation

Although the mechanisms for the generation and processing of soliton signals differs, many standard sinusoidal carrier modulation techniques could be implemented using soliton carriers. In this chapter, we define a soliton carrier as a signal which is composed of a periodically-repeated single soliton solution to a particular nonlinear system. For example, a soliton carrier signal for the Toda lattice is shown in Fig. 4-1 and can be written,

$$f_n(t) = \frac{m}{ab}\left\{\sum_{\ell=-\infty}^{\infty} \beta^2 \mathrm{sech}^2\left[\alpha(n-\lambda\ell) - \beta t\right] - 2\beta\nu\right\}, \tag{4.1}$$

where α and β are parameters related to the elliptic functions defined in Chap 2, Eq. (2.11). In addition to the Toda lattice, periodic soliton solutions of many soliton systems can be written in terms of Jacobian elliptic functions as in Eq. (2.10).

As a soliton carrier such as that for the Toda lattice in Fig. 4-1 is generated, a simple amplitude modulation scheme could be devised by modulating the soliton parameter β, since the amplitude of the Toda lattice solitons is proportional to β^2. Note that the pulse-width also changes with β, giving rise to a scale modulation

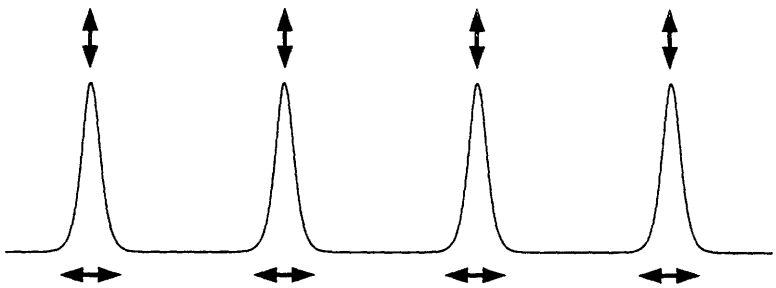

Figure 4-2: Modulating the relative amplitude or position of soliton carrier signal for the Toda lattice.

rather than a pure amplitude modulation. Similarly, an analog of FM/PM or pulse-position modulation could be achieved by modulating the relative position of each soliton in a given period, as shown in Fig. 4-2. Although the mechanisms developed for sinusoidal carrier demodulation would also have to be adapted, at least from a signal generation viewpoint, a variety of sinusoidal carrier modulation techniques can be directly mapped onto soliton carriers. We have again focused on the Toda lattice as an example, however, parameter modulation of soliton carriers could be applied to the large class of soliton signals that can be both generated and processed by solvable nonlinear systems.

4.2 Soliton Multiplexing

As a simple extension, the soliton modulation techniques described in Section 4.1 can be generalized to include multiple solitons in each period and accommodate multiple information-bearing signals, as shown in Fig. 4-3 for a four soliton example using the Toda lattice circuits developed in Chap. 3. In the figure, a signal is generated as a periodically-repeated train of four solitons of increasing amplitude. The relative amplitudes or positions of each of the component solitons could be independently modulated about their nominal values to accommodate multiple information signals in a single soliton carrier.

The nominal soliton amplitudes can be appropriately chosen so that as this signal is processed by the diode ladder circuit, the larger amplitude solitons propagate faster than the smaller solitons, and each of the solitons can become nonlinearly superim-

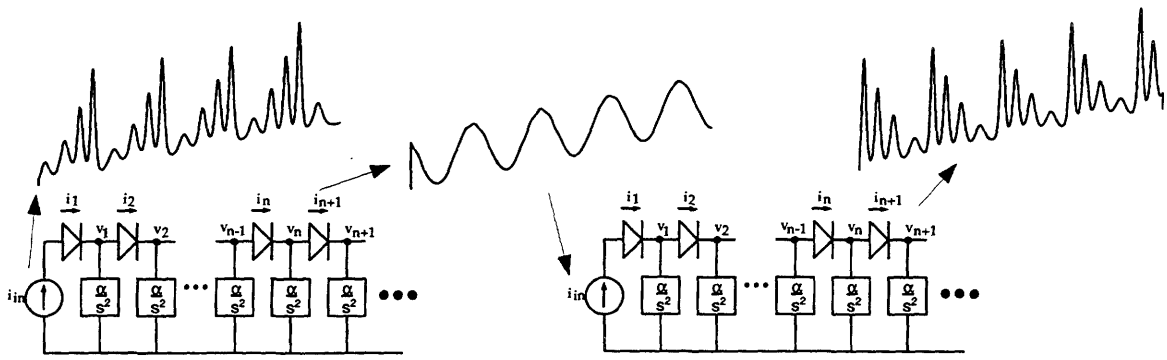

Figure 4-3: Multiplexing of a four soliton solution to the Toda lattice.

posed as viewed at a given node in the circuit. From an input-output perspective, the diode ladder circuit can be used to make each of the solitons coincidental in time. As indicated in the figure, this packetized soliton carrier could then be transmitted over a communication channel. At the receiver, the multi-soliton signal can be processed with an identical diode ladder circuit which is naturally-suited to perform the non-linear signal separation required to demultiplex the multiple soliton carriers. As the larger amplitude solitons emerge before the smaller, after a given number of nodes, the original multi-soliton carrier re-emerges from the receiver in amplitude-reversed order. At this point, each of the component soliton carriers could be demodulated to recover the individual message signals it contains. Aside from a packetization of the component solitons, we will see that multiplexing the soliton carriers in this fashion can lead to an increased energy efficiency for such carrier modulation schemes.

Since the Toda lattice equations are symmetric with respect to time and node index, solitons can propagate in either direction. As a result, a single diode ladder implementation could be used as both a modulator and demodulator simultaneously, as shown in Fig. 4-4. From the figure at time $t = 0$, a signal composed of three solitons is multiplexed by the system, by propagating the separated solitons along the lattice from node 0 to node 35. The resulting multiplexed signal can be extracted from node 35 around $t = 30$. Also at $t = 0$, a received signal composed of three multiplexed solitons is input to the system at node 35. These solitons are induced in the reverse direction, allowing them to separate by the time they arrive at node 0 around $t = 30$. Since the forward propagating solitons correspond to positive eigenvalues in

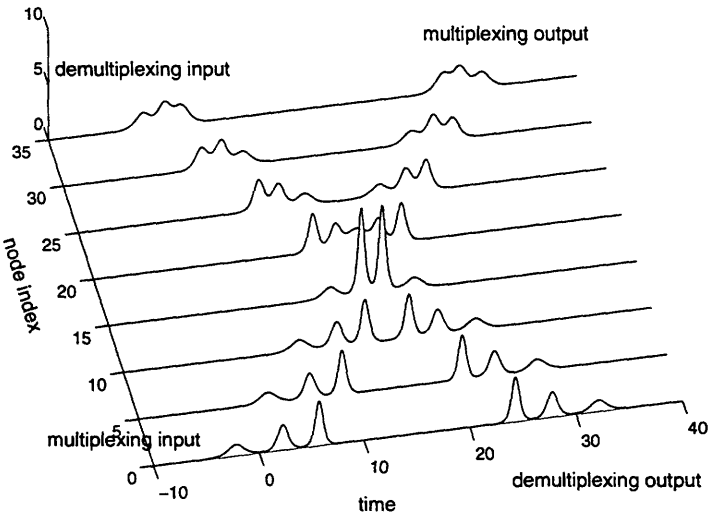

Figure 4-4: Toda lattice response to an outgoing signal at node 0 and to a received signal at node 35, each with three component solitons. The solitons that are input at node 0 are multiplexed by the system, as viewed on node 35. The solitons that are input to node 35, propagate in the reverse direction, and are demultiplexed by the system, as viewed on node 0.

the inverse scattering transform and the reverse propagating solitons have negative eigenvalues, the dynamics of the two signals will be completely decoupled. The ability to propagate solitons in both directions is a property shared by many soliton systems with dynamics governed by differential equations that are second order in time.

Although presented in the context of the Toda lattice equation, the soliton modulation techniques presented are applicable to a variety of soliton systems, both in discrete- and continuous-time. For example, a similar technique can be used for modulation of the discrete-time solitons generated by the discrete-KdV equation. Both the soliton amplitude and relative position for a multi-soliton solution of the dKdV equation could be independently modulated when the solitons are well-separated in time. This multi-soliton signal could then be used as the initial condition to a dKdV circuit developed in Chap. 3, and then iterated forward in time until the component solitons were mutually overlapping. This multiplexed signal could be transmitted to a receiver where identical dKdV circuitry is used to demultiplex the component solitons.

4.3 Spectrum of Toda Lattice Solitons

To draw comparisons with sinusoidal AM and FM modulation, we consider the Fourier spectrum of a periodic single soliton carrier for the Toda lattice. We consider a solution of the form of Eq. (4.1) for a fixed node,

$$f(t) = \sum_{\ell=-\infty}^{\infty} \beta^2 \mathrm{sech}^2(\beta(t - \ell T)) - 2\beta, \tag{4.2}$$

where T is the period of one message frame. The Fourier transform of a single soliton (or one frame) is given by[13]

$$\begin{aligned} F(\omega) &= \int_{-\infty}^{\infty} v(t) e^{-j\omega t} dt \\ &= \frac{\pi\omega}{\sinh(\pi\omega/2\beta)} - 2\pi\beta\delta(\omega). \end{aligned} \tag{4.3}$$

In the small amplitude limit, the periodic traveling wave solutions to the Toda lattice approach sinusoids. To see that this is reasonable, we consider the Fourier transform of the periodic soliton, Eq. (4.2), which, ignoring effects due to time aliasing, is given by

$$F(\omega) = \sum_{\ell=-\infty, \ell\neq 0}^{\infty} \frac{\pi\omega}{\sinh(\pi\omega/2\beta)} \delta(\omega - \ell\omega_c), \tag{4.4}$$

where $\omega_c = 2\pi/T$. Since the Fourier series coefficients fall off exponentially in frequency, for small amplitudes ($\beta \ll \omega_c$),

$$F(\omega) \approx 4\pi\beta\delta(\omega - \omega_c) + 4\pi\beta\delta(\omega + \omega_c), \tag{4.5}$$

which is in line with the asymptotic sinusoidal form of $f(t)$.

We now consider an AM modulation with a single soliton waveform,

$$f_{AM}(t) = f(t)(1 + m(t)), \tag{4.6}$$

where $m(t)$ is the message signal. We also assume that the modulation depth is small, i.e. the bandwidth of $m(t)$ is much smaller than ω_c. To illustrate the resulting

spectrum, we set $m(t) = m\cos(\omega_m t)$, which yields

$$F_{AM}(\omega) = \sum_{\ell=-\infty,\ell\neq 0}^{\infty} \frac{\pi\omega}{\sinh(\pi\omega/2\beta)}(\delta(\omega-\ell\omega_c)+\frac{1}{2}\delta(\omega-\ell\omega_c+\omega_m)+\frac{1}{2}\delta(\omega-\ell\omega_c-\omega_m)). \tag{4.7}$$

Again, making the small amplitude approximation ($\beta \ll \omega_c$), the positive half of the spectrum is given by

$$F_+(\omega) \approx 4\pi\beta\delta(\omega-\omega_c) + 2\pi\beta\delta(\omega-(\omega_c-\omega_m)) + 2\pi\beta\delta(\omega-(\omega_c+\omega_m)), \tag{4.8}$$

which is the same as the spectrum for a sinusoidal AM modulation.

In analogy to FM, we consider a soliton carrier with the relative position of the component solitons modulated,

$$f_{FM}(t) = f(t + m\cos(\omega_m t)), \tag{4.9}$$

again assuming that $\omega_m \ll \omega_c$. This expression can be expanded using a trigonometric identity, to

$$f_{FM}(t) = \sum_{\ell=-\infty}^{\infty} \frac{\beta^2}{(\cosh(\beta\tau_\ell)\cosh(\beta m\cos(\omega_m t)) + \sinh(\beta\tau_\ell)\sinh(\beta m\cos(\omega_m t)))^2} - 2\beta, \tag{4.10}$$

where $\tau_\ell = t - \ell T$. Making the assumption that $m \ll T$, this expression can be approximated to first order in m by

$$\begin{aligned} f_{FM}(t) &\approx \sum_{\ell=-\infty}^{\infty} \frac{\beta^2}{\cosh^2(\beta\tau_\ell) + 2\cosh(\beta\tau_\ell)\sinh(\beta\tau_\ell)m\cos(\omega_m t)} - 2\beta \\ &\approx \sum_{\ell=-\infty}^{\infty} \beta^2\mathrm{sech}^2(\beta\tau_\ell) - 2\beta^2\mathrm{sech}^2(\beta\tau_\ell)\tanh(\beta\tau_\ell)m\cos(\omega_m t) - 2\beta \end{aligned} \tag{4.11}$$

Noting that

$$\frac{d}{dt}\beta^2\mathrm{sech}^2(\beta t) = -2\beta^3\mathrm{sech}^2(\beta t)\tanh(\beta t), \tag{4.12}$$

we obtain the approximate Fourier transform of $f_{FM}(t)$ as

$$F_{FM}(\omega) \approx \frac{\pi\omega}{\sinh(\pi\omega/2\beta)} + \frac{j\pi(\omega-\omega_m)^2/2}{\sinh(\pi(\omega-\omega_m)/2\beta)} + \frac{j\pi(\omega+\omega_m)^2/2}{\sinh(\pi(\omega+\omega_m)/2\beta)}. \quad (4.13)$$

Again, making an approximation for $\beta \ll 1$, and noting that in the limit of small β, the period T of the signal must approach β, the positive half of the spectrum is approximated by

$$V_{FM,+}(\omega) \approx 4\pi\beta\delta(\omega-\omega_c) + j2\pi\beta\delta(\omega-(\omega_c-\omega_m)) + j2\pi\beta\delta(\omega-(\omega_c+\omega_m)), \quad (4.14)$$

which has the same magnitude as the spectrum for a sinusoidal AM modulation, and is the same spectrum that would be obtained by sinusoidal FM modulation.

For the two-soliton signal, from Chapter 2, Eq. (2.6), a single period of the signal is of the form

$$f(t) = \frac{\beta_1^2\mathrm{sech}^2(\eta_1) + \beta_2^2\mathrm{sech}^2(\eta_2) + A\mathrm{sech}^2(\eta_1)\mathrm{sech}^2(\eta_2)}{\left(\cosh(\phi/2) + \sinh(\phi/2)\tanh(\eta_1)\tanh(\eta_2)\right)^2}, \quad (4.15)$$

with $\eta_i = \beta_i(t-\delta_i)$. Thus, for positional modulation, $\delta_i = m_i(t)$, in addition to the spectral components of the individual messages, there is a contribution from the product of the individually modulated solitons. However, when the solitons do not overlap, $A \approx 0$ and the modulation is essentially the sum of the individually modulated waveforms. As the solitons begin to overlap, the contribution from the cross terms becomes significant, and spectral mixing of the component messages will occur. This results in an expansion of Fourier bandwidth of the multi-soliton signal. Examining the Fourier bandwidth of soliton signals is of interest for several reasons. First, such analysis offers comparisons to the spectral analyses of standard sinusoidal modulation techniques. Also, our engineering intuition often relates the bandwidth of a signal to the available degrees of freedom or information content of the signal. Finally, most transmission standards for electromagnetic as well as wired propagation are governed by an allocation of a finite region of Fourier spectrum or employ channels which are frequency-selective, making such analyses critical for use in any practical

transmission context.

However, in the absence of regulation on the Fourier content of signals, it is perhaps more appropriate to consider the nonlinear spectrum, as defined in Chap. 2, when analyzing soliton carrier modulation techniques. The nonlinear spectrum plays essentially the same role for soliton modulation that the Fourier spectrum plays for sinusoidal modulation. For example, in sinusoidal AM or FM, multiple carriers occupy disjoint regions of the Fourier spectrum, enabling signal separation via LTI processing. Similarly, in the soliton carrier modulation techniques outlined in this chapter, multiple carriers would occupy disjoint regions of the nonlinear spectrum, or different eigenvalues of the linear operator L in the inverse scattering transform. This enables separation of the different carrier signals through evolution of the nonlinear equations or through an inverse scattering analysis. In either a wired context or another situation where all of the signals are constructed for soliton modulation, although there may be Fourier spectral broadening of the component signals, there is no expansion of the nonlinear spectral composition of multi-soliton signals. This is due to the time-invariance of the eigenvalues in the inverse scattering transform under the evolution of the nonlinear dynamics.

4.4 Low Energy Signaling

In Chapters 2 and 3, we observed a compaction of signal amplitude as multiple solitons interact. This nonlinear coupling among the component solitons can be exploited to yield a reduction in transmitted signal energy for soliton carrier modulation techniques. Since the nonlinear coupling of multi-soliton signals is system-specific, we focus our attention on signal amplitude reduction in the Toda lattice. Specifically, it can be shown [29] that for a solution to the Toda lattice in the form of Eq. (3.1),

$$\int_{-\infty}^{\infty} v_n(t)dt = \text{constant}, \tag{4.16}$$

where v_n is the voltage on the n-th nonlinear capacitor,

$$\int_{-\infty}^{\infty} i_n(t)dt = \text{constant}, \tag{4.17}$$

where i_n is the current through the n-th inductor, and that

$$\int_{-\infty}^{\infty} v_n(t)i_{n-1}(t)dt = \text{constant}. \tag{4.18}$$

As a consequence of these conservation laws, we see that if two solitons are well separated, their individual contributions in Eqs. (4.16) and (4.17) are added, yet as they approach one another, their joint amplitude is restricted by Eq. (4.18). For example, if two solitons are well-separated in time as viewed on node k, and mutually overlapping as viewed on node ℓ, we obtain

$$\begin{aligned} \int_{-\infty}^{\infty} (v_\ell(t)i_{\ell-1}(t))dt &= \int_{-\infty}^{\infty} v_{1,k}(\tau_1)i_{1,k-1}(\tau_1)dt + \int_{-\infty}^{\infty} v_{2,k}(\tau_2)i_{2,k-1}(\tau_2)dt \\ &\neq \int_{-\infty}^{\infty} (v_{1,k}(\tau_1) + v_{2,k}(\tau_2))(i_{1,k-1}(\tau_1) + i_{2,k-1}(\tau_2))dt, \end{aligned} \tag{4.19}$$

where $v_{1,k}(\tau_1)$ is the voltage contribution from the first soliton when the solitons are separated as viewed on node k, and $v_\ell(t)$ is the voltage contribution from combined solitons as viewed on node ℓ. Note also that the time origin of each signal has been shifted, $t \to \tau_i$ so that each soliton is re-centered about $t = 0$. Due to the conservation law of Eq. (4.18), the joint amplitude of the solitons when combined must be less than the sum of the individual amplitudes when separated as illustrated in Fig. 4-5. A consequence of the restriction placed on the amplitude of the overlapping solitons is a reduction of energy in the transmitted signal for the modulation techniques of Section 4.2. In fact, as a function of the relative separation of the two solitons, the minimum energy of the transmitted signal is obtained precisely at the point of overlap. This can be shown for the two-soliton case by analysis of the form of the equation for the energy in the voltage waveform, $v(t)$,

$$E = \int_{-\infty}^{\infty} v(t;\delta_1,\delta_2)^2 dt, \tag{4.20}$$

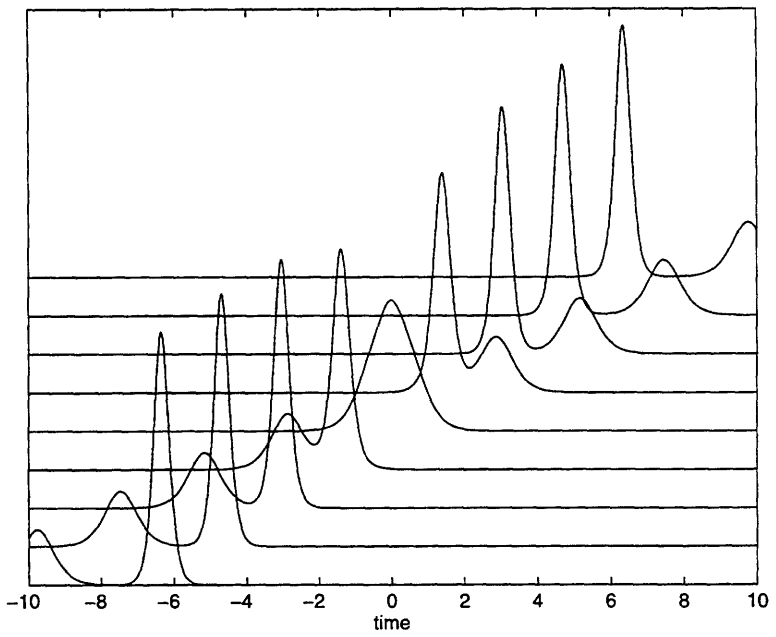

Figure 4-5: A two-soliton solution is depicted in the Toda lattice. Each horizontal trace is the response at a successive node in the lattice. In this case, the two soliton wavenumbers are $p_1 = 2$ and $p_2 = 1.3$.

where $v(t; \delta_1, \delta_2)$ is given in Eq. (4.15).

Without loss of generality, we assume $\delta_1 = 0$, and seek the value of δ_2 that minimizes (4.20). Differentiation of (4.20), yields,

$$\frac{dE}{d\delta_2} = \int_{-\infty}^{\infty} 2v(t)\frac{dv(t)}{d\delta_2}dt. \tag{4.21}$$

We now seek the value of δ_2 that makes the integral (4.21) equal to zero. This is accomplished by first noting that when the two solitons have the same phase, i.e., $\delta_1 = \delta_2$ in (4.15), then $v(t)$ is an even function of time, centered about $\delta_1 = \delta_2$. In this case, setting $\delta_2 = \delta_1 = 0$, makes $v(t)$ even. If it can be shown that by setting $\delta_2 = 0$, that $dv(t)/d\delta_2$ is an odd function, then the integral in (4.21) is trivially zero. This indeed turns out to be the case,

$$\frac{dv(t)}{d\delta_2} = \frac{\left(2\,\beta_1^2\mathrm{sech}^2(\beta_1\,t) + 2\,\beta_2^2\mathrm{sech}^2(\eta_2) + 2\,A\,\mathrm{sech}^2(\beta_1\,t)\mathrm{sech}^2(\eta_2)\right)}{\left(\cosh(\frac{\phi}{2}) + \sinh(\frac{\phi}{2})\tanh(\beta_1\,t)\tanh(\eta_2)\right)^3}$$

$$\times \sinh(\frac{\phi}{2})\tanh(\beta_1\,t)\left(1 - \tanh^2(\eta_2)\right)\beta_2$$

$$+\frac{2\,\beta_2^3\mathrm{sech}^2(\eta_2)\tanh(\eta_2) + 2\,A\,\mathrm{sech}^2(\beta_1\,t)\mathrm{sech}^2(\eta_2)\tanh(\eta_2)\beta_2}{\left(\cosh(\frac{\phi}{2}) + \sinh(\frac{\phi}{2})\tanh(\beta_1\,t)\tanh(\eta_2)\right)^2}. \tag{4.22}$$

Note that setting $\delta_2 = 0$ makes each of the terms in the numerator of the first line of (4.22) an even function of time. Setting $\delta_2 = 0$ also makes the denominator of the first term an even function. This term is then multiplied by the second line of (4.22), which is a constant, $\sinh(\phi/2)$, times an odd function, $\tanh(\beta_1 t)$, times an even function. Hence, we have several even functions multiplying an odd function, making the entire first term in (4.22) an odd function of time. The second term is also seen to be an odd function by similar analysis. As a result, setting $\delta_2 = 0$ is a stationary point of (4.20). To check that this is a minimum, we need to verify that

$$\frac{d^2}{d\delta_2^2}\int_{-\infty}^{\infty} v^2(t)dt\Big|_{\delta_2=0} > 0. \tag{4.23}$$

First we note that

$$\frac{d^2}{d\delta_2^2}\int_{-\infty}^{\infty} v^2(t)dt\Big|_{\delta_2=0} = \int_{-\infty}^{\infty} 2\left(\frac{dv(t)}{d\delta_2}\Big|_{\delta_2=0}\right)^2 + 2v(t)\,\frac{d^2v(t)}{d\delta_2^2}\Big|_{\delta_2=0} dt. \tag{4.24}$$

Since $dv(t)/d\delta_2|_{\delta_2=0}$ is real, the first term in (4.24) is positive. The second term contains $v(t)$, which is real, and positive, and $d^2v(t)/d\delta_2^2|_{\delta_2=0}$, which can be seen to also

be positive,

$$\left.\frac{d^2v(t)}{d\delta_2^2}\right|_{\delta_2=0} = \frac{4\,\beta_2^4\mathrm{sech}(\tau_2)^2\tanh(\tau_2)^2-2\,\beta_2^4\mathrm{sech}(\tau_2)^2\left(1-\tanh(\tau_2)^2\right)}{\left(\cosh(\frac{\phi}{2})+\sinh(\frac{\phi}{2})\tanh(\tau_1)\tanh(\tau_2)\right)^2}+$$

$$\frac{4\,A\,\mathrm{sech}(\tau_1)^2\mathrm{sech}(\tau_2)^2\tanh(\tau_2)^2\beta_2^2-2\,A\,\mathrm{sech}(\tau_1)^2\mathrm{sech}(\tau_2)^2\left(1-\tanh(\tau_2)^2\right)\beta_2^2}{\left(\cosh(\frac{\phi}{2})+\sinh(\frac{\phi}{2})\tanh(\tau_1)\tanh(\tau_2)\right)^2}+$$

$$\frac{\left(8\,\beta_2^3\mathrm{sech}(\tau_2)^2\tanh(\tau_2)+8\,A\,\mathrm{sech}(\tau_1)^2\mathrm{sech}(\tau_2)^2\tanh(\tau_2)\beta_2\right)\sinh(\frac{\phi}{2})\tanh(\tau_1)\left(1-\tanh(\tau_2)^2\right)\beta_2}{\left(\cosh(\frac{\phi}{2})+\sinh(\frac{\phi}{2})\tanh(\tau_1)\tanh(\tau_2)\right)^3}+$$

$$\frac{\left(6\,\beta_1^2\mathrm{sech}(\tau_1)^2+6\,\beta_2^2\mathrm{sech}(\tau_2)^2+6\,A\,\mathrm{sech}(\tau_1)^2\mathrm{sech}(\tau_2)^2\right)\sinh(\frac{\phi}{2})^2\tanh(\tau_1)^2\left(1-\tanh(\tau_2)^2\right)^2\beta_2^2}{\left(\cosh(\frac{\phi}{2})+\sinh(\frac{\phi}{2})\tanh(\tau_1)\tanh(\tau_2)\right)^4}+$$

$$\frac{\left(4\,\beta_1^2\mathrm{sech}(\tau_1)^2+4\,\beta_2^2\mathrm{sech}(\tau_2)^2+4\,A\,\mathrm{sech}(\tau_1)^2\mathrm{sech}(\tau_2)^2\right)\sinh(\frac{\phi}{2})\tanh(\tau_1)\tanh(\tau_2)\left(1-\tanh(\tau_2)^2\right)\beta_2^2}{\left(\cosh(\frac{\phi}{2})+\sinh(\frac{\phi}{2})\tanh(\tau_1)\tanh(\tau_2)\right)^3},$$

where $\tau_i = \beta_i\, t$. Since each term in (4.24) is positive, the integral is therefore positive, and $\delta_2 = \delta_1$ is indeed a minimum.

To illustrate the energy reduction, a two-soliton solution is shown in Fig. 4-6 as a function of both time and mutual separation, $\delta_1 - \delta_2$. As shown in the figure, when the two solitons are well-separated in time, $|\delta_1 - \delta_2| \gg 0$, the two component solitons are each distinguishable as a function of time and the signal appears as a linear superposition of the two. In this case, $A \approx 0$ in Eq. (4.15). However, as the solitons come to interact, $\delta_1 \approx \delta_2$, the nonlinear cross term in Eq. (4.15) becomes significant, and the combined signal amplitude decreases.

The effect of the energy reduction is illustrated in Fig. 4-7 for several different values of the parameter β_2 holding β_1 fixed, $\beta_1 > \beta_2$. When the smaller soliton is roughly the same amplitude as the larger, the energy decrease is on the order of 10% of the maximum signal energy. However as the smaller soliton reduces to roughly half the amplitude of the larger, we see that the energy reduction is almost 30%. Significant energy reduction occurs for a fairly wide range of separations, indicating that the modulation techniques described here could take advantage of this reduction.

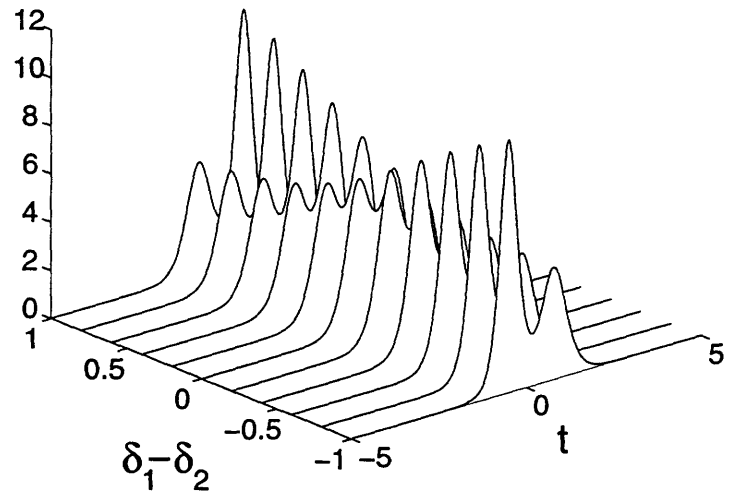

Figure 4-6: A two-soliton solution to the Toda lattice as a function of both time and mutual separation, $\delta_1 - \delta_2$.

4.5 Gain Normalization

In any practical communication context, a modulation system must be able to combat the presence of an unknown channel gain due to fluctuations in the channel characteristics. This is a potential drawback of using Toda lattice soliton carrier signals since these solitons have a specific relationship between the amplitude and pulse-width which must be preserved. If the soliton signal,

$$s(t) = \beta^2 \text{sech}^2(\beta t) \tag{4.25}$$

is transmitted through a channel and arrives at the receiver with an unknown gain, $r(t) = \alpha s(t)$, then the soliton dynamics of the signal $s(t)$ can no longer be observed from processing the signal $r(t)$. In general, the signal $r(t)$ will give rise to both soliton and non-soliton components, where the soliton component corresponds to a different soliton parameter $\tilde{\beta} \neq \beta$.

Many communication systems combat gain fluctuations by using a form of automatic gain control (AGC) to dynamically adjust the gain of a pre-amplifier in the receiver, $r(t) = \alpha\gamma s(t)$. To demonstrate the feasibility of such AGC techniques for

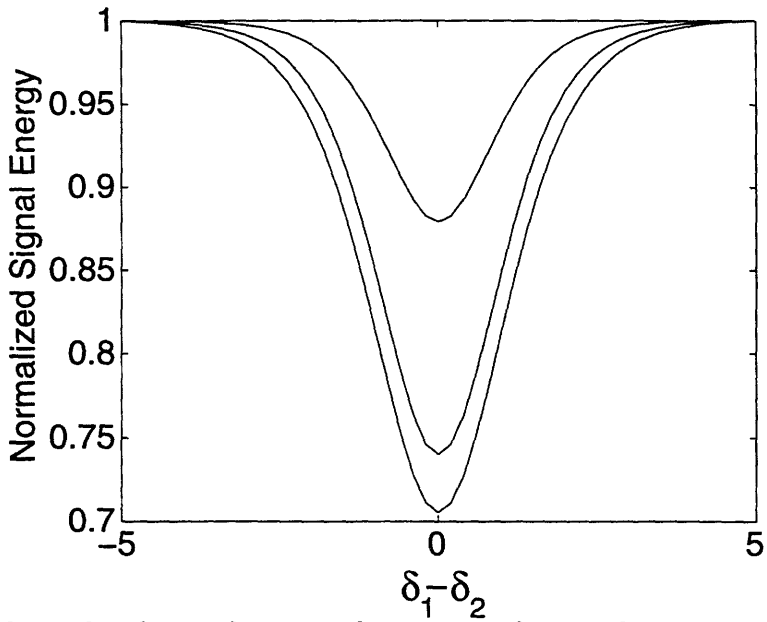

Figure 4-7: Normalized signal energy for a two-soliton solution to the Toda lattice holding β_1 fixed for 3 values of β_2. The signal energy is normalized by the maximum signal energy of the separated solitons.

the soliton modulation systems investigated in this chapter, we will explore the effect of an unknown gain on a single soliton as it is processed by the Toda lattice. Since the effect of processing the soliton will correspond to a simple time-delay only when the unknown gain has been removed, $\alpha\gamma = 1$, an AGC system might exploit differences between the input and the processed waveforms, and adjust the gain γ until the processed waveform is a pure time-delay of the input. If both the input and processed signals are made zero-mean, then the energy in the difference between the input and the output when the largest soliton in the output is time aligned with the input corresponds to

$$\begin{aligned} &\min_{\tau} \int ((r(t) - m_r) - (r_n(t-\tau) - m_{rn}))^2 dt = \\ &\min_{\tau} E_r + E_{rn} - 2\int (r(t) - m_r)(r_n(t-\tau) - m_{rn}) dt, \end{aligned} \tag{4.26}$$

where m_r and m_{rn} are the means and E_r and E_{rn} are the energies of the input and output, respectively. When the gain has been properly adjusted, $\alpha\gamma = 1$, this error will be a minimum. If each signal is energy normalized, $E_r = E_{rn} = 1$, then minimizing Eq. (4.26) amounts to maximizing the cross-correlation between the normalized

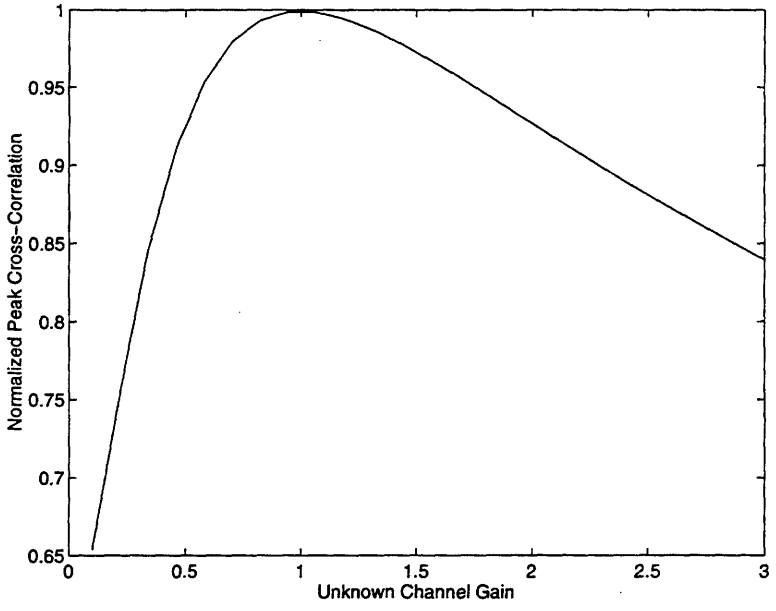

Figure 4-8: Normalized cross-covariance of input with the processed signal as a function of the unknown gain, α.

signals. The cross-correlation between the two normalized signals can be calculated as the peak of the cross-covariance function,

$$C_{r,rn}(\tau) = \frac{1}{E_r E_{rn}} \int (r(t) - m_r)(r_n(t-\tau) - m_{rn})dt. \tag{4.27}$$

Since $r_n(t) = r(t-\tau)$ only when $\alpha\gamma = 1$, then by the Schwartz inequality, the peak of $C_{r,rn}(\tau) \leq 1$, with equality only achieved when when $\alpha\gamma = 1$. As an example, in Fig. 4-8, the peak of the cross-covariance between the gain adjusted soliton signal $r(t) = \alpha\gamma s(t)$, and the processed signal at the n-th node of the lattice $r_n(t)$ is shown as a function of the unknown gain $\alpha\gamma$. For this example, $\beta = \sinh(2)$, and $0.1 \leq \alpha \leq 3$. As shown, the normalized cross-covariance has a unique maximum of $C = 1$, when the input to the Toda lattice has been properly rescaled, $\alpha\gamma = 1$. This gives an indication that AGC techniques based on a feedback of the normalized cross-covariance between the input and the processed signal might be effective in combating unknown channel gain. However, a variety of issues including how such AGC might be performed for multi-soliton signals or modulated multi-soliton carriers remains an interesting area for future research.

4.6 Other Potential Applications

We have explored in a very preliminary manner a modulation technique using solitons as carrier waveforms and nonlinear evolution equations as tuned transmitters and receivers. There are several interesting aspects of such techniques that warrant further study. For example, noting that the same nonlinear network can support a spectrum of solitons ranging from those with small amplitudes and wide pulse-widths, to relatively large amplitudes and narrow pulse-widths, indicates the potential for operating essentially the same modulator-demodulator networks at variable data rates depending on the bandwidth requirements. In the case of on-off keying modulation, where a bit could be indicated by the presence or absence of a soliton, a tradeoff may be made between the data rates and the power in the transmitted signal. When communication bandwidth requirements are low, small amplitude, wide solitons may be used and the necessary transmitted power is low. When bandwidth requirements increase, so does the requisite output power as narrower larger-amplitude solitons are used. This same analogy holds for either the amplitude or position modulation schemes addressed in this chapter.

Such signaling techniques may also prove useful in the context of recent advances in multi-resolution signal representations. In a hierarchical modulation technique reminiscent of fractal modulation [77] a multi-resolution representation of a signal might be transmitted such that each scale of the signal were encoded in a soliton of a different amplitude. If each of these soliton waveforms are combined and time-aligned according to the nonlinear superposition of the network, the response of the receiver network to this signal will be a gradual separation of each of the component soliton waveforms. In this manner, compactly represented signals might be constructed whereby varying amounts of processing, or equivalently, longer delay, yield signal representations of varying fidelity. As the received waveform is processed, the information present in the higher-amplitude, faster solitons emerges quickly from the composite waveform and may be decoded. As the message is passed further down the chain, the information in the next set of solitons may be decoded, and so on.

This type of modulation may be useful in a variety of communications or broadcast contexts which contain a large number of receivers of variable processing power. This may also be useful in a signaling context with messages of variable priority. In either case, successively more processing power, more accurate hardware, or more processing delay may be required to extract the messages encoded on the smallest amplitude solitons. This could correspond to either users of lower priority in a priority-based multiple access communications scenario, or to an incremental fidelity enhancement as envisioned for progressive transmission or embedded coding systems.

An essential ingredient in the modulation concepts explored in this chapter is the nonlinear superposition of the component soliton signals for combined packetization and energy reduction of the multi-soliton signal. As we shall see in Chap. 6 it is during this nonlinear superposition that the susceptibility to errors in the multi-soliton signal may be traded off between the component solitons. In fact, over certain ranges of parameter values, in addition to a net reduction in the transmitted signal energy, there can be net increase in fidelity of the recovered component messages.

A technique for modulation of information on soliton carriers was also proposed by Hirota, Suzuki and Yoshikawa in [64] and [65]. In their work, an amplitude and phase modulation of a two-soliton solution to the Toda lattice were presented as a technique for private communication. Although their signal generation and processing methods relied on an inexact phenomenon known as recurrence, the modulation paradigm they presented is essentially a two-soliton version of the carrier modulation paradigm presented in this chapter. Rather than generating multi-soliton signals in the lattice directly, a Toda lattice circuit was driven with a sinusoidal signal. For certain frequencies, a two-soliton-like solution is induced into the line. Each of the component solitons were separately modulated, and an appropriate length of the Toda chain was used to allow the solitons to recombine. This signal was then considered the transmitted signal, to be separated by another Toda circuit receiver. This overall process is illustrated in Fig. 4-9.

These methods were proposed as techniques for secure communication, the justification being that the nonlinear effects of the soliton superposition would cause

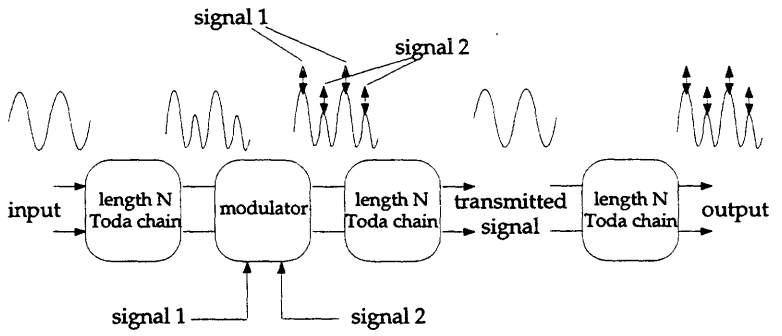

Figure 4-9: Schematic diagram of AM-like modulation of Hirota and Suzuki. Redrawn based on [64, 65]

enough spectral mixing of the component message waveforms that decoding without the correct nonlinear circuit would be difficult. However, in their experiments the message waveforms were pure sinusoids and as they point out from observations of the signal spectrum, these messages could be recovered by using a narrow band filter near the carrier frequency.

Before such methods could be considered for private or LPI (low probability of intercept) communications in practice, as is the case for direct-sequence spread spectrum systems, an additional level of security would have to be employed. Typically in direct sequence spread spectrum, the binary-valued symbol sequence is multiplied by a pseudo-random binary-valued sequence known only to the transmitter and receiver. In the soliton position modulation example, this could correspond to a pseudo-random perturbation to the relative phasing of the component solitons. Again, the efficacy of such techniques would have to be explored in detail.

The issue of the relative phasing of the soliton carrier signals brings to light another interesting analogy with more traditional modulation techniques. An issue of interest in modern multi-user communication systems is the relative performance of time-division-multiple-access (TDMA) versus code-division-multiple-access (CDMA) systems and the corresponding complexity of such systems. If the relative phases of the component solitons in the soliton PPM system are chosen such that they overlap temporally, then at least in the linear limit, a form of CDMA is approached. Conversely, if the relative phasing is chosen such that the solitons do not overlap,

then a TDMA system is employed. If the phasing is chosen such that only the highest amplitude soliton is separate from the composite, a hybrid TDMA/CDMA-like system is realized. In addition, a variety of digital communications techniques could be implemented using soliton carrier signals. However, the potential benefits of such techniques remain an area of future study.

Chapter 5

Noise Dynamics in Soliton Systems

We have seen that soliton solutions to nonlinear evolution equations provide an intriguing and potentially viable alternative to sinusoidal signals as carrier waveforms in the broad context of communication. In order to address the efficacy of the modulation techniques presented in Chapter 4, accurate models are needed for the effects of random fluctuations on the dynamics of soliton systems. Such disturbances could take the form of additive noise or interference or convolutional corruption incurred during terrestrial or wired transmission, circuit thermal noise, or modeling errors due to system deviation from the idealized soliton dynamics. A fundamental property of solitons that has made them appeal to such a broad area of science and engineering is that they are stable in the presence of a variety of disturbances. From their early discovery in the Scottish canal, it was the inherent stability of one such solitary wave that first attracted John Scott-Russell and influenced his study of the phenomena for many years [57]. For several decades, however, solitary waves were considered to be fluke solutions to a special class of nonlinear evolution equations and it was conjectured that two solitary waves would annihilate one another due to nonlinear interaction. It was after early computer experiments by Perring and Skyrme [57] with the sine-Gordon equation, and later numerical studies of KdV by Zabusky and Kruskal that revealed the contrary, prompting Zabusky and Kruskal to term these stable solitary waves *solitons* since they "pass through one another without losing their identity" [78].

In the literature, several measures of the stability or robustness of such nonlinear systems and their soliton solutions have been investigated. In addition to early numerical work, studies like [51] have empirically investigated the stability of soliton solutions in the presence of additive corruption. Lindgren and Buratti [43] have studied analytically the stability of solitons in the sine-Gordon equation through a linearization about a known soliton solution. Some success has also been achieved for such a study of one-dimensional nonlinear lattices by Flytzanis et al. [17]. Many forms of perturbation theory and approximate linear analysis have also been applied to the nonlinear Schrödinger equation, demonstrating the viability of proposed telecommunications systems as well [40]. In [5], Benjamin demonstrates the Lyapunov stability of a single soliton in the fully nonlinear KdV equation.

There has also been increasing interest in the solvability of soliton equations in the presence of additive noise. This area of the literature concerns systems such as the "stochastic KdV equation" which is a rather restrictive setting in which additive noise is additive and is a function of time, while remaining a constant function of space,

$$u_t + 6uu_x + u_{xxx} = n(t). \tag{5.1}$$

This system can be shown to possess an exact soliton solution with a phase drift that is given by a Wiener process, when $n(t)$ is a stationary white Gaussian process [44, 74].

With the development of the inverse scattering framework and the discovery that many soliton systems were conservative Hamiltonian systems, many of the questions regarding the stability of soliton solutions are readily answered. For example, since the eigenvalues of the associated linear operator remain unchanged under the evolution of the dynamics, then any solitons that are initially present in a system must remain present for all time, regardless of their interactions. Similarly, the dynamics of any non-soliton components that are present in the system are orthogonal to the dynamics of the solitons. However, in the communication scenario discussed in Chapter 4, soliton waveforms are generated and then propagated over a noisy channel. During transmission, these waveforms are susceptible to additive corruption

from the channel. When the waveform is received and processed, the inverse scattering framework can provide useful information about the soliton and noise content of the received waveform. Since the time evolution of the dynamics of such systems leaves the eigenvalues of a linear operator unchanged, investigations into their stability involves a study of the spectra of random linear operators. Although there has been recent work in this area [8, 54], little that has been published applies directly to our communication context.

In this chapter, we will assume that soliton signals generated in the communication contexts of Chapter 4 have been transmitted over an additive white Gaussian noise channel. We can then consider the effects of additive corruption on the processing of soliton signals with their nonlinear evolution equations. Two general approaches are taken to this problem. The first primarily deals with linearized models and investigates the dynamic behavior of the noise component of signals comprising an information bearing soliton signal and additive noise. The second approach is taken in the framework of inverse scattering and is based on some results from random matrix theory. Although the analysis techniques developed in this chapter are applicable to a large class of soliton systems, we focus our attention on the Toda lattice as a representative example.

5.1 Toda Lattice Small Signal Model

If a signal that is processed in a Toda lattice receiver contains only a small amplitude noise component, then the dynamics of the receiver can be approximated by a small signal model. Starting with the nonlinear transmission line model,

$$\frac{d^2}{dt^2}\ln(1+V_n(t)) = \frac{1}{LC}(V_{n-1}(t) - 2V_n(t) + V_{n+1}(t)), \tag{5.2}$$

and using the approximation, $\ln(1+x) \approx x$, we see that the lattice equations can be approximately described by the linear lattice equations

$$\frac{d^2V_n(t)}{dt^2} = \frac{1}{LC}(V_{n-1}(t) - 2V_n(t) + V_{n+1}(t)), \tag{5.3}$$

when the amplitude of $V_n(t)$ is appropriately small. Since this model is linear, we may decompose solutions into harmonic components of the form

$$V_n(t) = V_+ e^{j(kn-\omega t)} + V_- e^{j(kn+\omega t)}. \tag{5.4}$$

From Eqs. (5.3) and (5.4) we see that the frequency of a single forward propagating solution must satisfy the dispersion relation

$$-\omega^2 = \frac{1}{LC}(e^{-jk} - 2 + e^{jk}), \tag{5.5}$$

which reduces to

$$\omega = \frac{2\sin(k/2)}{\sqrt{LC}}. \tag{5.6}$$

Therefore the lattice is dispersive, with frequency-dependent velocity,

$$c(k) = \frac{2\sin(k/2)}{k\sqrt{LC}}, \tag{5.7}$$

or

$$c(\omega) = \frac{\omega}{2\sin^{-1}\left(\omega\sqrt{LC}/2\right)}. \tag{5.8}$$

Note that we can also write the dispersion relation as

$$k = 2\sin^{-1}\left(\omega\sqrt{LC}/2\right), \tag{5.9}$$

from which k is only real if

$$|\omega| \leq \frac{2}{\sqrt{LC}}, \tag{5.10}$$

for which there are propagating waves. When ω is outside this region, the wavenumber, k, is complex, corresponding to evanescent waves of the form

$$\omega = \frac{2}{\sqrt{LC}} \cosh(\mathrm{Im}(k)/2), \qquad \mathrm{Re}(k) = \pi. \tag{5.11}$$

These solutions decay as they pass through the lattice,

$$|V_n| = |V_+| e^{-2\cosh^{-1}(\omega\sqrt{LC}/2)n}, \tag{5.12}$$

which for $\omega \gg 2/\sqrt{LC}$ corresponds to

$$V_n = V_+ \left(\frac{-1}{\omega^2 LC}\right)^n. \tag{5.13}$$

If we consider processing signals with an infinite linear lattice and obtain an input-output relationship where a signal is input at the zeroth node and the output is taken as the voltage on the N-th node, we see that the input-output frequency response of the system can be given by

$$H_N(j\omega) = \begin{cases} e^{-2j\sin^{-1}(\omega\sqrt{LC}/2)N}, & |\omega| < 2/\sqrt{LC} \\ e^{[j\pi - 2\cosh^{-1}(\omega\sqrt{LC}/2)]N}, & \text{else.} \end{cases} \tag{5.14}$$

As shown in Fig. 5-1, the lattice behaves as a low pass filter, and for $N \gg 1$, approaches

$$|H_N(j\omega)|^2 = \begin{cases} 1, & |\omega| < \omega_c = 2/\sqrt{LC} \\ 0, & \text{else.} \end{cases} \tag{5.15}$$

5.2 Linearized Model

Our small signal model indicates that in the absence of solitons in the received signal, small amplitude noise will be processed by a low pass filter. If the received signal also contains solitons, then the small signal model of Eq. (5.3) will no longer hold. A

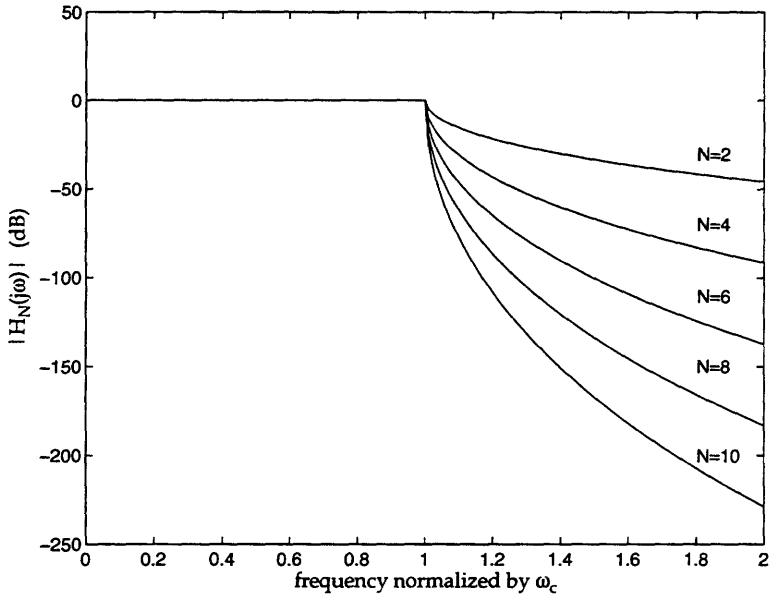

Figure 5-1: The log magnitude of the frequency response from the input node to the N-th node as a function of normalized frequency. As indicated, the response rapidly drops off as a function of N for $\omega > \omega_c$.

linear small signal model can still be used if we linearize Eq. (5.2) about the known soliton signal of the form

$$S_n(t) = \Omega^2 \text{sech}^2 \left(pn - \frac{\Omega t}{\sqrt{LC}} \right). \tag{5.16}$$

Assuming that the solution contains a single soliton in small amplitude noise, $V_n(t) = S_n(t) + v_n(t)$, we can write Eq. (5.2) as

$$\frac{d^2}{dt^2} \ln (1 + S_n + v_n) = \frac{1}{LC}(S_{n-1} - 2S_n + S_{n+1} + v_{n-1} - 2v_n + v_{n+1}). \tag{5.17}$$

After factoring the argument of the logarithm and cancelling terms from both sides that correspond to the known soliton solution, we have an exact equation that is satisfied by the non-soliton component,

$$\frac{d^2}{dt^2} \ln \left(1 + \frac{v_n(t)}{1 + S_n(t)} \right) = \frac{1}{LC}(v_{n-1}(t) - 2v_n(t) + v_{n+1}(t)), \tag{5.18}$$

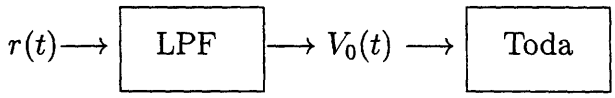

Figure 5-2: Receiver model comprising a low pass filter followed by a Toda lattice circuit.

which can be viewed as the fully nonlinear model with a time-varying parameter, $(1+S_n(t))$. As a result, over short time scales relative to $S_n(t)$, we would expect this model to behave in a similar manner to the small signal model of Eq. (5.3). With $v_n(t) \ll (1+S_n(t))$, we obtain

$$\frac{d^2}{dt^2}\frac{v_n(t)}{1+S_n(t)} \approx \frac{1}{LC}(v_{n-1}(t) - 2v_n(t) + v_{n+1}(t)). \tag{5.19}$$

When the contribution from the soliton is small, Eq. (5.19) reduces to the linear system of Eq. (5.3). We would therefore expect that both before and after a soliton has passed through the lattice, the system essentially low pass filters the noise. However, as the soliton is processed, there will be a time-varying component to the filter.

5.3 Simulation of the Lattice in Noise

To confirm the intuition developed through small signal analyses, we have simulated the fully nonlinear dynamics. As indicated in Chap. 3, we will work with a finite-length lattice which is terminated with its linearized impedance. We then focus on the dynamics of the small amplitude noise component in the response of the lattice to a signal comprising a single soliton in white Gaussian noise with noise power N_0.

Our primary interest in this chapter is to characterize the effects of additive noise in a receiver for a potential soliton modulation system. Since the bandwidth limitations of the receiver for any of the communications scenarios discussed in Chap. 4 will restrict the possible range of soliton parameters, without loss of generality, we may assume that the receiver comprises a low pass filter followed by a Toda lattice circuit as shown in Fig. 5-2. We also assume that the bandwidth, $2\pi/\Delta$, of the low pass filter in Fig. 5-2 is wide enough to pass the soliton component of $r(t)$ completely. The

input to the Toda lattice circuit, $V_0(t)$, then comprises the soliton signal in low pass Gaussian noise. Simulations are performed using a Runge-Kutta integration routine with a fixed step size, Δ. To model the effects of the noise, an i.i.d. Gaussian random sequence, $w(k\Delta) \sim N(0, \sigma_w^2)$, was added to the samples of the input sequence $V_0(k\Delta)$ resulting in an effective white noise power of $N_0 = \Delta\sigma_w^2$.

The circuit equations governing the resistance-terminated lattice are given in Eq. (5.2) for $n < N$. At the termination, $n = N$, we have

$$\ddot{V}_N(t) = \left(\frac{V_{N-1}(t) - V_N(t)}{LC} - \frac{\dot{V}_N(t)}{RC}\right)(1 + V_N(t)) + \frac{\dot{V}_N^2(t)}{1 + V_N(t)}. \tag{5.20}$$

Writing Eq. (5.2) and (5.20) as $2N$ first-order differential equations, we obtain

$$\dot{V}_n(t) = W_n(t), \qquad 1 \le n \le N \tag{5.21}$$

$$\dot{W}_n(t) = \frac{W_n^2(t)}{1 + V_n(t)} + \frac{1 + V_n(t)}{LC}(V_{n+1}(t) - 2V_n(t) + V_{n-1}(t)), \quad 1 \le n < N$$

$$\dot{W}_N(t) = \left(\frac{V_{N-1}(t) - V_N(t)}{LC} - \frac{W_N(t)}{RC}\right)(1 + V_N(t)) + \frac{W_N^2(t)}{1 + V_N(t)}. \tag{5.22}$$

From our linearized analyses, we anticipate that the response of the lattice to a soliton in small amplitude Gaussian noise will essentially comprise the unperturbed soliton with an additional small amplitude low pass Gaussian component. In Fig. 5-3 we show the response of the lattice to a single soliton at 20dB signal-to-noise ratio, where the SNR is calculated using

$$\text{SNR} = 10 \log \left(\frac{\int_{-\infty}^{\infty} s(t)^2 dt}{N_0} \right). \tag{5.23}$$

As expected, the response to the lattice is essentially the unperturbed soliton with an additional low pass perturbation. The noise component of the response on the third node of the lattice is indicated in Fig. 5-4. The spectrum of the noise remains essentially flat over the bandwidth of the soliton and is attenuated out of band.

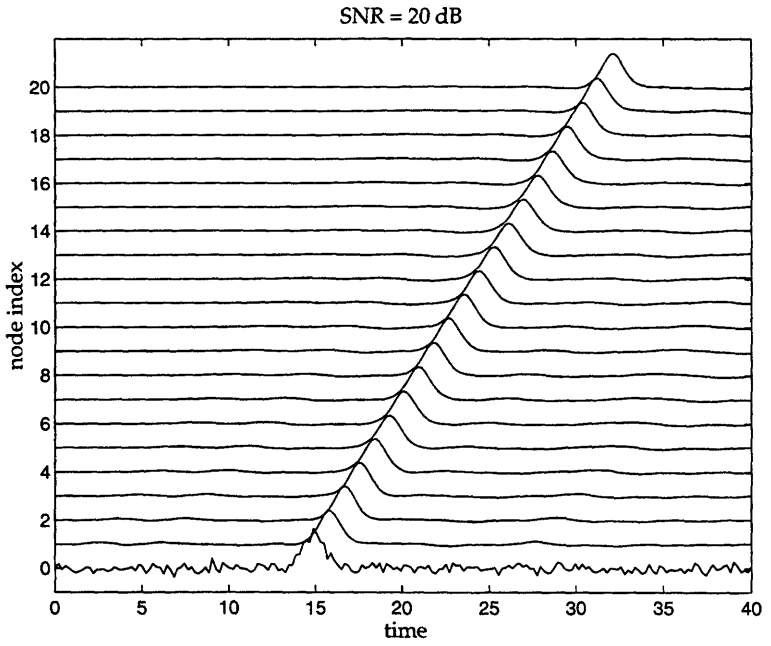

Figure 5-3: Response to a single soliton with $\beta = \sinh(1)$ in 20 dB Gaussian noise. The spectrum of the noise process is flat out to half the sample-rate of the integration routine. The corresponding in-band SNR is approximately 24 dB.

As the SNR decreases, and correspondingly $v_n(t)/(1 + S_n(t))$ becomes significant relative to unity, the linear approximation no longer applies and the noise dynamics must be described with the fully nonlinear equations. As shown in Fig. 5-5, the response to the noise term, $v_n(t)$, contains small-amplitude solitons as well as non-soliton components. The behavior of solitons induced by noise is better handled in the framework of inverse scattering, which is the topic of Sec. 5.6.

5.4 Noise Correlation

The statistical correlation of the system response to the noise component can also be estimated from our linear analyses. From Sec. 5.1, the small signal model for the nonlinear lattice approximately satisfies the linear equations,

$$\frac{d^2}{dt^2}v_n(t) = \frac{1}{LC}(v_{n-1}(t) - 2v_n(t) + v_{n+1}(t)), \tag{5.24}$$

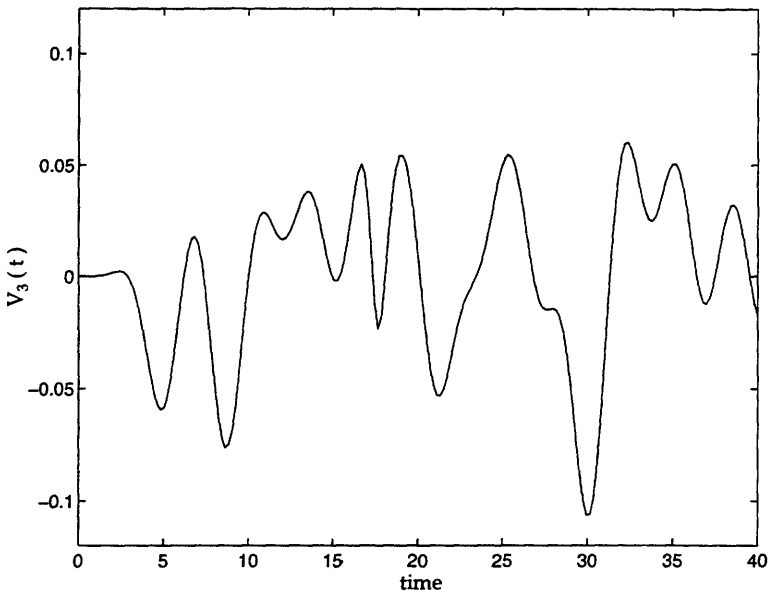

Figure 5-4: Noise response to a single soliton in 20 dB Gaussian noise as viewed from the third node in the lattice.

which has a magnitude-squared frequency response at the n-th node, $n \gg 1$, of

$$|H_n(j\omega)|^2 \approx \begin{cases} 1, & |\omega| < 2/\sqrt{LC} \\ 0, & \text{else.} \end{cases} \tag{5.25}$$

Therefore, $v_n(t)$ is zero mean and has an auto-correlation function given by

$$R_{n,n}(\tau) = E\{v_n(t)v_n(t+\tau)\} \approx N_0 \frac{\sin(\omega_c \tau)}{\pi \tau}, \tag{5.26}$$

and a variance $\sigma_{v_n}^2 \approx N_0\omega_c/\pi$, for $n \gg 1$.

Although the autocorrelation of the noise at each node is only affected by the magnitude response of Eq. (5.14), the cross-correlation between nodes is also affected by the phase response. The cross-correlation between nodes m and n is given by

$$R_{m,n}(\tau) = h_m(\tau) * h_n(-\tau) = h_m(\tau) * h_m(-\tau) * h_{n-m}(-\tau), \tag{5.27}$$

where $h_m(\tau)$ is the inverse Fourier transform of $H_m(j\omega)$ in Eq. (5.14). Since $h_m(\tau) * h_m(-\tau)$ approaches the impulse response of an ideal low pass filter for $m \gg 1$, we

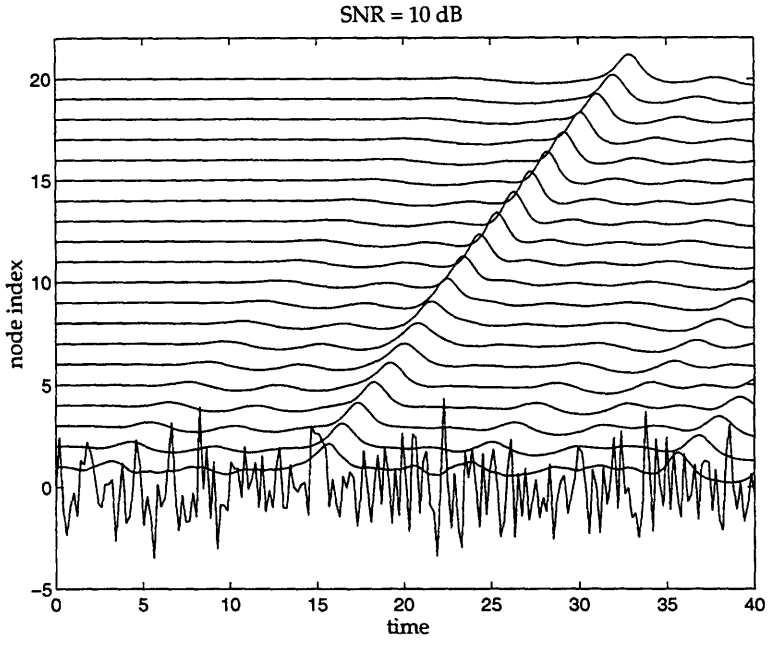

Figure 5-5: Response to a single soliton with $\beta = \sinh(1)$ in 10 dB Gaussian noise.

have

$$R_{m,n}(\tau) \approx N_0 \frac{\sin(\omega_c \tau)}{\pi \tau} * h_{n-m}(\tau). \tag{5.28}$$

In Fig. 5-6, $R_{m,n}(\tau)$ is shown for $n > m \gg 1$. Note that for ω small in Eq. (5.14), $\sin^{-1}(\omega/\omega_c) \approx \omega/\omega_c$, and the lattice looks like a pure delay of $\alpha = 2(n-m)/\omega_c$, corresponding to $R_{m,n}(\tau) \approx \sin(\omega_c(\tau - \alpha))/(\pi(\tau - \alpha))$. This approximation is only valid in the low frequency limit and corresponds to the diagonal translation of the largest lobe of $R_{m,n}(\tau)$ in Fig. 5-6.

For small amplitude noise, the correlation structure can be examined through the linear lattice, which acts as a dispersive low pass filter. A corresponding analysis of the nonlinear system in the presence of solitons becomes prohibitive in closed form. However we can explore the analyses numerically by linearizing the dynamics of the system about the known soliton trajectory.

To examine the correlation structure in the presence of soliton components, we use the state space framework of linear dynamic systems. The state space model

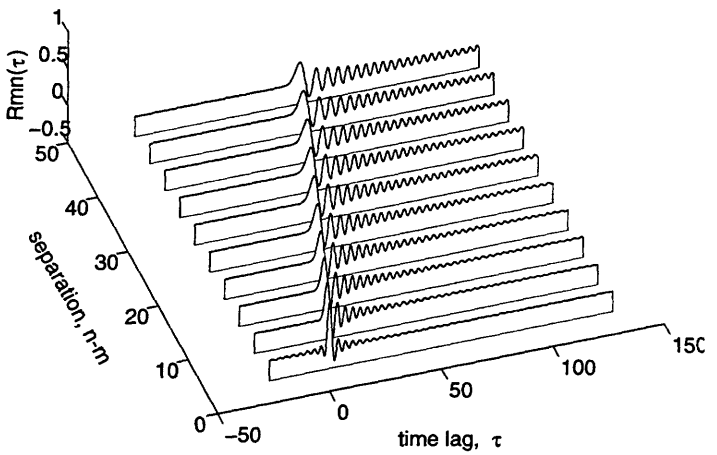

Figure 5-6: Cross-correlation, $R_{m,n}(\tau)$, between the m-th and the n-th node voltages in the linearized lattice.

comprises a linear system of finite dimension, N, with state vector

$$\mathbf{x}(t) = [x_0(t), \ldots, x_{N-1}(t)]^\top$$

and dynamics in state space form,

$$\dot{\mathbf{x}}(t) = A(t)\mathbf{x}(t) + \mathbf{b}(t)u(t), \tag{5.29}$$

where $A(t)$ is an $N \times N$ state transition matrix, $\mathbf{b}(t)$ is an $N \times 1$ vector, and $u(t)$ is a scalar input. We consider $u(t)$ to be a zero-mean, white Gaussian noise process with noise power σ_u^2.

For a linear system of the form (5.29), the state covariance matrix,

$$P(t) = E\left\{(\mathbf{x}(t) - E\{\mathbf{x}(t)\})(\mathbf{x}(t) - E\{\mathbf{x}(t)\})^\top\right\}, \tag{5.30}$$

satisfies the following differential equation [19]

$$\dot{P}(t) = A(t)P(t) + P(t)A(t)^\top + \mathbf{b}(t)\sigma_u^2\mathbf{b}(t)^\top. \tag{5.31}$$

To limit the number of state variables in $\mathbf{x}$, we again terminate the nonlinear lattice with its linearized impedance. If we assume that the input to the nonlinear lattice is of the form,

$$V_{\text{in}}(t) = V_0^0(t) + u(t), \tag{5.32}$$

where $u(t)$ is a small amplitude white Gaussian noise process, and $V_0^0(t)$ corresponds to a known soliton input, we may linearize the dynamics about the known response of the system.

By seeking a response $V_n(t) = V_n^0(t) + v_n(t)$, and $W_n(t) = \dot{V}_n(t) = W_n^0(t) + w_n(t)$, where $V_n^0(t)$ and $W_n^0(t)$ are the known responses to the input $V_0^0(t)$, and $v_n(t)$ and $w_n(t)$ are the responses to the small amplitude noise component, $u(t)$, we obtain

$$\begin{aligned}
\dot{V}_n^0 + \dot{v}_n &= W_n^0 + w_n^0, \qquad 1 \le n \le N \\
\dot{W}_n^0 + \dot{w}_n &= \frac{(W_n^0 + w_n)^2}{1 + V_n^0 + v_n} \qquad 1 < n \le N \\
&+ \frac{1 + V_n^0 + v_n}{LC}(V_{n+1} - 2V_n + V_{n-1} + v_{n+1} - 2v_n + v_{n-1}), \\
\dot{W}_N^0 + \dot{w}_N &= \left(\frac{V_{N-1} - V_N + v_{N-1} - v_N}{LC} - \frac{W_N + w_N}{RC}\right)(1 + W_N + w_n) \\
&+ \frac{(W_N + w_n)^2}{1 + V_N + v_n},
\end{aligned} \tag{5.33}$$

where $V_0^0 = V_0^0(t)$ and $v_0 = u(t)$. Cancelling terms that correspond to the known input and response and terms higher than first order, we obtain

$$\begin{aligned}
\dot{v}_n &= w_n^0, \qquad 1 \le n \le N \\
\dot{w}_n &= \left[\frac{V_{n+1}^0 - 2V_n^0 + V_{n-1}}{LC} - \frac{(W_n^0)^2}{(1 + V_n^0)^2} - \frac{2(1 + V_n^0)}{LC}\right] v_n \\
&+ \frac{1 + V_n^0}{LC}(v_{n+1} + v_{n-1}) + \frac{2W_n^0}{1 + V_n^0} w_n, \qquad 1 \le n < N \\
\dot{w}_N &= \left[\frac{V_{N-1}^0 - V_N^0}{LC} - \frac{W_N^0}{RC}\right] v_N \\
&+ \left[\frac{v_{N-1} - v_N}{LC} - \frac{w_N}{RC}\right](1 + V_N^0) + \frac{2W_N^0}{1 + V_N^0} w_N.
\end{aligned} \tag{5.34}$$

Eqs. (5.34) can be written in the form,

$$\begin{bmatrix} \dot{\mathbf{v}}(t) \\ \dot{\mathbf{w}}(t) \end{bmatrix} = A(t) \begin{bmatrix} \mathbf{v}(t) \\ \mathbf{w}(t) \end{bmatrix} + \mathbf{b}(t)u(t), \tag{5.35}$$

where $\mathbf{v}(t) = [v_1(t), \ldots, v_N(t)]^\top$, and $\mathbf{w}(t) = [w_1(t), \ldots, w_N(t)]^\top$.

From our earlier linearized analyses, the linear time-varying small signal model can be viewed over short time scales as a linear time-invariant chain, with a slowly varying parameter. The resulting input-output transfer function can be viewed as a low pass filter with time varying cutoff frequency equal to ω_c when a soliton is far from the node, and to $\omega_0\sqrt{1+V_n^0}$ as a soliton passes through. Thus, we would expect the variance of the node voltage to rise from a nominal value as a soliton passes through.

We numerically integrate the corresponding Riccati equation, (5.31), for the node covariance and in Fig. 5-7, the resulting variance of the noise component on each node is shown. In this example, the input to the lattice was a periodically repeated single soliton with an initial SNR of 30 dB. Since the lattice was assumed initially at rest, there is a startup transient, as well as an initial spatial transient at the beginning of the lattice, after which we see that the variance of the noise is amplified from the nominal variance as each soliton passes through, confirming our earlier intuition.

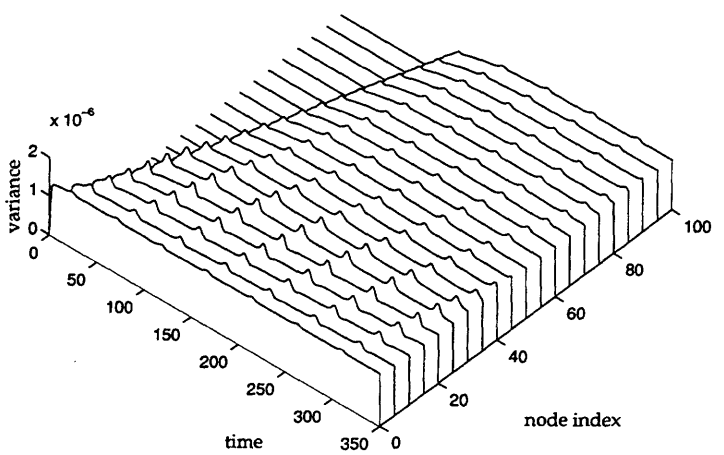

Figure 5-7: The variance of each node voltage as a function of time.

5.5 Noise Dynamics for the Diode Ladder Circuit

The prior analyses developed in this chapter apply to the Toda lattice when the noise component of the signal can be considered small in comparison to the remaining arguments of the logarithm in

$$\frac{d^2}{dt^2}\ln\left(1+\frac{V_n(t)}{V_0}\right)=\frac{1}{LCV_0}(V_{n-1}(t)-2V_n(t)+V_{n+1}(t)). \tag{5.36}$$

When $V_n(t)$ is small as compared with V_0, then Eq. (5.36) behaves like a linear LC ladder. However, for the diode ladder circuit which satisfies,

$$\frac{d^2}{dt^2}\ln\left(1+\frac{I_n(t)}{I_s}\right)=\frac{\alpha}{v_t}(I_{n-1}(t)-2I_n(t)+I_{n+1}(t)), \tag{5.37}$$

for a similar small signal analysis, $I_n(t)$ would have to be small in comparison to the saturation current, I_s. This would either require diodes with an unusually large saturation current or very small signal levels.

For a solution containing a soliton signal, $I_n(t)$, and a small amplitude noise signal, $i_n(t)$, an exact expression for the small amplitude component is given by

$$\frac{d^2}{dt^2}\ln\left(1+\frac{i_n(t)}{I_n(t)+I_s}\right)=\frac{\alpha}{v_t}(i_{n-1}(t)-2i_n(t)+i_{n+1}(t)). \tag{5.38}$$

The linearization that results from the assumption that the current $i_n(t)$ is small in comparison to the saturation current is tantamount to replacing the diodes with their equivalent linearized resistance, $R_{eq}=v_t/I_s$, which is on the order of $M\Omega$. The resulting small signal model has a low pass characteristic with a cutoff frequency of $\omega_c=\alpha/R_{eq}\approx 8kHz$ for the range of circuit parameters used in Chap. 3. Since the soliton pulse-widths considered there were on the order of μs for mA amplitudes, the bandwidth of the small signal model is extremely narrow in comparison to that of the soliton.

Observations of our circuit implementation of the diode ladder circuit seem to indicate that this bandwidth is too narrow to explain the level of higher-frequency

circuit noise present. This is partially explained by the change in the cutoff frequency as solitons are processed through a node. That is, over regions where the soliton component is significant, the equivalent resistance of the diode becomes $R_{eq} = v_t/I_n(t)$, which is on the order of 25Ω for a 1mA soliton. The effect this has on the linearized lattice is to make the lattice effectively an all pass filter in the vicinity of propagating solitons.

As a practical matter, we note that there appears to be a small amount of diode leakage current present in the circuit implementation and will explore the effect of a small bias current on the dynamics of both the soliton components and the small amplitude perturbation. For a solution containing a soliton, $I_n(t)$, a small amplitude component, $i_n(t)$, and a small bias current, I_b, the resulting system dynamics are

$$\frac{d^2}{dt^2}\ln\left(1+\frac{I_n+i_n+I_b}{I_s}\right)=\frac{\alpha}{v_t}(I_{n-1}-2I_n+I_{n+1}+i_{n-1}-2i_n+i_{n+1}), \tag{5.39}$$

which reduces to

$$\frac{d^2}{dt^2}\ln\left(1+\frac{i_n(t)+I_b}{I_n(t)+I_s}\right)=\frac{\alpha}{v_t}(i_{n-1}(t)-2i_n(t)+i_{n+1}(t)). \tag{5.40}$$

When the noise component $i_n(t)$ is small as compared with I_b, and away from the peaks of the soliton signal, $I_n(t) < I_b$, the dynamics further reduce to

$$\frac{d^2}{dt^2}i_n(t)\approx\frac{I_b\alpha}{v_t}(i_{n-1}(t)-2i_n(t)+i_{n+1}(t)), \tag{5.41}$$

where, the diodes are replaced by their linearization about the bias current, $R_{eq} = v_t/I_b$, leading to an increase in the bandwidth of the effective low pass filter.

In summary, due of the scaling of the diode ladder circuit, in order for the linear analyses to hold, the noise must be small in comparison to the diode saturation current, I_s. When a soliton is present, if the noise is small compared with the soliton, then a linear model can hold as with the LC ladder. When there is no soliton, if there is a small bias current that is larger than the noise, this can also lead to a simple linear model. When there is neither a bias nor a soliton present, if the noise is not

small as compared with the diode saturation current, then the noise satisfies the fully nonlinear system. The resulting disturbance is better described in terms of inverse scattering and leads to the problem of determining the spectrum of random linear operators, or random matrices.

5.6 Inverse Scattering-Based Noise Modeling

The inverse scattering transform provides a particularly useful mechanism for exploring the long term behavior of soliton systems. In a similar manner to the use of the Fourier transform for describing the ability of linear processors to extract a signal from a stationary random background, the nonlinear spectrum of a received soliton signal in noise can effectively characterize the ability of the nonlinear system to extract or process the component solitons. In this section, we focus on the effects of random perturbations on the dynamics of solitons in the Toda lattice from the viewpoint of inverse scattering. A discussion of this topic for soliton systems in general would require a level of mathematical background that is largely outside the scope of this thesis. However, some interesting results can be obtained for the Toda lattice through an application of some results from matrix theory, highlighting some potential directions for future research in the broad context of soliton signal processing.

As seen in Sec. 2.2, the dynamics of the Toda lattice may be described by the evolution of the matrix

$$L(t) = \begin{bmatrix} \ddots & a_{n-2}(t) & & & & \\ a_{n-2}(t) & b_{n-1}(t) & a_{n-1}(t) & & & \\ & a_{n-1}(t) & b_n(t) & a_n(t) & & \\ & & a_n(t) & b_{n+1}(t) & a_{n+1}(t) & \\ & & & & \ddots \end{bmatrix}, \tag{5.42}$$

whose eigenvalues outside the range $|\lambda| \leq 1$ give rise to soliton behavior. By considering the effects of small amplitude perturbations to the sequences $a_n(t)$ and $b_n(t)$ on

the eigenvalues of $L(t)$, we can observe the effects on the soliton dynamics through the eigenvalues corresponding to solitons. There is a large body of literature on the perturbation of eigenvalues of linear operators and matrices, e.g. [6, 37, 73, 76]. We will largely use results from [73] for randomly perturbed symmetric matrices with simple eigenvalues, since both the matrix $L(t)$ and its perturbation will be symmetric.

Following [73], we write the $N \times N$ matrix L in the form

$$L = L_0 + D, \tag{5.43}$$

where L_0 is the unperturbed symmetric matrix, and D is the symmetric random perturbation. It is further assumed that each element of the perturbation matrix is almost-surely bounded, such that

$$|D| = \left(\sum_{i,j=1}^{N} d_{ij}^2 \right)^{1/2} < \epsilon \ \ a.s., \tag{5.44}$$

where $\epsilon > 0$ is sufficiently small. By expanding the eigenvalues of the matrix L in a convergent series and matching terms in the expansion, vomScheidt and Purkert derive expressions for the first four terms in the expansion,

$$\lambda_g = \mu_g - \sum_{k=1}^{\infty} \lambda_{gk}, \tag{5.45}$$

where μ_g is the g-th eigenvalue of L_0 and λ_{gk} is of k-th order in the elements of D. The expectations and correlations of the eigenvalues can also be derived up to fourth order in the elements of D. To second order, the eigenvalues are given by

$$\begin{aligned} \lambda_{g1} &= -\hat{d}_{gg}, \\ \lambda_{g2} &= \sum_{i=1, i \neq g}^{N} \frac{\hat{d}_{gi}\hat{d}_{ig}}{\mu_{ig}}, \end{aligned} \tag{5.46}$$

where $\mu_{ig} = \mu_i - \mu_g$, and $\hat{d}_{ij}$ are the elements of the matrix $\hat{D}$ defined by,

$$\hat{D} = C^{\top} D C, \tag{5.47}$$

and C is a matrix that diagonalizes L,

$$C^{\top} L_0 C = \mathrm{diag}(\mu_1, \ldots, \mu_N). \tag{5.48}$$

To second order, the means of the eigenvalues are given by

$$E\{\lambda_g\} = \mu_g - \sum_{i=1, i \neq g}^{N} \frac{\hat{d}_{gi}\hat{d}_{ig}}{\mu_{ig}}, \tag{5.49}$$

indicating that the eigenvalues of L are asymptotically unbiased estimates of the eigenvalues of L_0. To first order,

$$\lambda_g \approx \mu_g - \hat{d}_{gg}, \tag{5.50}$$

and $\hat{d}_{gg}$ is a linear combination of the elements of D,

$$\hat{d}_{gg} = \sum_{r=1, s=1}^{N} c_{gr} c_{gs} d_{rs}. \tag{5.51}$$

Therefore, if the elements of D are jointly Gaussian, then to first order, the eigenvalues of L will be jointly Gaussian, distributed about the eigenvalues of L_0.

Note that the second order perturbation to the eigenvalues depends not only on the perturbation matrix, $\hat{D}$, but also on the proximity to the other eigenvalues. Also apparent from (5.49) is that the smallest and largest eigenvalues are biased, that is $E\{\lambda_1\} \leq \mu_1$ and $E\{\lambda_N\} \geq \mu_N$. This is of particular interest, since the largest eigenvalue typically corresponds to a soliton.

The variance of the eigenvalues are in general given by

$$\mathrm{Var}(\lambda_g) = E\left\{\hat{d}_{gg}^2\right\} - 2 \sum_{p=1, p \neq g}^{N} \frac{1}{\mu_{pg}} E\left\{\hat{d}_{pg}^2 \hat{d}_{gg}\left(1 + \frac{\hat{d}_{gg}}{\mu_{pg}}\right)\right\}, \tag{5.52}$$

to third order. When there is only small amplitude noise in the processed signal, we

can evaluate (5.52) to second order. If the perturbation matrix is given by

$$D = \begin{bmatrix} \ddots & \alpha_{n-2} & & & \\ \alpha_{n-2} & \beta_{n-1} & \alpha_{n-1} & & \\ & \alpha_{n-1} & \beta_n & \alpha_n & \\ & & \alpha_n & \beta_{n+1} & \alpha_{n+1} \\ & & & & \ddots \end{bmatrix}, \tag{5.53}$$

where β_n and α_n are independent, identically-distributed (iid) random sequences with variances σ_α^2, and σ_β^2, then the variances of the eigenvalues reduce to

$$\mathrm{Var}(\lambda_g) \approx \frac{\sigma_\beta^2 + 2\sigma_\alpha^2(1 + \cos(4\pi g/N))}{N}, \tag{5.54}$$

to second order. This indicates that the eigenvalues of L are consistent estimates of the eigenvalues of L_0.

Although we have only given a cursory investigation of this area, the inverse scattering framework appears to provide unique perspective on the effects of perturbations on the long-term behavior of the soliton solutions. If this method is to be applied to the driven Toda lattice as discussed in Chap. 3, then the sequences α_n and β_n would no longer be i.i.d., although to first order, they would remain jointly Gaussian. However, for the communication example using the dKdV equation, the transmitted signal could correspond to the sequence a_n and this analysis would apply directly. Although the methods developed in [73] assume a bounded perturbation, D, it can be shown that such methods remain accurate for Gaussian perturbations of small variance.

In this chapter, we have examined some of the effects of small amplitude noise on the processing of soliton signals with the Toda lattice. When processing small amplitude noise alone, the lattice can be viewed as a dispersive low pass filter. Therefore, the response of the system will be low pass Gaussian noise at each node. When solitons are processed in noise, our linearized analyses indicate that the solitons will be essentially unperturbed, and the noise will remain Gaussian and low pass. These

conclusions are validated through numerical integration of the fully nonlinear system and through a state space approach. Through numerical solution, we see that the variance of the noise at each node is essentially the variance that would be observed at the output of the low pass filter with a time-varying cutoff frequency. Useful insight can also be obtained from the nonlinear spectrum of the inverse scattering approach. We see that when processing small amplitude noise alone, the noise only excites eigenvalues corresponding to non-soliton components. When solitons are also processed, the noise induces a small Gaussian perturbation to the soliton eigenvalues as well.

Chapter 6

Estimation of Soliton Signals

In the communication techniques suggested in Chapter 4, the parameters of a multi-soliton carrier are modulated with message-bearing signals and the carrier is then processed with the corresponding nonlinear evolution equation. A potential advantage to transmission of this packetized soliton carrier is a net reduction in the transmitted signal energy. However during transmission, the multi-soliton carrier signal can be subjected to distortions due to propagation, which we have assumed can be modeled as additive white Gaussian noise, (AWGN). In Chapter 5, we characterized some of the effects of additive channel distortion on the generation and processing of soliton signals using their associated nonlinear evolution equations. In this chapter, we investigate the fidelity of the demodulated message signals from the perspective of the ability of a receiver to estimate the parameters of a multi-soliton carrier.

Specifically, if a message is encoded in a soliton carrier by modulating the relative spacing of the component solitons in each period, then it is important to understand the problem of time-of-arrival estimation both in terms of algorithm performance as well as theoretical performance bounds. More generally, the efficacy of any system employing soliton signals will be fundamentally influenced by the ability to detect, estimate, or otherwise process the signals themselves. The nonlinear interaction of the component waveforms make the signal dynamics unique to soliton systems, and it is therefore important to begin to understand how such signals behave under the influence of traditional signal processing algorithms.

In this chapter, we consider the problems of estimating the scaling parameters and the relative positions of component solitons of multi-soliton solutions and once again focus on the Toda lattice as an example. For each of these problems, we derive Cramér-Rao lower bounds for the estimation error variance through which several properties of multi-soliton signals can be observed. Specifically, we will see that although the net transmitted energy in a multi-soliton signal can be reduced through nonlinear interaction, the estimation performance for the parameters of the component solitons can also be enhanced. However, at the receiver there are inherent difficulties in parameter estimation imposed by this nonlinear coupling. We will demonstrate that the Toda lattice can act as a tuned receiver for the component solitons, naturally decoupling them so that the parameters of each soliton can be independently estimated. Based on this strategy, we develop asymptotically optimal algorithms for maximum likelihood parameter estimation. We also extend the analogy of the inverse scattering transform as an analog of the Fourier transform for linear techniques, by developing a maximum likelihood estimation algorithm based on the nonlinear spectrum of the received signal.

6.1 Soliton Parameter Estimation: Bounds

In order to understand the effects of additive channel corruption on some of the modulation techniques discussed in Chap. 4, we consider some of the basic signal processing issues that must be addressed by any receiver. Specifically, in this section we will determine bounds on the performance of any unbiased estimator for the problem of estimating both the scale parameters, β_i, and the relative positions, δ_i, of multi-soliton signals in stationary AWGN. In our simplified channel model, the received signal $r(t)$ contains a multi-soliton signal $s(t)$ in an additive noise background $n(t)$ with noise power, N_0.

A bound on the variance of an estimate of the parameter β may be useful in determining the demodulation performance of an AM-like modulation or PAM, where the component soliton wavenumbers are slightly amplitude modulated by a message-

bearing waveform. The fidelity of the recovered message will be directly affected by the ability of a receiver to estimate the soliton amplitude, β^2. When $s(t)$ contains a single soliton for the Toda lattice,

$$s(t) = \beta^2 \mathrm{sech}^2(\beta t), \tag{6.1}$$

the variance of any unbiased estimator $\hat{\beta}$ of β must satisfy the Cramér-Rao lower bound (CRB),

$$\mathrm{Var}\left(\hat{\beta}\right) \geq \frac{N_0}{\int_{t_i}^{t_f} \left(\frac{\partial s(t;\beta)}{\partial \beta}\right)^2 dt}, \tag{6.2}$$

where the observation interval is assumed to be $t_i < t < t_f$. For the infinite observation interval, $-\infty < t < \infty$, the CRB (6.2) is given by

$$\mathrm{Var}\left(\hat{\beta}\right) \geq \frac{N_0}{\left(\frac{8}{3} + \frac{4\pi^2}{45}\right)\beta} \approx \frac{N_0}{3.544\beta}. \tag{6.3}$$

Note that the CRB is a decreasing function of β. Although the width of $s(t)$ increases as $\beta \to 0$, the amplitude decreases proportional to β^2, and $s(t) \to 0$. Therefore, in a fixed level of noise, estimation of β will eventually become impossible, and the CRB becomes unbounded. On the other hand, as β increases, the amplitude increases as β^2 and in the limit, β can be estimated arbitrarily well and the CRB vanishes.

The proof of the bound (6.3) is based on the evaluation of the following integral,

$$\int_{-\infty}^{\infty} \left(\frac{\partial s(t;\beta)}{\partial \beta}\right)^2 dt. \tag{6.4}$$

For the single soliton this becomes,

$$\int_{-\infty}^{\infty} \left(\frac{\partial \beta^2 \mathrm{sech}^2(\beta t)}{\partial \beta}\right)^2 dt. \tag{6.5}$$

Expanding the integrand yields,

$$\int_{-\infty}^{\infty} \left(4\beta^2 \mathrm{sech}^3(\beta t) - 8\beta^3 \mathrm{sech}^4(\beta t)t + 4\beta^4 \mathrm{sech}^4(\beta t)\tanh(\beta t)t^2\right) dt. \tag{6.6}$$

The first two integrands evaluate to

$$4\beta^2\left(\frac{4}{3\beta}\right), \quad \text{and} \quad 8\beta^3\left(\frac{1}{3\beta^2}\right), \tag{6.7}$$

respectively. It is the third integrand in (6.6) that causes difficulty,

$$\frac{16}{30}\int_{-\infty}^{\infty}\frac{tdt}{e^{2t}+1} - \tag{6.8}$$

$$\frac{4(1+5e^{2t}-5e^{4t}+15e^{6t})t^2-4(e^{2t}-3e^{4t}-3e^{6t}+e^{8t})t+2(e^{2t}+e^{4t}-e^{6t}-e^{8t})}{15\left(e^{2t}+1\right)^5}\Bigg|_{-\infty}^{\infty} \tag{6.9}$$

The second term on the right is easily seen to vanish. The integral (6.9) evaluates to [22]

$$\frac{32}{30}\frac{1}{4}\frac{1}{2}\Gamma(2)\zeta(2) = \frac{\pi^2}{45}. \tag{6.10}$$

A slightly different bound may be useful in determining the demodulation performance of an FM-like modulation or PPM, where the soliton position, or time-delay, is slightly modulated by a message-bearing waveform. The fidelity of the recovered message waveform will be directly affected by the ability of a receiver to estimate the soliton position. When the signal $s(t)$ contains a single soliton,

$$s(t) = \beta^2\text{sech}^2(\beta(t-\delta)), \tag{6.11}$$

where δ is the relative position of the soliton in a period of the carrier, the CRB for $\hat{\delta}$ is given by [72]

$$\text{Var}\left(\hat{\delta}\right) \geq \frac{N_0}{\int_{t_i}^{t_f}\left(\frac{\partial s(t;\delta)}{\partial\delta}\right)^2 dt}, \tag{6.12}$$

which evaluates to

$$\text{Var}\left(\hat{\delta}\right) \geq \frac{N_0}{\int_{t_i}^{t_f} 4\beta^6\text{sech}^4(\beta(t-\delta))\tanh^2(\beta(t-\delta))dt} = \frac{N_0}{\left(\frac{16}{15}\right)\beta^5}. \tag{6.13}$$

As a comparison, for estimating the time of arrival of the raised cosine pulse,

$$s(t) = \beta^2 \left(1 + \cos\left(2\pi\beta(t-\delta)\right)\right), \tag{6.14}$$

the CRB for this more traditional pulse position modulation would be

$$\mathrm{Var}\left(\hat{\delta}\right) \geq \frac{N_0}{\pi^2\beta^5}, \tag{6.15}$$

which has the same dependence on signal amplitude as (6.13).

6.2 Multi-soliton Parameter Estimation: Bounds

When the received signal comprises a multi-soliton waveform where the multiple solitons are not time resolved and are therefore combined according to the nonlinear superposition of the system, the estimation problem becomes more difficult. Appropriately, the bounds for estimating the parameters of such signals must also be sensitive to the relative positions of the component solitons. The ability to estimate the soliton parameters based on observations of the multi-soliton received waveform will give direct insight to the potential performance of any demodulation algorithm.

We will focus our attention on the two-soliton solution to the Toda lattice,

$$s(t) = \frac{\beta_1^2 \mathrm{sech}^2(\eta_1) + \beta_2^2 \mathrm{sech}^2(\eta_2) + A\mathrm{sech}^2(\eta_1)\mathrm{sech}^2(\eta_2)}{\left(\cosh(\phi/2) + \sinh(\phi/2)\tanh(\eta_1)\tanh(\eta_2)\right)^2}, \tag{6.16}$$

where

$$A = \sinh(\phi/2)\left(\left(\beta_1^2 + \beta_2^2\right)\sinh(\phi/2) + 2\beta_1\beta_2\cosh(\phi/2)\right), \tag{6.17}$$

and when both solitons travel in the same direction and $\beta_1 > \beta_2$,

$$\phi = \ln\left(\frac{\sinh((p_1 - p_2)/2)}{\sinh((p_1 + p_2)/2)}\right), \tag{6.18}$$

where $\beta_i = \sinh(p_i)$, and $\eta_i = \beta_i(t - \delta_i)$.

From the modulation techniques discussed in Chapter 4, we are generally inter-

ested in estimating the parameters of the multi-soliton carrier for an unknown relative spacing among the solitons present in the carrier signal. Either the relative spacing of the solitons has been modulated, and is therefore unknown, or the parameters β_1 and β_2 are slightly modulated and the induced phase shift in the received solitons, ϕ, is unknown. In either case, the CRB for jointly estimating the parameters of a multi-soliton signal from observations of $r(t)$ can be obtained numerically by forming the Fisher information matrix, $I(\Theta)$, where $\Theta = [\delta_1 \delta_2 \beta_1 \beta_2]^\top$,

$$[I(\Theta)]_{i,j} = \frac{1}{N_0} \int_{t_i}^{t_f} \left(\frac{\partial s(\tau;\Theta)}{\partial \Theta_i} \frac{\partial s(\tau;\Theta)}{\partial \Theta_j} \right) dt, \tag{6.19}$$

where Θ_i is the i-th element of Θ. The resulting bound on the estimation variance for parameter i is given by [72]

$$\mathrm{Var}\left(\hat{\Theta}_i\right) \geq \left[I^{-1}(\Theta)\right]_{ii}. \tag{6.20}$$

For large separations, $\delta = \delta_1 - \delta_2$, the CRB for estimating the parameters of any of the component solitons will be unaffected by the parameters of the other solitons. As shown in Fig. 6-1, when the component solitons are well separated, the CRB for either β_1 or β_2 approaches the CRB for estimation of a single soliton with that parameter value in the same level of noise. The bounds for estimating β_1, and β_2 are shown in Fig. 6-1 as a function of the relative separation, δ.

Note that both of the bounds are reduced by the nonlinear superposition, indicating that the potential performance of the receiver is *enhanced* by the nonlinear superposition. However, if we let the parameter difference $\beta_2 - \beta_1$ increase, we notice a different character to the bounds. Specifically, we maintain $\beta_1 = \sinh(2)$, and let $\beta_1 = \sinh(1.25)$ and plot in Fig. 6-2, the same bounds as Fig. 6-1.

Note that now, the performance of the larger soliton is inhibited by the nonlinear superposition, while the smaller soliton is still enhanced. In fact, the CRB for the smaller soliton becomes lower than that for the larger soliton near the range $\delta = 0$. The reason for this has to do with the relative sensitivity of the signal $s(t)$ to each of the parameters β_1 and β_2.

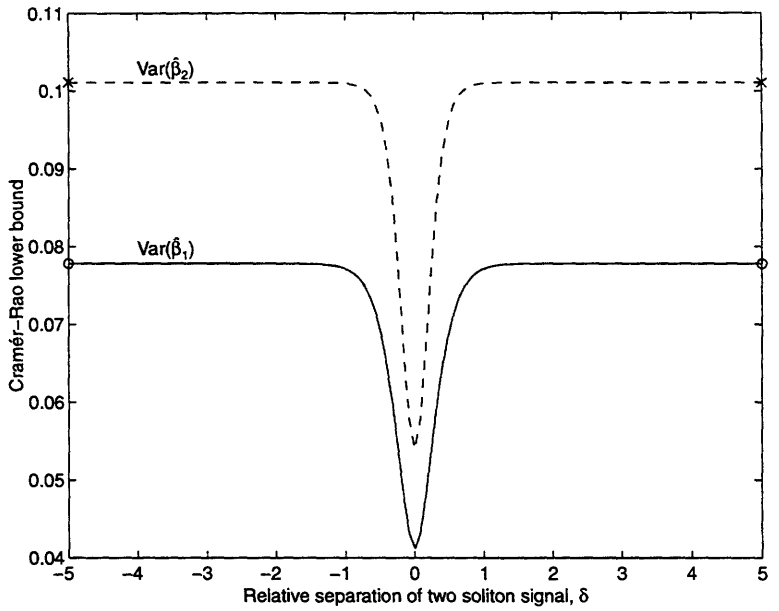

Figure 6-1: The Cramér-Rao lower bound for estimating $\beta_1 = \sinh(2)$ and $\beta_2 = \sinh(1.75)$ with all parameters unknown in AWGN with $N_0 = 1$. The bounds are shown as a function of the relative separation, $\delta = \delta_1 - \delta_2$. The CRB for estimating β_1 and β_2 of a single soliton with the same parameter value is indicated with 'o' and '×' marks, respectively.

The ability to simultaneously enhance estimation performance while decreasing signal energy is an inherently nonlinear phenomena. From Eq. (6.2), we see that the CRB for linear estimation in AWGN is inversely proportional to the signal energy,

$$\mathrm{Var}\left(\hat{\beta}\right) \geq \frac{N_0}{\int_{t_i}^{t_f} \left(\frac{\partial \beta s(t)}{\partial \beta}\right)^2 dt} = \frac{N_0}{\int_{t_i}^{t_f} s^2(t) dt} = \mathrm{SNR}^{-1}. \tag{6.21}$$

However, for nonlinear parameter estimation, the CRB is dependent upon the energy in the derivative of the signal with respect to the parameter, rather than signal energy.

The bounds for estimating the times of arrival of the two component solitons can also be seen to agree with the single soliton bounds, as shown in Fig. 6-3. Note that while the estimation performance of the larger of the two solitons is inhibited by nonlinear superposition, the estimation of the smaller of the two solitons is enhanced.

For the two-soliton signal, the nonlinear interaction of the component solitons can therefore enhance the parameter estimation performance or permit a tradeoff in performance between the component solitons. This potential performance enhancement

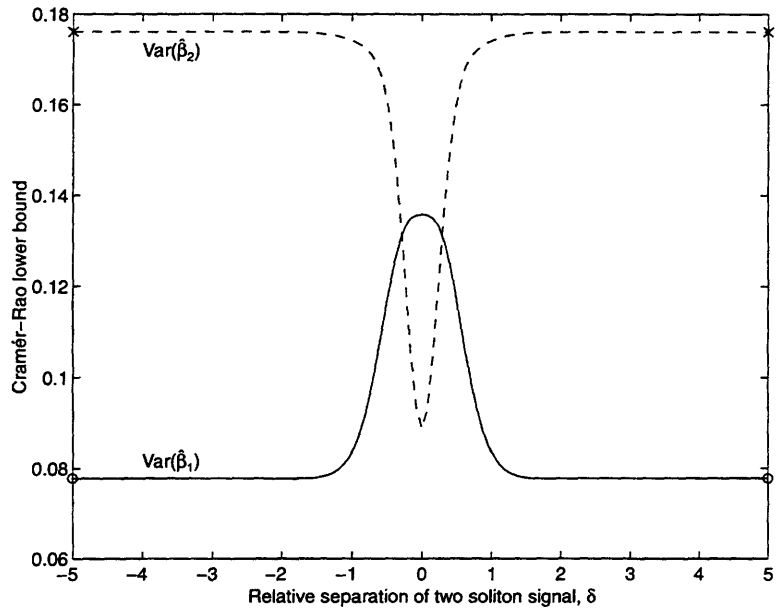

Figure 6-2: The Cramér-Rao lower bound for estimating $\beta_1 = \sinh(2)$ and $\beta_2 = \sinh(1.25)$ with all parameters unknown in AWGN with $N_0 = 1$. The bounds are shown as a function of the relative separation, $\delta = \delta_1 - \delta_2$. The CRB for estimating β_1 and β_2 of a single soliton with the same parameter value is indicated with 'o' and '×' marks, respectively.

is achieved in combination with a net energy reduction in the multi-soliton signal. The combination of these properties may make the superimposed solitons particularly attractive for a variety of communications contexts by providing an overall signal to noise ratio enhancement.

6.3 Estimation Algorithms

6.3.1 General Approach

In this section we will present and analyze the performance of several algorithms for estimating the parameters of soliton signals. Although the algorithms presented do not amount to a demodulation of any of the communication techniques suggested in Chap. 4, the bounds presented in the previous sections should give an idea of the best achievable performance of any such demodulation hardware. Similarly, the performance of the algorithms presented here may indicate the degree to which such

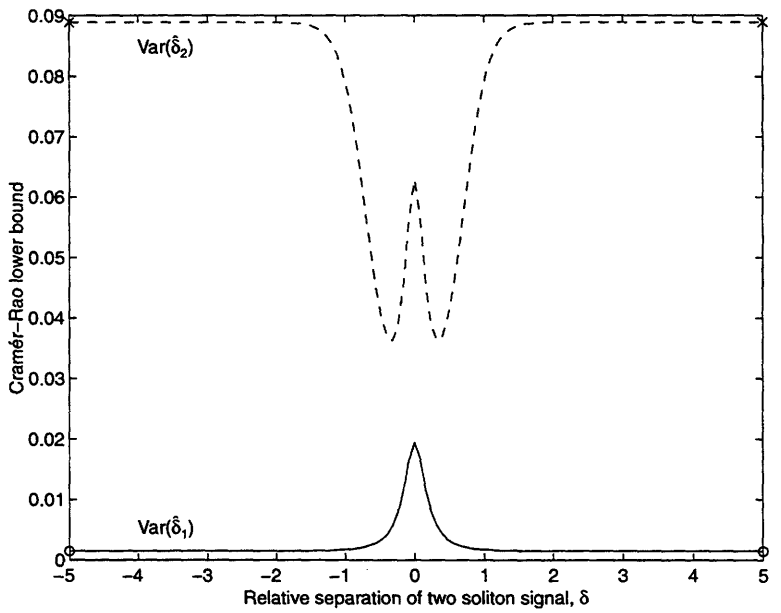

Figure 6-3: The Cramér-Rao bounds for estimating the time of arrival for each soliton in a two-soliton signal with $\beta_1 = \sinh(2)$ and $\beta_2 = \sinh(1.25)$ in AWGN with $N_0 = 1$. The asymptotic values of each of the bounds agree with the CRB for estimating the time of arrival of a single soliton with the same parameter value as indicated with 'o' and '×' marks.

bounds may be approached.

As an example, we will focus on the diode ladder circuit implementation of the Toda lattice equations,

$$\frac{d^2}{dt^2}\ln(1 + i_n(t)) = (i_{n-1}(t) - 2i_n(t) + i_{n+1}(t)), \tag{6.22}$$

where $i_n(t)$ is the current through the n-th diode, $i_0(t) = i_{\text{in}}(t)$, and for simplicity, the parameters of all circuit elements have been normalized to unity.

In order to motivate the general approach, we start by considering the problem of estimating the position, δ, of a single soliton solution to (6.22),

$$s(t;\delta) = \beta^2 \text{sech}^2(\beta(t - \delta)), \tag{6.23}$$

with the parameter β known. This is a classical time-of-arrival estimation problem. For observations $r(t) = s(t) + n(t)$, where $n(t)$ is a stationary white Gaussian process,

the maximum likelihood estimate is given by the value of the parameter δ which maximizes the likelihood of the observation, or equivalently minimizes the exponent of the likelihood function yielding the expression

$$\hat{\delta} = \arg\min_{\tau} \int_{t_i}^{t_f} (r(t) - s(t;\tau))^2 dt, \tag{6.24}$$

where $s(t;\tau)$ is the set of "replica signals" corresponding to $s(t-\tau)$ for all possible values of the parameter δ. Since the replica signals all have the same energy, we can represent the minimization in (6.24) as a maximization of the correlation,

$$\hat{\delta} = \arg\min_{\tau} \int_{t_i}^{t_f} r(t)s(t-\tau)dt. \tag{6.25}$$

It is well-known that an efficient way to perform the correlation (6.25) with all of the replica signals $s(t-\tau)$ over the range $\delta_{\min} < \tau < \delta_{\max}$, is through convolution with a matched filter followed by a peak-detector [72]. The estimate $\hat{\delta}$ is then determined from the time-location of the peak.

When the signal $r(t)$ contains a multi-soliton signal, $s(t;\underline{\beta},\underline{\delta})$, where we wish to estimate the parameter vector $\underline{\delta}$, the estimation problem becomes more involved. If the component solitons are well separated in time, then the maximum likelihood estimator for the positions of each of the component solitons would again involve a matched filter processor followed by a peak-detector for each soliton.

If the component solitons are not well-separated and are therefore nonlinearly combined, the estimation problems are tightly coupled and should not be performed independently. For observations in AWGN, the maximum likelihood processor would involve a minimization of the energy in the difference between the observed signal $r(t)$ and a replica signal $s(t;\underline{\beta},\underline{\delta})$ over the parameter space,

$$\hat{\underline{\delta}} = \arg\min_{\underline{\theta}} \int_{t_i}^{t_f} (r(t) - s(t;\underline{\beta},\underline{\theta}))^2 dt. \tag{6.26}$$

Note that, since the set of signals $s(t;\underline{\beta},\underline{\theta})$ are not all of equal energy, the minimization cannot be represented as a correlation. Further, since the signals are not all related

by a time-shift, there is no simple way to reproduce each member of the set.

The estimation problems can be decoupled by preprocessing the signal $r(t)$ with the Toda lattice. By setting $i_{\text{in}}(t) = r(t)$, that is the current through the first diode in the diode ladder circuit, then as the signal propagates through the lattice, the component solitons will naturally separate.

Defining the signal and noise components as viewed on the k-th node in the lattice as $i_k(t)$ by $s_k(t)$ and $n_k(t)$, respectively, i.e.,

$$i_k(t) = s_k(t) + n_k(t), \tag{6.27}$$

where $n_0(t)$ is the stationary white Gaussian noise process $n(t)$, in Chapter 5, we saw that in the high SNR limit, $n_k(t)$ will be low pass and Gaussian. In this limit, the ML estimator for the positions, δ_i, can again be formulated using matched filters for each of the component solitons. Since the lattice equations are invertible, at least in principle through inverse scattering, then the ML estimate of the parameter $\underline{\delta}$ based on $r(t)$ must be the same as the estimate based on $i_n(t) = T(r(t))$, for any invertible transformation $T(\cdot)$. If the component solitons are well-separated as viewed on the N-th node of the lattice, $i_N(t)$, then an ML estimate based on observations of $i_N(t)$ will reduce to the aggregate of ML estimates for each of the separated component solitons in low pass Gaussian noise. For soliton position estimation, this amounts to a bank of matched filters. We can view this estimation procedure as a form of nonlinear matched filtering, whereby first, dynamics matched to the soliton signals are used to perform the necessary signal separation, and then filters matched to the separated signals are used to estimate their arrival time.

To examine the empirical performance of this approach, we consider a soliton signal in AWGN with noise power N_0. Since the bandwidth limitations of the receiver will restrict the possible range of parameters, and to simplify our simulations, we assume that the receiver comprises a low pass filter followed by a Toda lattice circuit as shown in Fig. 6-4. We also assume that the bandwidth, $2\pi/\Delta$, of the low pass filter in Fig. 6-4, is wide enough to pass the soliton components of $r(t)$ completely. The

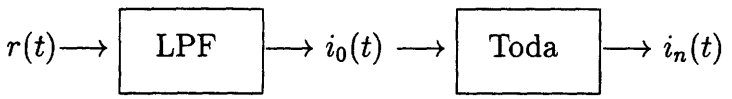

Figure 6-4: Toda lattice receiver model.

input to the Toda lattice circuit, $i_{\text{in}}(t)$, then comprises the soliton signal in low pass Gaussian noise. Simulations are performed using a Runge-Kutta integration routine with a fixed step size, Δ. To model the effects of the noise, an i.i.d. Gaussian random sequence, $w(k\Delta) \sim N(0, \sigma_w^2)$, is added to the samples of the input sequence $i_{\text{in}}(k\Delta)$ resulting in an effective white noise power of $N_0 = \Delta\sigma_w^2$. Equivalently, to simulate the effect of a white noise component in $r(t)$ with noise power N_0, and a bandwidth of the low pass filter of $2\omega_c$, the Runge-Kutta time step should be set to $\Delta = \pi/\omega_c$ and the variance of the Gaussian i.i.d. sequence should be $\sigma_w^2 = N_0/\Delta$.

6.3.2 Position Estimation

We will focus our attention on the two-soliton signal (6.16). If the component solitons are well-separated as viewed on the N-th node of the Toda lattice, the signal appears to be a linear superposition of two solitons,

$$\begin{aligned} i_N(t) &\approx \beta_1^2 \text{sech}^2(\beta_1(t-\delta_1) - p_1 N - \phi/2) \\ &+ \beta_2^2 \text{sech}^2(\beta_2(t-\delta_2) - p_2 N + \phi/2), \end{aligned} \tag{6.28}$$

where $\phi/2$ is the time-shift incurred due to the nonlinear interaction. Matched filters can now be used to estimate the time of the arrival of each soliton at the N-th node. We formulate the estimate

$$\hat{\delta}_1 = \left(t_{N,1}^a - \frac{p_1 N + \phi/2}{\beta_1}\right), \quad \hat{\delta}_2 = \left(t_{N,2}^a - \frac{p_2 N - \phi/2}{\beta_2}\right), \tag{6.29}$$

where $t_{N,i}^a$ is the time of arrival of the i-th soliton an node N. The performance of this algorithm for a two-soliton signal with $\underline{\beta} = [\sinh(2), \sinh(1.5)]$ is shown in Fig. 6-5. Note that although the error variance of each estimate appears to be a constant multiple of the CRB, the estimation error variance approaches the CRB in

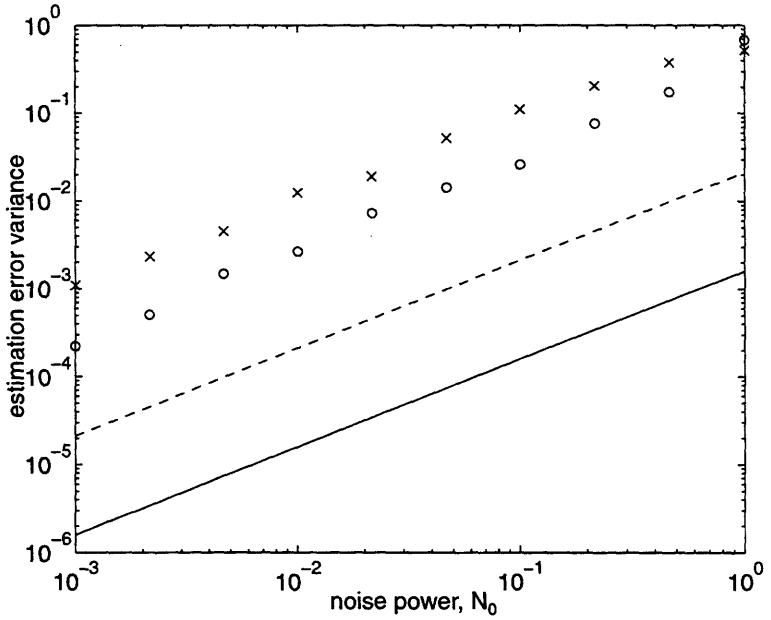

Figure 6-5: The CRBs for δ_1 and δ_2 are shown with solid and dashed lines, while the estimation error results of 100 Monte-Carlo trials are indicated with 'o' and '×' marks, respectively.

an absolute sense as $N_0 \to 0$.

6.3.3 Velocity Estimation

Since the velocity of a soliton in the Toda lattice is related to the scale parameter, β, and the velocity can be estimated based on the arrival times of the soliton, we may also form an estimate of β through velocity estimation. From the set of arrival times, $t^a_{N,i}$ we have a set of equations for each of the unknown parameters, β_i,

$$p_1 N + \phi/2 = \beta_1 t^a_{1,N}, \quad p_2 N - \phi/2 = \beta_2 t^a_{2,N}, \tag{6.30}$$

which are nonlinear in the parameter β_i, since $p_i = \sinh^{-1}(\beta_i)$. Solving for the parameter p_i, we obtain,

$$\frac{\sinh(p_i)}{p_i} = \frac{1}{t^d_{i,N}}, \tag{6.31}$$

where $t^d_{i,N}$ are the time-difference of arrivals of the i-th soliton between nodes N and $N+1$. Equation (6.31) can be solved numerically using Newton's method and for

large p, the solution can also be expressed in terms of Lambert's omega function, $p_i = -\Omega(-t^d_{i,N})$ [9]. We may then formulate the estimate $\hat{\beta}_i = \sinh(p_i)$. This technique is similar to "velocity-filtering" commonly used in seismic signal processing [55]. Note that in estimating β_i, the arrival times $t^a_{N,i}$ must be selected based on peak detection of the signal $i_N(t)$ alone without the aid of the matched filter which would require knowledge of the unknown parameter β_i.

A scalar closed-form sufficient statistic for the estimation of β based on observations of a single soliton in Gaussian noise does not exist due to the highly nonlinear manner in which the parameter appears both in the time and the amplitude scales of the signal which preclude factorization of the likelihood function for $r(t)$. Although an ML solution could be found by numerical maximization of the likelihood function, such a solution would be computationally intensive. We therefore look at the performance of the ad-hoc estimate based on the most salient characteristics of the soliton through the lattice, namely the scale-dependent velocity.

The results of 100 Monte Carlo trials for the velocity-based estimation algorithm using a Toda lattice with $N = 10$ nodes are shown in Fig. 6-6. The parameter values estimated were $\beta_1 = \sinh(2)$ and $\beta_2 = \sinh(1.5)$ with both solitons time-aligned. Therefore the CRB for the smaller soliton is actually lower than that for the larger soliton.

6.3.4 Estimation Based on Inverse Scattering

Although an ML estimate of the parameter β cannot be formulated directly based on observations of the received signal $r(t)$, we can use the inverse scattering framework along with some of the results from Chapter 5 to demonstrate a procedure for constructing the ML estimate in the high SNR limit. We have argued that ML parameter estimation based on a received multi-soliton signal, $r(t)$, is equivalent to ML estimation based on the signal as observed on the N-th node in the Toda lattice, $i_N(t)$. We may also consider the transformation

$$L(t) = T\{r(t)\}, \tag{6.32}$$

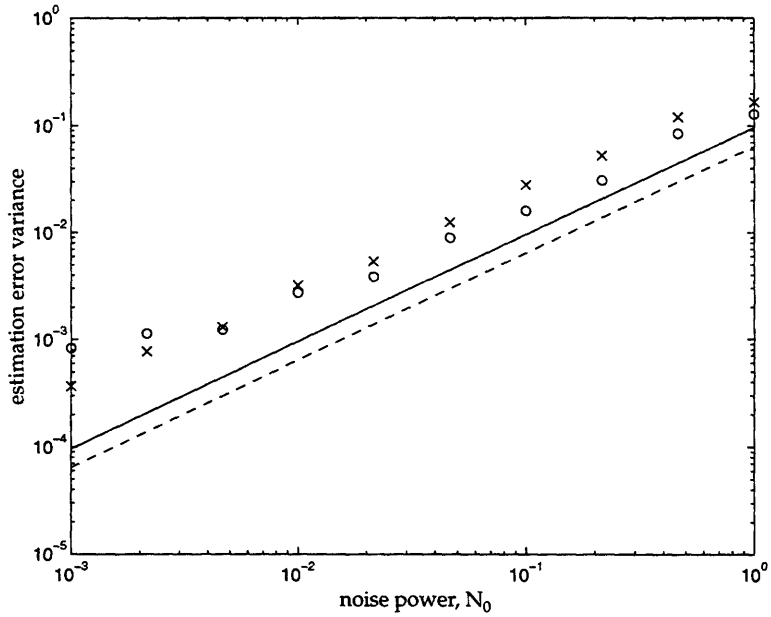

Figure 6-6: The estimation error variance for the velocity-based algorithm. The CRB for β_1 and β_2 is shown with a solid and dashed line, and the estimation error variances are indicated by the points labeled 'o' and '×' respectively.

where $L(t)$ is the symmetric matrix from the inverse scattering transform. This transformation $T\{\cdot\}$ is also invertible in principle through inverse scattering. Therefore, an ML estimate based on the signal $L(t)$ must be the same as an ML estimate based on $r(t)$. We therefore seek to form an estimate of the parameters of the signal $r(t)$ by performing the estimation in the nonlinear spectral domain. This can be accomplished as shown in Fig. 6-7 where the Toda lattice can be viewed as a nonlinear filterbank which projects the signal $r(t)$ onto the spectral components of $L(t)$. This use of the inverse scattering transform is analogous to performing frequency estimation with the Fourier transform.

From Chapter 2 we saw that if $v_n(t)$ evolves according to the Toda lattice,

$$\ddot{v}_n(t) = \left(e^{-(v_n(t)-v_{n-1}(t))} - e^{-(v_{n+1}(t)-v_n(t))}\right), \tag{6.33}$$

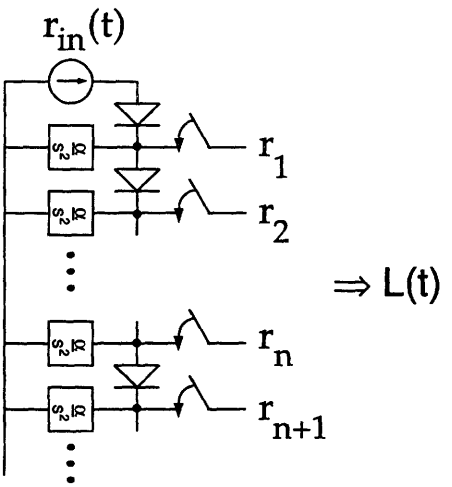

Figure 6-7: Procedure for computing $L(t)$ by processing the signal $r(t)$ with the Toda lattice.

then the eigenvalues of the matrix,

$$L(t) = \begin{bmatrix} \ddots & a_{n-2}(t) & & & & \\ a_{n-2}(t) & b_{n-1}(t) & a_{n-1}(t) & & & \\ & a_{n-1}(t) & b_n(t) & a_n(t) & & \\ & & a_n(t) & b_{n+1}(t) & a_{n+1}(t) & \\ & & & & \ddots \end{bmatrix}, \tag{6.34}$$

are time-invariant, where, $a_n(t) = \frac{1}{2}e^{(v_n(t)-v_{n+1}(t))/2}$, and $b_n = \dot{v}_n(t)/2$. Note that $v_n(t)$ could correspond to the voltages on the double capacitors in the diode ladder circuit. Further, the eigenvalues of $L(t)$ for which $|\lambda_i| > 1$ correspond to soliton solutions, with $\beta_i = \sinh(\cosh^{-1}(\lambda_i)) = \sqrt{\lambda_i^2 - 1}$. We also saw in Chapter 5, that the eigenvalues of $L(t)$ are, to first order, jointly Gaussian and distributed about the true eigenvalues corresponding to the original multi-soliton signal, $s(t)$. Therefore, estimation of the parameters β_i from the eigenvalues of $L(t)$ as described above constitutes a maximum likelihood approach in the high SNR limit.

The parameter estimation algorithm now amounts to an estimation of the eigenvalues of $L(t)$. Note that since $L(t)$ is tridiagonal, very efficient techniques for eigenvalue

estimation may be used [21]. The estimate of the parameter β is then found by the relation $\hat{\beta}_i = \sqrt{\lambda_i^2 - 1}$, where $|\lambda_i| > 1$, and the sign of β_i can be recovered from the sign of λ_i. Clearly if there is a pre-specified number of solitons, k, present in the signal, then the k largest eigenvalues would be used for the estimation. If the number k were unknown, then a simultaneous detection and estimation algorithm would be required.

In order to perform eigenvalue estimation, we must once again deal with the finite length of the Toda lattice. This can be resolved by either using the periodic Jacoby matrix $L(t)$ that results from making the periodic assumption $a_N(t) = a_0(t)$,

$$L(t) = \begin{bmatrix} b_1(t) & a_1(t) & 0 & \cdots & a_N(t) \\ a_1(t) & b_2(t) & a_2(t) & & \\ & \ddots & & & \\ & & \ddots & a_{N-2}(t) & \\ & & a_{N-2}(t) & b_{N-1}(t) & a_{N-1}(t) \\ a_N(t) & 0 & \cdots & a_{N-1}(t) & b_N(t) \end{bmatrix}, \tag{6.35}$$

or by simply truncating the matrix. It can be shown that for the periodic Toda lattice, the eigenvalues of the periodic Jacoby matrix are time-invariant [68]. In practice, truncating the matrix around the region of support of the solitons has little effect on the eigenvalues. Note the similarity once again to the frequency estimation problem, whereby the Fourier transform cannot be computed explicitly, however the discrete Fourier Transform, (DFT), is often used which makes similar assumptions about the region of support of the underlying signal.

An example of the joint estimation of the parameters of a two-soliton signal is shown in Fig. 6-8. The estimation error variance decreases with the noise power at the same exponential rate as the CRB. The normalized mean estimation error, $(\hat{\beta}_i - \beta_i)/\beta_i$ for each estimate $\hat{\beta}_i$ are shown in Fig. 6-9, indicating that the estimates are empirically unbiased.

To verify that the performance of the estimation algorithm has the same dependence on the relative separation of solitons as indicated in Sec 6.2, the estimation

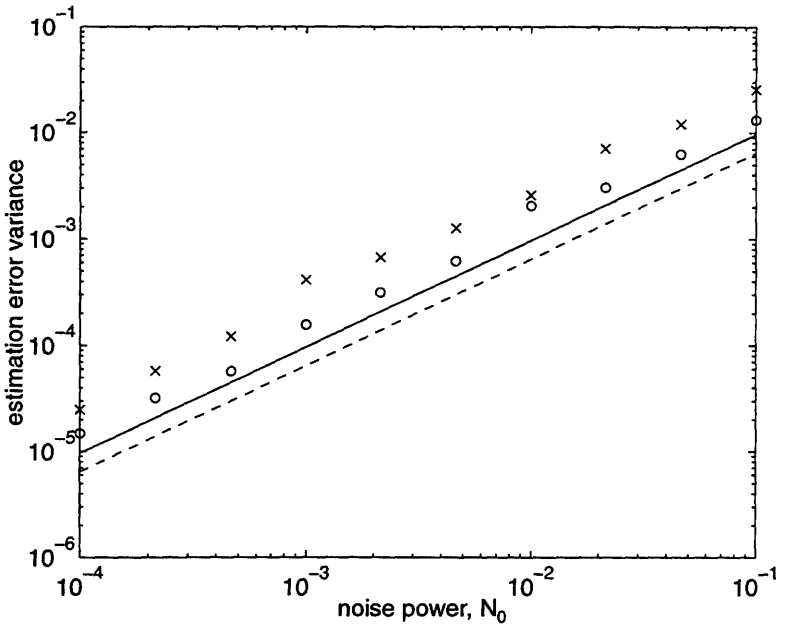

Figure 6-8: The estimation error variance for the inverse scattering-based estimates of $\beta_1 = \sinh(2), \beta_2 = \sinh(1.5)$. The bounds for β_1 and β_2 are indicated with solid and dashed lines respectively. The estimation results for 100 Monte Carlo trials with a diode lattice of $N = 10$ nodes for β_1 and β_2 are indicated by the points labeled 'o' and '$\times$' respectively.

error variance is also indicated in Fig. 6-10 versus the relative separation, δ. In the figure, the mean-squared parameter estimation error for each of the parameters β_i are shown along with their corresponding CRB. At least empirically, we see that the fidelity of the parameter estimates are indeed enhanced by their nonlinear interaction, even though this corresponds to a signal with lower energy, and therefore lower observational SNR.

6.4 Summary

In this chapter, we have explored some of the properties of multi-soliton signals from the viewpoint of parameter estimation. In fact, some of the rich structure of these signals is apparent from the behavior of the Cramér-Rao bounds for estimating their parameters. In Chap. 4, we observed that the energy in a two-soliton signal is reduced when the component solitons are nonlinearly superimposed. In this chapter,

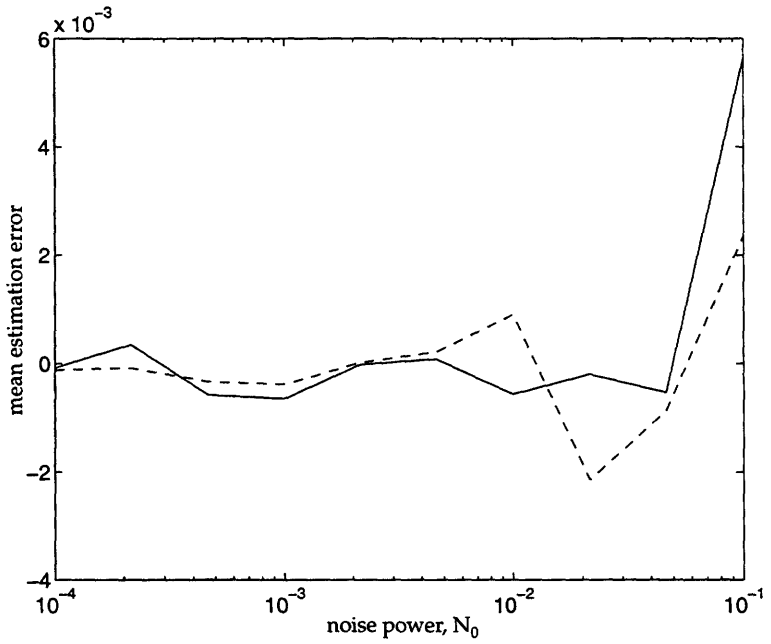

Figure 6-9: Normalized mean parameter estimation error for the inverse scattering-based estimation.

we observed that the nonlinear interaction of solitons can also improve the estimation performance of each. For certain parameter ranges, the coupling enables the larger soliton components to enhance the estimation performance of the smaller components.

For multi-soliton parameter estimation, we noted that the coupling of component solitons can make traditional techniques prohibitively complex. However, using the nonlinear evolution equations as a preprocessor to perform signal separation, we were able to perform maximum likelihood time-delay estimation and an associated velocity estimation.

We also demonstrated an algorithm for multi-soliton parameter estimation based on the inverse scattering transform. In the high SNR limit, the discrete eigenvalues in the nonlinear spectrum can be used to formulate maximum likelihood estimates of the scaling parameters for Toda lattice solitons. This approach is analogous to a filterbank which measures the content of the received signal in the nonlinear spectrum of the associated linear operator. Parameter estimation based on inverse scattering techniques also has many direct analogies to estimation based on Fourier methods for linear systems.

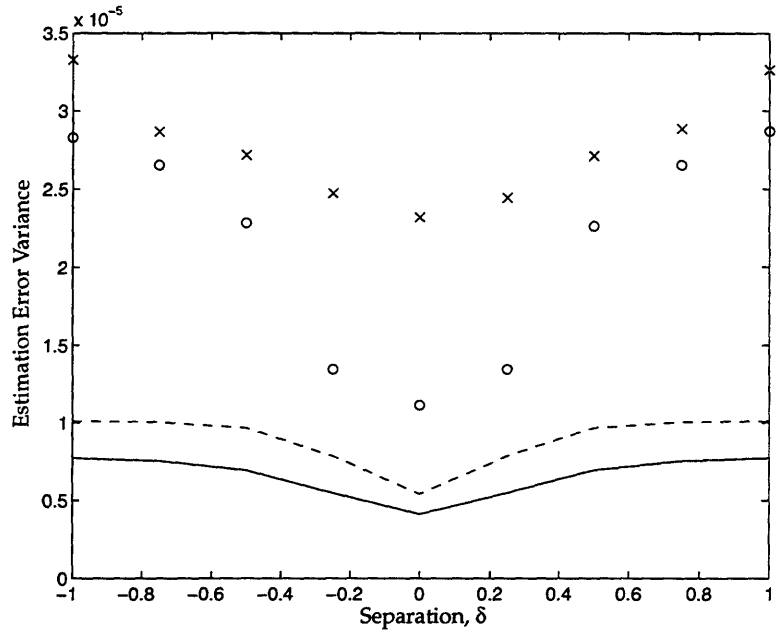

Figure 6-10: The estimation error variance for estimating $\beta_1 = \sinh(2), \beta_2 = \sinh(1.5)$ are indicated with the points labeled 'o' and '$\times$' and the CRBs for each are indicated with solid and dashed lines, respectively.

Perhaps there is something to be gained from a more thorough investigation of the inverse method in looking for a sufficient statistic for soliton parameter estimation. The lack of a sufficient statistic for estimation of the parameter β stems from the highly nonlinear manner in which the parameter appears both in the time-scale and the amplitude scale of the signal

$$s_n(t;\beta) = \beta^2 \mathrm{sech}^2(\sinh^{-1}(\beta)n - \beta t). \tag{6.36}$$

An investigation into exploiting the scale-invariance of such signals and the potential for multi-scale processing of soliton signals also represents an interesting area for future work.

Chapter 7

Detection of Soliton Signals

7.1 General Approach

The problem of detecting a single soliton or multiple non-overlapping solitons in AWGN falls within the theory of classical detection. The general approach to such problems involves first mapping the observation waveform, $r(t)$ onto a convenient and suitably compact decision space [72]. The detection problem then reduces to a partitioning of the decision space into decision regions according to a particular criteria of optimality. Consider the following binary hypothesis problem,

$$\begin{aligned} H_0 &: r(t) = n(t), \\ H_1 &: r(t) = \sqrt{E}s(t) + n(t), \end{aligned}$$

where the received waveform comprises the soliton signal $\sqrt{E}s(t)$ in white Gaussian observational noise $n(t)$ under hypothesis 1, or just the observational noise under the null hypothesis, for later convenience we have normalized $s(t)$ to have unit energy. The first task, reduction of $r(t)$ into a convenient decision space, is accomplished through the sufficient statistic,

$$r = \int_{t_i}^{t_f} r(t)s(t), \tag{7.1}$$

which can be efficiently computed with a matched filter.

Once the received signal has been transformed into the decision space, we have the simple binary hypothesis test

$$\begin{aligned} H_0 &: r = n, \\ H_1 &: r = \sqrt{E} + n, \end{aligned}$$

where under $H_0 : r \sim N(0, N_0)$, and under $H_1 : r \sim N(\sqrt{E}, N_0)$, where N_0 is the noise power of the white noise process, $n(t)$. The optimal receiver for a variety of measures, including the Bayes or Neyman-Pearson criteria, involves a likelihood ratio test, where the likelihood function is given by

$$\Lambda(r) = \frac{p_{r|H_1}(R|H_1)}{p_{r|H_0}(R|H_0)}, \tag{7.2}$$

resulting in the test

$$\frac{\sqrt{E}}{N_0} \int_{t_i}^{t_f} r(t)s(t)dt \underset{\hat{H}_0}{\overset{\hat{H}_1}{>}} \ln \eta + \frac{E}{2N_0}. \tag{7.3}$$

When the signal $r(t)$ contains a multi-soliton signal where the component solitons are not resolved, the detection problem becomes more involved. Specifically, consider a signal comprising a two-soliton solution to the Toda lattice, where we wish to make one of four decisions,

$$\begin{aligned} H_0 &: \text{neither soliton is present,} \\ H_1 &: \text{only soliton one is present,} \\ H_2 &: \text{only soliton two is present,} \\ H_{12} &: \text{both solitons are present.} \end{aligned}$$

If the relative positions of the component solitons are known *a priori*, then the de-

tection problem reduces to deciding which among 4 possible signals is present,

$$\begin{aligned} H_0 &: r(t) = n(t), \\ H_1 &: r(t) = s_1(t) + n(t), \\ H_2 &: r(t) = s_2(t) + n(t), \\ H_{12} &: r(t) = s_{12}(t) + n(t), \end{aligned}$$

where $s_1(t), s_2(t)$, and $s_{12}(t)$ are soliton one, soliton two and the multi-soliton signals respectively. Once again, this problem can be solved with standard Gaussian detection theory.

If the relative positions of the solitons are unknown, as would be the case for a modulated soliton carrier, then the signal $s_{12}(t)$ will vary significantly as a function of the relative separation. Similarly, if the signals are to be transmitted over a soliton channel where different users occupy adjacent soliton wavenumbers, any detection at the receiver would have to be performed with the possibility of another soliton component present at an unknown position. We therefore obtain a composite hypothesis testing problem, whereby under each hypothesis, we have

$$\begin{aligned} H_0 &: r(t) = n(t), \\ H_1 &: r(t) = s_1(t; \delta_1) + n(t), \\ H_2 &: r(t) = s_2(t; \delta_2) + n(t), \\ H_{12} &: r(t) = s_{12}(t; \underline{\delta}) + n(t), \end{aligned}$$

where $\underline{\delta} = [\delta_1, \delta_2]^\top$. The general problem of detection with an unknown parameter, $\underline{\delta}$, can be handled in a number of ways. For example, if the parameter can be modeled as random and the distribution for the parameter were known, $p_{\underline{\delta}}(\underline{\delta})$, along with the distributions $p_{r|\underline{\delta},H}(R|\underline{\delta}, H_i)$ for each hypothesis, then the Bayes or Neyman-Pearson criteria can be used to formulate a likelihood ratio test based on the likelihood func-

tions,

$$\Lambda(r) = \frac{\int d\underline{\delta} p_{\underline{\delta}}(\underline{\delta}) p_{r|\underline{\delta},H}(R|\underline{\delta}, H_i)}{\int d\underline{\delta} p_{\underline{\delta}}(\underline{\delta}) p_{r|\underline{\delta},H}(R|\underline{\delta}, H_j)} \tag{7.4}$$

for $i \neq j$. Unfortunately, even when the distribution for the parameter $\underline{\delta}$ is known, the likelihood ratios given in (7.4) cannot be found in closed form for even the single soliton detection problem.

Another approach that is commonly used in radar processing [72, 24] applies when the distribution of δ does not vary rapidly over range of possible values while the likelihood function (7.4) has a sharp peak as a function of δ. In this case, the major contribution to the integral in the averaged likelihood function (7.4) is due to the region around the value of δ for which $\Lambda(r;\delta)$ is maximum, and therefore this value of the likelihood function is used as if the maximizing value, $\hat{\delta}_{\mathrm{ML}}$, were the *actual* value. Since this amounts to a generalization of the standard likelihood ratio test, it is often called a "generalized likelihood ratio test" (GLRT).

If we plan to employ a GLRT for the multi-soliton detection problem, we are again faced with the need for an ML estimate of the position, $\hat{\underline{\delta}}_{\mathrm{ML}}$. A standard approach to such problems would involve turning the current problem into one with hypotheses H_0, H_1, and H_2 as before, and an additional M hypotheses — one for each value of the parameter $\underline{\delta}$ sampled over a range of possible values. Additionally, the complexity of the detection problem increases exponentially with the number of component solitons, N_s, resulting in a hypothesis testing problem with $(M+1)^{N_s}$ hypotheses.

However, as with the estimation problems in Chap. 6, the detection problems can be decoupled by preprocessing the signal $r(t)$ with the Toda lattice. If the component solitons separate as viewed on the N-th node in the lattice, then the detection problem can be more simply formulated using $i_N(t)$. The invertibility of the lattice equations implies that a Bayes optimal decision based on $r(t)$ must be the same as that based on $i_N(t)$. Since the Bayes optimal decision can be performed based on the likelihood function $\Lambda(r(t))$, and $\Lambda(i_N(t)) = \Lambda(T\{r(t)\}) = \Lambda(r(t))$, the optimal decisions based on $r(t)$ and $i_N(t)$ must be the same for any invertible transformation $T\{\cdot\}$. Although we will be using a GLRT, where the value of $\hat{\underline{\delta}}_{\mathrm{ML}}$ is used for the unknown positions

of the multi-soliton signal, since the ML estimates based on $r(t)$ and $i_N(t)$ must also be the same, as shown in Chap. 6, the detection performance of a GLRT using those estimates must also be the same. Since at high SNR, the noise component of the signal $i_N(t)$ can be assumed low pass and Gaussian, as in Chap. 6, the GLRT can be performed by pre-processing $r(t)$ with the Toda lattice equations followed by matched filter processing.

7.2 Simulations

To illustrate the algorithm, we consider the hypothesis test between H_0 and H_{12}, where the separation of the two solitons, $\delta_1 - \delta_2$, varies randomly in the interval $[-1/\beta_2, 1/\beta_2]$. The detection processor comprises a Toda lattice of $N = 20$ nodes, with the detection performed based on the signal $i_{10}(t)$. To implement the GLRT, we search over a fixed time interval about the expected arrival time for each soliton. In this manner we obtain a sequence of 1000 Monte Carlo values of the processor output for each hypothesis. A set of Monte Carlo runs has been completed for each of 3 different levels of the noise power, N_0.

The receiver operating characteristic (ROC) for the soliton with $\beta_2 = \sinh(1.5)$ is shown in Fig. 7-1, where the probability of detection, P_D, for this hypothesis test is shown as a function of the false alarm probability, P_F. For comparison, we also show the ROC that would result from a detection of the soliton alone, at the same noise level and with the time-of-arrival known. The detection index, $d = \sqrt{E/N_0}$, is indicated for each case, where E is the energy in the component soliton. The corresponding results for the larger soliton are qualitatively similar, although the detection indices for that soliton alone, with $\beta_1 = \sinh(2)$, are 5.6, 4, and 3.3, respectively. Therefore the detection probabilities are considerably higher for a fixed probability of false alarm. Note that the detection performance for the smaller soliton is well modeled by the theoretical performance for detection of the smaller soliton alone. This implies, at least empirically, that the ability to detect the component solitons in a multi-soliton signal appears to be unaffected by the nonlinear coupling with other solitons.

Further, although the unknown relative separation results in significant waveform uncertainty and would require a prohibitively complex receiver for standard detection techniques, Bayes optimal performance can still be achieved with a minimal increase in complexity.

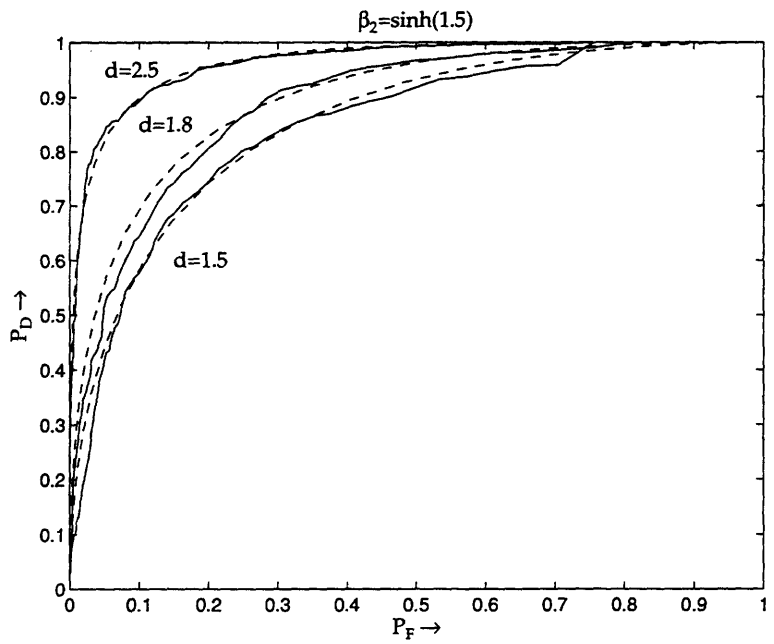

Figure 7-1: A set of empirically generated ROCs are shown for the detection of the smaller soliton from a two-soliton signal. For each of the three noise levels, the ROC for detection of the smaller soliton alone is also indicated along with the corresponding detection index, d.

7.3 Summary and Further Considerations

In this chapter we address the problem of multi-soliton detection in an AWGN environment. Our approach is to exploit the soliton evolution equations as a preprocessor, separating the multi-soliton observation into component solitons. Focusing on the Toda lattice as an example, at high signal-to-noise ratios, the noise component in the receiver remains low pass and Gaussian and is decoupled from the solitons. This allows each of the component solitons to be detected with standard matched filter processing using a GLRT. Empirically generated ROCs seem to indicate that

the detection performance for the component solitons is comparable to that for single soliton observations.

One outstanding issue is the determination of appropriate bounds on the theoretical performance of the GLRT for the detection of soliton and multi-soliton signals. Both when the Toda lattice is used for signal separation of a multi-soliton signal and when a single soliton is observed with unknown arrival time, the probability of detection and the false alarm rate have to be computed empirically, due to the complexity of the required calculations. The false alarm rate of a GLRT for a single soliton detection with unknown arrival time is determined by the level crossing problem, whereby we seek the probability that the output of the matched filter will cross a given threshold over a fixed time interval. A description of this problem is given in [24]. In general, determination of the false alarm rate is difficult, however there are a few well-studied cases. For example, based on Siegert's work with Markov processes, Helstrom shows that for a first order Gauss-Markov process with auto-covariance, $R_{xx}(\tau) = R(0)e^{-\alpha|\tau|}$, for large time intervals, $\alpha T \gg 1$, the probability of false alarm is given approximately by [24]

$$P_{fa} \approx 1 - e^{-vT}, \quad v = \frac{\alpha\eta}{\sqrt{2\pi R(0)}} e^{-\eta^2/2R(0)}, \tag{7.5}$$

where it is assumed that the threshold, $\eta \gg \sqrt{R(0)}$. When a matched filter is used for detecting a single soliton of unknown arrival time, our matched filter can be roughly approximated by a filter with impulse response, $h(t) = \beta^2 e^{-2\beta|\tau|}$. The corresponding matched filter output for a white noise input will have auto-covariance of the form $\beta^4(2 + |\tau|)e^{-2\beta|\tau|}$ and for $\beta \gg 1$ will behave much like a first order Gauss Markov process. In this manner, we might obtain a better estimate of the expected false alarm rate for single and multi-soliton detection with unknown position. For modest signal to noise ratios, the detection probability is well-modeled by the detection probability of a processor with the arrival time known.

Chapter 8

Conclusions and Directions for Future Work

In this thesis, we have developed a framework for exploring the generation and processing of soliton signals and introduced some potentially important applications of solitons in the broad context of communications.

We have taken the viewpoint of using solitons as carrier signals for transmission over linear, rather than nonlinear channels. The nonlinear evolution equations can then be viewed as specialized processors of this class of signals, which are naturally suited to performing a number of complex signal processing tasks. For example, these systems can efficiently generate soliton signals and can perform the nonlinear signal separation of multi-soliton carriers necessary for multiplexing and demultiplexing multiple users in a potential soliton wireless communications context.

Focusing specifically on two soliton systems, the Toda lattice and the discrete-KdV equation, we develop new electrical analogs for the generation and processing of soliton signals. Although analog circuit models have been previously developed for a variety of nonlinear wave equations in general, and for the Toda lattice in particular, our diode ladder implementation is the first direct electrical analog of this soliton system. Further, this appears to be the first circuit model of the Toda lattice which is sufficiently accurate to demonstrate true soliton interactions. The diode ladder circuit was implemented in hardware using standard components and provides a platform for

the further development and testing of real-time soliton processing techniques. We have also developed a new circuit model for the discrete-KdV equation; a nonlinear system which was largely ignored for having no prior electrical or mechanical analog. The discrete-KdV circuit provides a framework for processing discrete-time soliton signals.

Based on these nonlinear circuit models, we have suggested and explored a number of communications techniques whereby message-bearing signals are used to modulate the parameters of soliton carriers. The nonlinear circuits are used to generate and to multiplex multiple message-signals onto a multi-soliton carrier. We have demonstrated that the nonlinear interaction of multiple solitons can be exploited as a means of reducing the transmitted signal energy in a multi-user communication context.

To assess the efficacy and the robustness of these communication techniques in the presence of background noise, we have analyzed the effects of small amplitude disturbances on the processing of soliton signals in the Toda lattice and characterized the statistics of the noise as it is processed. We have shown that in a high SNR AWGN background, the dynamics of soliton signals are practically unperturbed. Also, the noise component of the received signal remains essentially low pass and Gaussian. Through an analysis of the nonlinear spectrum from the inverse scattering transform, we also have shown that at high SNR, virtually all of the background noise maps onto the non-soliton (continuum) component of the nonlinear spectrum, and the soliton spectrum experiences only a small Gaussian perturbation. This result furthers the analogy of the inverse scattering transform to the Fourier transform for linear systems.

We were also able to develop maximum likelihood parameter estimation algorithms for soliton signals corrupted by white Gaussian noise. Calculation of the Cramér-Rao bounds for the estimation error variance of soliton parameters reveals the potential for estimation enhancement due to multiple soliton interaction. By using the nonlinear circuits as preprocessors which perform the necessary signal separation, the joint estimation of multiple soliton parameters can be achieved through standard Gaussian techniques. We have also developed a maximum likelihood parameter estimation algorithm in the nonlinear spectral domain of the inverse scattering transform. Both

the theoretical bounds and the empirical algorithm performance demonstrate that the nonlinear coupling of multiple solitons can actually enhance parameter estimation performance. This indicates the potential for wireless multi-soliton communication techniques to simultaneously reduce the transmitted signal energy while enhancing communication performance.

By a similar technique, soliton circuits can be used to decompose a multi-soliton detection problem with $(M+1)^{N_s}$ hypotheses into N_s-separate binary hypothesis tests without sacrificing Bayes optimality in high SNR Gaussian environments. Of particular interest is the case of multi-soliton position uncertainty which can gives rise to dramatic changes in the received multi-soliton signal and therefore would have a significant impact on the structure of a traditional detector. However, since the soliton circuits decompose the multi-soliton detection problem into single soliton detections, our detection framework is unchanged.

8.1 Future Directions

In this thesis, we began an exploration of a number of new and interesting applications of soliton signals and systems from a signal processing viewpoint. As a result, there are a number outstanding issues relating to many of the topics considered. Although many areas of future study have been identified in the body of the thesis, we mention several particularly intriguing directions here.

Much of the mathematical foundation for soliton dynamics lies within the framework of solvable nonlinear systems. In Sec. 2.2 we have attempted to present some of the essential ideas behind this class of nonlinear systems and relate them to linear system theory. Although many of the results in this thesis pertain to the detection and estimation of parameters of received soliton signals, there are many interesting signal processing questions regarding the dynamics these integrable nonlinear systems themselves. Specifically, it may be possible to address the problems of recursive estimation, e.g., prediction, extrapolation, filtering, and smoothing of such systems with the aid of the inverse scattering. Traditional barriers to such investigations for nonlin-

ear systems lie in both the state propagation and the propagation of state probability densities. For integrable Hamiltonian systems, the state propagation can be solved explicitly via inverse scattering, while the propagation of the state density remains a difficult problem.

Another potentially interesting area of future research involves extending the results of integrable system theory to include totally discrete (discrete-time, finite dimensional) systems. Some work in this area has led to discretized versions of the inverse scattering theory for the Toda lattice [20, 26, 28] the Korteweg-de Vries equation[25], as well as others in [1, 27]. Such systems may lead to applications using discrete soliton signals for digital communication.

In Chap. 3 we illustrate how analog circuits could be used in the context of the communication ideas shown in Chap. 4. These results along with those of Hirota and Suzuki [29, 64, 65], Toda [68], Scott [56, 57], and others illustrate the potential for development of a variety of analog hardware for soliton modulation techniques. However, there are several outstanding issues regarding the detailed implementation of the communications techniques discussed in Chap. 4 using such circuits. Specifically, the demodulation of individual soliton carriers still must be addressed along with a more complete investigation into the effects of realistic non-additive channel disturbances. There may also be benefit to further exploration of the soliton-like behavior of certain cellular automata [1, 7, 53, 66] and the possible use of such systems for digital communication or computation [32, 62, 63].

The nonlinear circuit models developed for the Toda lattice demonstrate an interesting similarity to the models used by Keshner in his analysis of $1/f$ noise [38]. Specifically, a small signal model for the diode ladder circuit yields a driving point impedance inversely proportional to frequency, and thus would produce a "double Brownian" motion process in response to a white noise input. Such an analogy leads directly to the observation that at least for the small signal model, noise at the input of the nonlinear circuits will lead to $1/f$-type disturbances. Another interesting link between the $1/f$ generators and soliton circuits, is that, like the family of $1/f$ random processes, the family of soliton solutions to such equations also have a multi-

scale component. This apparent multi-scale invariance of the soliton dynamics along with the similarity in the circuit models to those which generate $1/f$ noise, may indicate the presence of a fundamental nonlinear multi-scale behavior inherent in the dynamics.

Although we have explored some basic strategies for using soliton signals for communication, there remain a number of unanswered questions regarding the efficacy of such techniques in comparison to standard methods. For example, a quantitative investigation of the spectral efficiency, the effects of inter-symbol interference, the error probability, or decoder complexity for such methods in comparison to standard techniques ought to be undertaken. Finally, we note that solitons represent a rich class of signals that are potentially applicable to a variety of signal processing and communications contexts beyond those mentioned in this thesis. Indeed, perhaps the most exciting and potentially rewarding direction for future research lies in the discovery of new and promising applications.

Bibliography

[1] M.J. Ablowitz and A.P. Clarkson. *Solitons, Nonlinear Evolution Equations and Inverse Scattering.* Number 149 in London Mathematical Society Lecture Note Series. Cambridge University Press, Cambridge, Great Britain, 1991.

[2] M. Abramowitz and I.A. Stegun, editors. *Handbook of Mathematical Functions.* Dover, New York, NY, 1965.

[3] V.I. Arnold and A. Avez. *Ergodic Problems of Classical Mechanics.* Addison-Wesley Publishing Company, Inc., 1989.

[4] G.J. Ballantyne, P.T. Gough, and D.P. Taylor. Periodic solutions of Toda lattice in loop nonlinear transmission line. *Electronics Letters*, 29(7):607–609, April 1993.

[5] T.B. Benjamin. The stability of solitary waves. *Proceedings of the Royal Society of London*, A(328):1553–183, 1972.

[6] Rajendra Bhatia. *Perturbation bounds for matrix eigenvalues.* Pitman research notes in mathematics series. Wiley, 1987.

[7] Alexander Bobenko, Martin Bordermann, Charlie Gunn, and Ulrich Pinkall. On two integrable cellular automata. *Communications in Mathematical Physics*, 158:127–134, 1993.

[8] Rene Carmona. *Spectral theory of random Schrödinger operators.* Birkhauser, 1990.

[9] B. Char, K. Geddes, G. Gonnet, B. Leong, M. Monagan, and S. Watt. *Maple V Library Reference Manual.* Springer-Verlag, 1992.

[10] Yasuo Cho, Junji Wakita, and Nozomu Miyagawa. Nonlinear equivalent circuit model analysis of acoustic devices and propagation of surface acoustic wave. *Japan Journal of Applied Physics*, 32(5B):2261–2264, 1993.

[11] *Proceedings of the IEEE*: Special issue on surface acoustic wave devices and applications. L.T. Claiborne, G.S. Kino and E. Stern, editors, May 1976.

[12] P.G. Drazin and R.S. Johnson. *Solitons: an Introduction.* Cambridge Texts in Applied Mathematics. Cambridge University Press, New York, 1989.

[13] A. Erdelyi, editor. *Tables of Integral Transforms*, volume I. McGraw-Hill Book Company, 1954. Based, in part, on notes left by Harry Bateman, and compiled by The Bateman Manuscript Project.

[14] E. Fermi, J.R Pasta, and S.M Ulam. Studies of nonlinear problems. In *Collected Papers of E. Fermi*, volume II, pages 977–988. University of Chicago Press, 1965.

[15] H. Flaschka. On the Toda lattice. ii. *Progress of Theoretical Physics*, 51(3):703–716, March 1974.

[16] H. Flaschka and D.W. McLaughlin. Some comments on Bäcklund transformations, canonical transformations, and the inverse scattering method. In Robert Miura, editor, *Backlund transformations, the inverse scattering method, solitons, and their applications: Proceedings NSF Research Workshop on Contact Transformations*, number 515 in Lecture notes in mathematics, pages 253–295, Berlin, 1976. Springer-Verlag.

[17] Nikos Flytzanis, Boris Malomed, and Jonathan A.D. Wattis. Analysis of stability of solitons in one-dimensional lattices. *Physics Letters*, A(180):107–112, 1993.

[18] Clifford S. Gardner, John M. Greene, Martin D. Kruskal, and Robert Miura. Method for solving the Korteweg-deVries equation. *Physical Review Letters*, 19(19):1095–1097, November 1967.

[19] A. Gelb, editor. *Applied Optimal Estimation.* MIT Press, Cambridge, MA, 1974.

[20] John Gibbons and Boris Kupershmidt. Time discretizations of lattice integrable systems. *Physics Letters*, A(165):105–110, May 1992.

[21] Gene H. Golub and Charles F. Van Loan. *Matrix Computations.* The Johns Hopkins University Press, Baltimore, Maryland, 1989.

[22] I.S. Gradshteyn and I.M. Ryzhik. *Table of Integrals, Series and Products.* Academic Press, fourth edition, 1965.

[23] Hermann A. Haus. Molding light into solitons. *IEEE Spectrum*, pages 48–53, March 1993.

[24] Carl W. Helstrom. *Statistical Theory of Signal Detection.* Pergamon Press, New York, second edition, 1968.

[25] Ryogo Hirota. Nonlinear partial difference equations. I. a difference analogue of the Korteweg-de Vries equation. *Journal of the Physical Society of Japan*, 43(4):1424–1433, October 1977.

[26] Ryogo Hirota. Nonlinear partial difference equations. II. discrete-time Toda equation. *Journal of the Physical Society of Japan*, 43(6):2074–2078, December 1977.

[27] Ryogo Hirota. Nonlinear partial difference equations. III. discrete sine-Gordon equation. *Journal of the Physical Society of Japan*, 43(6):2079–2087, December 1977.

[28] Ryogo Hirota. Nonlinear partial difference equations. IV. Bäcklund transformation for the discrete-time Toda equation. *Journal of the Physical Society of Japan*, 45(1):321–332, July 1978.

[29] Ryogo Hirota and Kimio Suzuki. Theoretical and experimental studies of lattice solitons in nonlinear lumped networks. *Proc. IEEE*, 61(10):1483–1491, October 1973.

[30] Paul Horowitz and Winfield Hill. *The Art of Electronics.* Cambridge University Press, New York, second edition, 1989.

[31] Eryk Infeld and George Rowlands. *Nonlinear Waves, Solitons and Chaos.* Cambridge University Press, New York, 1990.

[32] Nayeem Islam, J.P. Singh, and Kenneth Steiglitz. Soliton phase shifts in a dissipative lattice. *J. Appl. Phys.*, 62(2):689–693, July 1987.

[33] M. Kac and P. van Moerbeke. On an explicitly soluble system of nonlinear differential equations related to certain Toda lattices. *Advances in Mathematics*, 16:160–169, 1975.

[34] M. Kac and P. van Moerbeke. On some periodic Toda lattices. *Proc. Nat. Acad. Sci.*, 72(4):1627–1629, April 1975.

[35] J.F. Kaiser. On a simple algorithm to calculate the 'energy' of a signal. In *Proc. Int. Conf. Acoust. Speech, Signal Processing*, pages 381–384, Albuquerque, NM, 1990.

[36] J.F. Kaiser. personal communication, June 1994.

[37] Tosio Kato. *Perturbation theory for linear operators.* Springer-Verlag, 1980.

[38] M.S. Keshner. $1/f$ noise. *Proc. IEEE*, 70:212–218, March 1982.

[39] Joseph A Kolosick, Don L Landt, H.C. Hsuan, and Karle E. Lonngren. Properties of solitary waves as observed on a nonlinear dispersive transmission line. *Proc. IEEE*, 62(5):578–581, May 1974.

[40] Yinchieh Lai. Noise analysis of soliton communication systems—a new approach. *Journal of Lightwave Technology*, 11(3):462–467, March 1993.

[41] L.D. Landau and E.M. Lifshitz. *Mechanics.* Pergamon Press, New York, 1976.

[42] Peter D. Lax. Integrals of nonlinear equations of evolution and solitary waves. *Communications on Pure and Applied Mathematics*, XXI:467–490, 1968.

[43] A.G. Lindgren and R.J. Buratti. Stability of waveforms on active nonlinear transmission lines. *IEEE transactions on Circuit Theory*, CT-16:274–279, Aug 1969.

[44] V.M. Loginov. Exact separation of an additive mixture of a determinate signal and gaussian noise by the use of Korteweg-de Vries solitons. *Tech. Phys. Lett.(Pis'ma Zh. Tekh. Fiz.)*, 19(7):433–434, July 1993.

[45] S.V. Manakov. Complete integrability and stochastization of discrete dynamical systems. *Sov. Phys. JETP*, 40(2):269–274, 1975.

[46] N. Margolus and T. Toffoli. Cellular automata machines. In G.D. Doolen, editor, *Lattice Gas Methods for Partial Differential Equations*, pages 219–249, Reading, Ma, 1990. Addison-Wesley.

[47] Meta Software, Inc., Campbell, CA. *HSPICE User's Manual*, 1992.

[48] J. Moser. Finitely many mass points on the line under the influence of an exponential potential – an integrable system. In J. Moser, editor, *Dynamical Systems, Theory and Applications: Battelle Seattle 1974 Rencontres*, number 38 in Lecture Notes in Physics, pages 467–497, New York, 1975. Springer Verlag.

[49] Alan C. Newell. *Solitons in Mathematics and Physics.* Regional Conference Series in Applied Mathematics. Society for Industrial and Applied Mathematics, Philadelphia, 1985.

[50] Yoshiko Okada, Shinsuke Watanabe, and Hiroshi Tanaca. Solitary wave in periodic nonlinear lattice. *Journal of the Physical Society of Japan*, 59(8):2647–2658, August 1990.

[51] Naotake Ooyama and Nobuhiko Saito. On the stability of lattice solitons. *Supplement of the Progress of Theoretical Physics*, 45:201–208, 1970.

[52] T.S. Papatheodorou, M.J. Ablowitz, and Y.G. Saridakis. A rule for fast computation and analysis of soliton automata. *Studies in Applied Mathematics*, 79:173–184, 1988.

[53] James K. Park, Kenneth Steiglitz, and William P. Thurston. Soliton-like behavior in automata. *Physica 19D*, pages 423–432, 1986.

[54] V.N. Popov, editor. *Operator theory with a random potential, and some questions of statistical physics: collection of papers.* American Mathematical Society, 1991.

[55] Enders A. Robinson and Sven Treitel. *Geophysical Signal Analysis.* Prentice-Hall, Inc., 1980.

[56] A.C. Scott. *Active and Nonlinear Wave Propagation in Electronics.* Wiley - Interscience, New York, 1970.

[57] Alwyn C. Scott, F.Y.F. Chu, and David McLaughlin. The soliton: A new concept in applied science. *Proc. IEEE*, 61(10):1443–1483, October 1973.

[58] John Scott-Russell. Report on waves. In *Rep. 14th Meet. Brit. Assoc. Adv. Sci.*, pages 319–320, 1844.

[59] William McC. Siebert. *Circuits, Signals, and Systems.* The MIT Electrical Engineering and Computer Science Series. The MIT Press and The McGraw-Hill Book Company, Cambridge MA, 1986.

[60] Andrew C. Singer. A new circuit for communication using solitons. In *Proc. IEEE Workshop on Nonlinear Signal and Image Processing*, volume I, pages 150–153, 1995.

[61] Merrill I. Skolnik. *Radar Handbook.* McGraw-Hill Book Company, 1970.

[62] Richard K. Squire and Ken Steiglitz. Subatomic particle machines: parallel processing in bulk material. *submitted to IEEE Signal Processing Letters*, 1995.

[63] Kenneth Steiglitz, Irfan Kamal, and Arthur Watson. Embedding computation in one-dimensional automata by phase coding solitons. *IEEE Transactions on Computers*, 37(2):138–145, February 1988.

[64] Kimio Suzuki, Ryogo Hirota, and Kazufumi Yoshikawa. Amplitude modulated soliton trains and coding-decoding applications. *Int. J. Electronics*, 34(6):777–784, 1973.

[65] Kimio Suzuki, Ryogo Hirota, and Kazufumi Yoshikawa. The properties of phase modulated soliton trains. *Japanese Journal of Applied Physics*, 12(3):361–365, March 1973.

[66] D. Takahashi. On a fully discrete soliton system. In M. Boiti, L. Martina, and F. Pempinelli, editors, *Nonlinear Evolution Equations and Dynamical Systems*, pages 245–249, New Jersey, June 1991. World Scientific.

[67] Morikazu Toda. *Theory of Nonlinear Lattices.* Number 20 in Springer Series in Solid-State Science. Springer-Verlag, New York, 1981.

[68] Morikazu Toda. Nonlinear lattice and soliton theory. *IEEE Transactions on Circuits and Systems*, CAS-30(8):542–554, August 1983.

[69] Morikazu Toda. *Nonlinear Waves and Solitons.* Mathematics and Its Applications. Klewer Academic Publishers, Boston, 1989.

[70] T. Toffoli and N. Margolus. *Cellular Automata Machines - A New Environment for Modeling.* MIT Press, Cambridge, Ma, 1987.

[71] T. Toffoli and N. Margolus. Programmable matter: Concepts and realizations. *Physica D*, 47(1-2):263–272, 1991.

[72] Harry L. Van Trees. *Detection, Estimation, and Modulation Theory: Part I Detection, Estimation and Linear Modulation Theory.* John Wiley and Sons, 1968.

[73] J. vomScheidt and W. Purkert. *Random Eigenvalue Problems.* Probability and Applied Mathematics. North Holland, 1983.

[74] Miki Wadati. Stochastic Korteweg-de Vries equation. *Journal of the Physical Society of Japan*, 52(8):2642–2648, Aug 1983.

[75] G.B. Whitham. *Linear and Nonlinear Waves.* Wiley, New York, 1974.

[76] J.H. Wilkinson. *The algebraic eigenvalue problem.* Oxford science publications. Oxford University Press, 1988.

[77] G.W. Wornell and A.V. Oppenheim. Wavelet-based representations for a class of self-similar signals with application to fractal modulation. *IEEE Trans. Inform. Theory*, 38(2):785–800, March 1992.

[78] N.J. Zabusky and M.D. Kruskal. Interaction of solitons in a collisionless plasma and the recurrence of initial states. *Physical Review Letters*, 15(6):240–243, August 1965.

[79] V.E. Zakharov and A.B. Shabat. A refined theory of two-dimensional self-focussing and one-dimensional self-modulation of waves in nonlinear media. *Zh. Eksp. Teor. Fiz.*, 61(1):118–134, 1971.